



THE HONG KONG  
POLYTECHNIC UNIVERSITY

香港理工大學

Pao Yue-kong Library

包玉剛圖書館

---

## Copyright Undertaking

This thesis is protected by copyright, with all rights reserved.

**By reading and using the thesis, the reader understands and agrees to the following terms:**

1. The reader will abide by the rules and legal ordinances governing copyright regarding the use of the thesis.
2. The reader will use the thesis for the purpose of research or private study only and not for distribution or further reproduction or any other purpose.
3. The reader agrees to indemnify and hold the University harmless from and against any loss, damage, cost, liability or expenses arising from copyright infringement or unauthorized usage.

### IMPORTANT

If you have reasons to believe that any materials in this thesis are deemed not suitable to be distributed in this form, or a copyright owner having difficulty with the material being included in our database, please contact [lbsys@polyu.edu.hk](mailto:lbsys@polyu.edu.hk) providing details. The Library will look into your claim and consider taking remedial action upon receipt of the written requests.

**A STUDY OF NOVEL TUBULAR BRAIDED STRUCTURE WITH  
NEGATIVE POISSON'S RATIO**

**JIANG NING**

**MPhil**

**The Hong Kong Polytechnic University**

**2019**

The Hong Kong Polytechnic University

Institute of Textile and Clothing

A STUDY OF NOVEL TUBULAR BRAIDED STRUCTURE WITH  
NEGATIVE POISSON'S RATIO

Jiang Ning

A thesis submitted in partial fulfilment of the requirements for the  
degree of Master of Philosophy

July 2018

## CERTIFICATE OF ORIGINALITY

I hereby declare that this thesis is my own work and that, to the best of my knowledge and belief, it reproduces no material previously published or written, nor material that has been accepted for the award of any other degree or diploma, except where due acknowledgement has been made in the text.

\_\_\_\_\_ (Signed)

\_\_\_\_\_ Jiang Ning \_\_\_\_\_ (Name of student)

*To My Family*  
*For their Love, Patience and Support*

## **Abstract**

Auxetics are the materials and structures that display a negative Poisson's ratio. Differing from the common materials which tend to be thinner when stretched, auxetics will actually expand in the transverse direction upon stretching. This novel and counterintuitive behaviour allows auxetics to exhibit a series of improved material properties, such as increased shear stiffness, higher energy absorption, enhanced acoustic behaviour and superior indentation resistance, compared with conventional positive Poisson's ratio materials. Thus, in the past three decades, auxetics have gained great popularity in research and numerous studies have been conducted to explore the nature of them. However, none of auxetic braided structures has been reported among the considerable number of auxetic materials and structures proposed, fabricated, or synthesized in the previous studies. The study on structural characterization, manufacturing process and structure-properties relationships of auxetic braided structures are still lacking.

This study then was set to introduce auxetic effect into the field of braid, notably the field of tubular braid. The aims of this study were to propose novel tubular braided structures with negative Poisson's ratio, to explore the nature of their deformation mechanism and to investigate the effect of the structural parameters on the auxetic behaviour of developed braid. In order to reach the above goals, several types of auxetic braids were designed and fabricated using a standard or modified circular braiding technology. In the meantime, preliminary experimental investigations were conducted on those fabricated auxetic braids in order to evaluate and confirm the negative Poisson's ratio effect of them under tensile conditions. To examine the influence of the structural parameters on the auxetic behaviour of developed braid, a theoretical analysis on structure-property relationships was also adopted besides the

experimental investigation. Based on the established analytical model, the Poisson's ratio of the structure at any given longitudinal strain can be calculated, and the effects of three structural parameters, i.e., the initial wrap angle, component yarns diameter and the Poisson's ratio of component yarns, on auxetic behaviour are studied. With conducted experimental investigation and theoretical analysis, it is possible to optimize the developed structure for desired performance criteria.

It is expected that such a study could shed light on the development of the auxetic braided structures and provide an alternative way to fabricate auxetics from positive Poisson's ratio materials. Meanwhile, the developed new kinds of auxetic braids may solve the problems of unsolid knots that exist in currently commercialized medical sutures, shoelaces or secure threads.

## **Lists of Publications Arising from the Thesis**

Referred journal papers:

1. Ning Jiang, Hong Hu. (2018). A study of tubular braided structure with negative Poisson's ratio behavior. *Textile Research Journal*, 88(24), 2810–2824.
2. Ning Jiang, Hong Hu. (2018). Auxetic yarn made with circular braiding technology. *Physica Status Solidi B: Basic Solid State Physics*. Doi: 10.1002/pssb.201800168.
3. Ning Jiang, Hong Hu. (2018). Theoretical analysis of deformation behaviour of auxetic tubular braid made from modified braiding technique. To be submitted to *Smart Materials and Structure*.

Conference papers:

1. Ning Jiang, Hong Hu. Design and fabrication of tubular braids with negative Poisson's ratio. The 91st Textile Institute World Conference 2018, 23rd – 26th July 2018, Leeds, UK. The Textile Institute.
2. Ning Jiang, Hong Hu. Braided structure with negative Poisson's ratio, The fiber society 2016 Fall Meeting and Technical Conference 10-12 October, 2016, Ithaca, New York, USA.

## **Acknowledgements**

First of all, I am deeply indebted to my chief supervisor Professor Hu Hong to whom goes my deepest gratitude for his academic supervision and personal support throughout all my years in graduate school. Without his kindly guidance, constructive comments, and great patience, this dissertation would not have been possible.

I am also grateful to: Institute of Textile and Clothing, The HK PolyU, my home institution, for providing supportive and stimulating working environments during my two-year MPhil study here.

I wish to give my thanks to my colleague and my friends, Adeel Zulifqar and Wang Zhengyue, for their kind and warm help during my time at PolyU and for academic collaborations that have profoundly influenced my way of thinking about the subject of this thesis.

Lastly, but most importantly, I wish to thank my grandparents, Jiang Kangqin and Jiang Nenge, my parents, Jiang Zhijie and Sun Huiping and my girlfriend Liu Tianyi who give me braveness and confidence in my life. My gratitude to them is beyond words.

May 2018

Jiang Ning

## Table of Contents

ABSTRACT .....	I
LISTS OF PUBLICATIONS ARISING FROM THE THESIS .....	III
TABLE OF CONTENTS .....	V
LIST OF FIGURES.....	VIII
LIST OF TABLES.....	XIV
NOMENCLATURE .....	XV
CHAPTER 1 INTRODUCTION .....	1
1.1 Motivation of the research .....	1
1.2 Objectives.....	2
1.3 Methodology .....	3
1.4 Thesis outline .....	4
CHAPTER 2 LITERATURE REVIEW.....	6
2.1 Introduction .....	6
2.2 Poisson's ratio .....	6
2.2.1 Definition of Poisson's ratio .....	6
2.2.2 Poisson's ratio and materials' properties.....	6
2.3 Textile materials and structures with negative Poisson's ratio.....	9
2.3.1 Auxetic fibers .....	9
2.3.2 Auxetic yarns.....	12
2.3.3 Auxetic fabrics .....	16
2.3.4 Research gaps.....	24
2.4 Braiding technology and braided structures.....	25
2.4.1 The definition of braiding .....	25
2.4.2 History of braiding technique .....	26
2.4.3 Three primary braided structures in textile .....	27
2.4.4 Braid geometry.....	30
2.4.5 The advantage of auxetic braided structures .....	31
2.5 Conclusions .....	32
CHAPTER 3 DESIGN AND FABRICATE AUXETIC BRAIDED STRUCTURES.....	34
3.1 Introduction .....	34
3.2 Three auxetic braids developed using first approach.....	34
3.2.1 Geometry design and deformation mechanism.....	34

3.2.2 Fabrication process .....	38
3.3 Other three auxetic braids developed using second approach. ....	41
3.3.1 Geometry design and deformation mechanism.....	41
3.3.2 Fabrication process .....	43
3.4 Conclusions .....	45
<b>CHAPTER 4 EXPERIMENTAL ANALYSIS OF SIX AUXETIC BRAIDED</b>	
<b>STRUCTURES .....</b>	<b>47</b>
4.1 Introduction .....	47
4.2 Negative Poisson's ratio effect of six structures .....	47
4.2.1 Sample fabrication .....	47
4.2.2 Poisson's ratio testing method.....	49
4.2.3 Results and discussion .....	52
4.3 Effects of parameters on the negative Poisson's ratio effect.....	62
4.3.1 Sample fabrication .....	64
4.3.2 Poisson's ratio testing method.....	66
4.3.3 Experimental results and discussion for HL structure .....	67
4.3.4 Experimental results and discussion for R1 structure.....	71
4.4 Conclusions .....	76
<b>CHAPTER 5 THEORETICAL ANALYSIS OF THE AUXETIC BRAIDED</b>	
<b>STRUCTURE .....</b>	<b>78</b>
5.1 Introduction .....	78
5.2 Analytical modelling .....	78
5.2.1 Uniaxial extension structural deformation analysis .....	78
5.2.2 Basic assumptions .....	79
5.2.3 The Poisson's ratio of structure in the first stage. ....	81
5.2.4 The Poisson's ratio of structure in the second stage. ....	86
5.3 Model validation .....	88
5.4 Effects of parameters on the Poisson's ratio based on the analytical model....	90
5.4.1 Effects of initial wrap angle of stiff yarn .....	90
5.4.2 Effects of the diameter of component yarns .....	91
5.4.3 Effects of the Poisson's ratio of component yarns .....	93
5.5 Conclusions .....	95
<b>CHAPTER 6 CONCLUSIONS AND FUTURE WORK .....</b>	<b>97</b>
6.1 Conclusions .....	97

6.1.1 Design and fabrication of the novel braided structures with negative Poisson's ratio .....	97
6.1.2 Experimental investigation on the developed six auxetic braided structures .....	97
6.1.3 Theoretical analysis of the developed six auxetic braided structures .....	98
6.2 Contributions.....	98
6.3 Limitations .....	99
6.4 Recommendation for future work .....	100
REFERENCES.....	102

## List of Figures

Figure 1.1 Flowchart of overall methodology.....	3
Figure 2.1 Interrelations between Poisson's ratio and elastic properties.....	8
Figure 2.2 The schematics for the deformation of 2D materials under uni- longitudinal load: (a) materials with positive Poisson's ratio; (b) materials with negative PR. ....	9
Figure 2.3 When an object was hitting on the material: (a) a non-auxetic material immediately flows away in the lateral direction; (b) an auxetic material flows into the region of the impact rather than flow away.....	9
Figure 2.4 The Poisson's ratio of auxetic fibers: (a) auxetic polypropylene fibers; (b) auxetic polyester fibers and conventional positive Poisson's ratio polyester fibers. ....	10
Figure 2.5 Nodule-fibril network structure in auxetic fibers: (a) schematic diagram of nodule-fibril model in the polypropylene polymer; (b) expansion of nodule- fibril under tension. ....	11
Figure 2.6 Fully densified (left) and expanded (right) hexagonal interlocked structures. The coordinate system, a unit cell (dashed box) and geometrical parameters are indicated. ....	12
Figure 2.7 Helical auxetic yarn (HAY): (a) at an initial state; (b) at the maximum strain.....	13
Figure 2.8 Geometric definitions of a helical auxetic yarn.....	14
Figure 2.9 Poisson's ratio – strain curve of HAY structure with an initial wrap angle of 13°. ....	14
Figure 2.10 The novel plied yarn with negative PR: (a) geometry; (b) deformation mechanism responsible for auxetic behaviour. ....	15
Figure 2.11 The semi-auxetic yarn structure: (a) geometry; (b) deformation	

mechanism responsible for auxetic behaviour. ....	16
Figure 2.12 Fabrication method of auxetic knitted fabric with a zigzag arrangement. .....	17
Figure 2.13 Auxetic knitted fabric with a zigzag arrangement: (a) initial state; (b) when stretched. ....	17
Figure 2.14 The Poisson's ratio-strain curves of produced auxetic knitted fabric with a zigzag arrangement. ....	18
Figure 2.15 Fabrication method of auxetic knitted fabric: (a) with a rectangular arrangement; (b) with a horizontal and vertical stripes arrangement.....	19
Figure 2.16 Auxetic knitted fabric with a rectangular arrangement: (a) initial state and (b) when stretched; Auxetic knitted fabric with a horizontal and vertical stripes arrangement: (c) initial state and (d) when stretched.....	19
Figure 2.17 The photograph of auxetic woven fabrics: (a) made from HAY yarn; (b) made from plied yarn with negative PR.....	20
Figure 2.18 The auxetic woven fabric with a zigzag geometry shape. ....	22
Figure 2.19 The Poisson's ratio versus longitudinal strain curve for developed auxetic woven fabrics with different geometry settings. ....	22
Figure 2.20 The approach of producing auxetic non-woven fabric. ....	23
Figure 2.21 The schematic of buckled fibers responsible for producing auxetic behaviour in auxetic non-woven fabric.....	23
Figure 2.22 Auxetic composite based on non-auxetic braided rods: (a): with missing rib' geometry; (b) with 're-entrant honeycomb' geometry.....	24
Figure 2.23 From A to F indicates the process to braid a three-strand hairstyle.....	27
Figure 2.24 Tubular braid: (a) geometry; (b) the manufacturing process. ....	28
Figure 2.25 Flat braid: (a) geometry; (b) the manufacturing process. ....	29
Figure 2.26 Three dimensional (3D) braids: (a) application in the reinforcement of	

bicycle body; (b) production process (rotary braiding method). .....	30
Figure 2.27 Geometry of braided structure. ....	31
Figure 3.1 The auxetic tubular braided structures developed via wrapping or inserting extra stiff yarns: (a) HL; (b) HC; (c) FC. ....	36
Figure 3.2 Auxetic behaviour of HL structures under tension. ....	36
Figure 3.3 Auxetic behaviour of HC structure under tension. ....	37
Figure 3.4 Auxetic behaviour of FC structure under tension. ....	37
Figure 3.5 The conventional vertical circular braiding machine utilized for manufacturing developed auxetic braided structures. ....	38
Figure 3.6 The manufacturing process for structure HL: (a) set-up of the braiding system; (b) the moving path of extra stiff yarn; (c) fixation of the stiff yarn. ...	39
Figure 3.7 The manufacturing process for structure HC: (a) set-up of the braiding system; (b) the moving path of extra stiff yarn; .....	40
Figure 3.8 The manufacturing process for structure FC: (a) set-up of the braiding system; (b) the moving path of extra stiff yarn; .....	41
Figure 3.9 The auxetic tubular braided structure R1: (a) geometry; (b) auxetic deformation under tension. ....	42
Figure 3.10 The auxetic tubular braided structure R2: (a) geometry; (b) auxetic deformation under tension. ....	43
Figure 3.11 The auxetic tubular braided structure R3: (a) geometry; (b) auxetic deformation under tension. ....	43
Figure 3.12 Structure R1: (a) the manufacturing process; (b) the yarn arrangement on 16 carriers.....	45
Figure 3.13 Structure R2: (a) the manufacturing process; (b) the yarn arrangement on 16 carriers.....	45
Figure 3.14 Structure R3: (a) the manufacturing process; (b) the yarn arrangement on	

16 carriers.....	45
Figure 4.1 The tensile testing system used to calculate the Poisson's ratio of developed structures: (a) schematic; (b) photograph. ....	50
Figure 4.2 Digital Image Processing for yarn image obtained: (a) captured photograph; (b) binary and threshold image; (c) image for the calculation of effective transverse width of auxetic yarn. ....	51
Figure 4.3 The negative PR effect of structure HL: (a) transverse length–longitudinal length curve; (b) Poisson's ratio-strain curve. ....	53
Figure 4.4 The negative PR effect of structure HC: (a) transverse length–longitudinal length curve; (b) Poisson's ratio-strain curve. ....	55
Figure 4.5 The negative PR effect of structure FC: (a) transverse length–longitudinal length curve; (b) Poisson's ratio-strain curve. ....	56
Figure 4.6 The photograph of Sample FC1 at critical tensile strains. ....	57
Figure 4.7 The negative PR effect of structure R1: (a) transverse length–longitudinal length curve; (b) Poisson's ratio-strain curve. ....	58
Figure 4.8 The path of stiff yarn in structure R1 when rolled out into a flat surface: (a) crimp shape at an initial state; (b) helical shape when slightly stretched. ....	58
Figure 4.9 The negative PR effect of structure R2: (a) transverse length–longitudinal length curve; (b) Poisson's ratio-strain curve. ....	59
Figure 4.10 The negative PR effect of structure R3: (a) transverse length–longitudinal length curve; (b) Poisson's ratio-strain curve. ....	61
Figure 4.11 The negative PR effect of all produced structures: (a) transverse length–longitudinal length curve; (b) Poisson's ratio-strain curve. ....	62
Figure 4.12 Poisson's-strain curves for samples of HL with different initial wrap angles. ....	68
Figure 4.13 Poisson's-strain curves for samples of HL with different initial braiding	

angles. ....	69
Figure 4.14 Poisson's-strain curves for samples of HL with different braiding yarn diameters. ....	70
Figure 4.15 Poisson's-strain curves for R1 samples with a different number of stiff yarns. ....	72
Figure 4.16 Poisson's-strain curves for R1 samples with two stiff yarns in the different distance. ....	73
Figure 4.17 Poisson's-strain curves for R1 samples with two stiff yarns with the same stiff yarn, but with different elastic yarns and core yarns. ....	75
Figure 5.1 The deformation of the structure in the first stage. ....	79
Figure 5.2 The deformation of the structure HL in the second stage. ....	79
Figure 5.3 One geometry cycle of the structure in the initial state. ....	82
Figure 5.4 Trigonometric relationship exists between $r$ and $\epsilon_l$ . ....	83
Figure 5.5 The cross-section of the structure when the structure is deformed into a helical shape. ....	84
Figure 5.6 The triangle relationship between the helical radius of the core yarn and the longitudinal strain of the whole structure. ....	85
Figure 5.7 The triangle relationship between the helical radius of the core yarn and the longitudinal strain of the stiff yarn. ....	87
Figure 5.8 The comparison between results calculated from the established model and experimental results obtained from the testing for structures HL and R1...	90
Figure 5.9 Effects of the initial wrap angle of the stiff yarn. ....	91
Figure 5.10 Effects of the diameter of components yarns on the negative PR effect of the structure: (a) effects of core yarn diameters; (b) effects of braiding yarn diameters; (c) effects of stiff yarn diameters. ....	92
Figure 5.11 Effects of the Poisson's ratio of components yarns on the negative PR	

effect of the structure: (a) effects of core yarn Poisson's ratios; (b) effects of braiding yarn Poisson's ratios; (c) effects of stiff yarn Poisson's ratios. ....94

## **List of Tables**

Table 2.1 Comparison of four textile processes. ....	25
Table 4.1 Component yarn materials used to construct samples of the structures. ....	47
Table 4.2 The details of samples for six auxetic tubular braided structures. ....	48
Table 4.3 The details of used component yarns for samples with different parameters. .....	63
Table 4.4 The details of samples with various parameter settings for structures HL. ....	64
Table 4.5 The details of samples with various parameter settings for structures R1. ....	66
Table 4.6 The photographs of three samples of the R1 structure at different critical tensile strains. ....	74
Table 5.1 The geometrical parameters in the initial state used for theoretical calculation. ....	89

## Nomenclature

### Symbol

$\nu$	Poisson's ratio	[-]
$\nu_c$	Poisson's ratio of core yarn	[-]
$\nu_b$	Poisson's ratio of elastic braiding yarns	[-]
$\nu_w$	Poisson's ratio of stiff yarn	[-]
$\varepsilon_l$	The longitudinal strain	[-]
$\varepsilon_t$	The transverse strain	[-]
$\varepsilon_c$	The longitudinal strain of core yarn	[-]
$\varepsilon_b$	The longitudinal strain of elastic braiding yarn	[-]
$\varepsilon_w$	The longitudinal strain of stiff yarn	[-]
$L$	Longitudinal length	[mm]
$\Delta L$	Change in longitudinal length	[mm]
$L_s$	Longitudinal length of the stiff yarn	[mm]
$H$	The transverse length of the braid	[mm]
$D_c$	The diameter of core yarn	[mm]
$D_b$	The diameter of elastic braiding yarn	[mm]
$D_w$	The diameter of stiff yarn	[mm]
$\alpha$	Helical angle of core yarn and elastic braiding yarn	[°]
$\beta$	Helical angle of stiff yarn	[°]
$R$	Helical radius of core yarn and elastic braiding yarn	[mm]
$r$	Helical radius of stiff yarn	[mm]
$\lambda$	Cyclic pitch of the stiff yarn	[mm]

### Subscript

0 the value of parameters at the initial state.

# CHAPTER 1 INTRODUCTION

## 1.1 Motivation of the research

Braid is a minor and yet distinctive form of textile fabric which consists of three or more flexible materials interlaced diagonally with each other. The form of braided products can be linear fabrics (ropes and cables), curved or solid fabrics (three-dimensional preforms for composites) with constant or variable cross-sections as well as fabrics of closed or open appearance [1]. By virtue of its diagonal network architecture, braided fabrics have exhibited improved dimensional stability, impact resistance, torsional integrity and energy absorption. As a result, braided fabrics, which have thousand years history, are still prevalent in various applications. However, in some specific situations currently existed braided products failed to meet the needs perfectly due to their positive Poisson's ratio values. For example, braided sutures with positive Poisson's ratio have a problem of the unsolid knot when use and could result in a secondary infection. Based on that, a thought is to tailor the Poisson's ratio of braided sutures into negative values so that the structure can expand in the transverse direction when stretched and therefore resulting a solid knot.

Materials with negative Poisson's ratio are termed auxetic materials [2] and have gained increasingly scientific interest over the past three decades due to their unique features. Besides the counterintuitive behaviour under loading, the negative Poisson's ratio also leads to the enhancement of a series of material properties, such as increased shear stiffness, enhanced fracture toughness, superior indentation resistance [3, 4], improved acoustic behaviour [5] and synclastic curvature on out-of-plane flexure [6]. Thus, it is reasonable to expect that braided products with negative Poisson's ratio may also have potential applications in civil engineering, aerospace and transportation

industries besides the medical applications mentioned before. However, in contrast to the achievement of negative Poisson's ratio in textile fibers [18, 24, 25], yarns [19, 26, 27], knitted and woven fabrics [21-23, 28, 29], the development of auxetic braid is lagging. Currently, only conventional positive Poisson's ratio braided rods have been utilized to manufacture an auxetic composite. The research and studies on developing truly auxetic braid, i.e., the braid itself exhibiting a negative value of Poisson's ratio, are still lacking. Therefore, the production of an accessible auxetic braid is needed both in academia and in industry.

## **1.2 Objectives**

Given the above, this study was aimed at developing novel kinds of braided structures exhibiting negative Poisson's ratio with the following specific objectives:

- 1). to design and fabricate the novel braided structures with negative Poisson's ratio;
- 2). to experimentally examine the negative Poisson's ratio behaviour of developed braided structures and investigate the effects of parameters on their negative Poisson's ratio behaviour.
- 3). to theoretically predict the negative Poisson's ratio behaviour of developed braided structures and analyze the effects of parameters on their negative Poisson's ratio behaviour.

With the successful completion of this study, several types of braided structures exhibiting negative Poisson's ratio will be fabricated, with their tension deformation mechanism identified and manufacturing process described. The relationships between structural parameters and Poisson's ratio can be established. On the other hand, the conducted study is helpful to the further development of various auxetic braided structures and to optimize braided structures with negative Poisson's ratio for desired performance criteria.

### 1.3 Methodology

In accordance with above specific objectives, both experimental and theoretical approaches have been adopted. A flowchart in Figure 1.1 summarizes the research methodology used to address stated objectives.

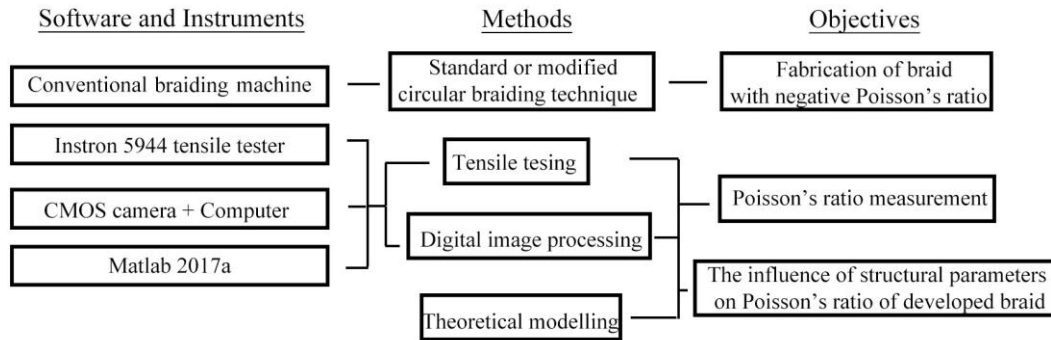


Figure 1.1 Flowchart of overall methodology.

To design and fabricate the braided structures with negative Poisson's ratio, a review of literature related to the past work in fields of Poisson's ratio, materials with negative Poisson's ratio and braiding technique was conducted. The definition, the physical significance of Poisson's ratio; the typical textile structures with negative Poisson's ratio, such as helical auxetic yarn structure [7], auxetic weft and warp knitted fabrics [8-11] and auxetic woven fabric [12-14] as well as the technique and features of braiding process and braided structures were surveyed in order to have a solid background knowledge of developing novel auxetic braids. Given above, two approaches, including wrapping or inserting extra stiff yarns onto the tubular braided structure according to specific geometry designs and employing both stiff and elastic yarns in the tubular braided structure, were employed to develop novel auxetic braids. These designed auxetic braided structures could be manufactured using a standard or modified circular braiding technology.

To experimentally examine the negative Poisson's ratio behaviour of novel braided

structures, samples produced for these structures were tested under a proper condition on an Instron 5544 Universal Testing Machine equipped with 2.5 cm x 2.5 cm face size mechanical jaws (Instron Worldwide Headquarters, Norwood, Massachusetts, USA). For assessment of the negative Poisson's ratio behaviour, an in-situ photograph system consisting of a high-resolution CMOS camera and a computer was employed at the same time. By using this system, a photograph of the tested sample was taken at every 1% elongation during the stretching process. These obtained photos were used to calculate the transversal strain of the sample at every 1% elongation. Eventually, with the calculated transversal strain and the longitudinal strain read from the tester, the Poisson's ratio of the sample can be obtained. On the other hand, to experimentally investigate the effects of parameters on negative Poisson's ratio effect, samples of two selected representative structures, which have different yarn combination and structural parameters were produced and were tested using above method.

To theoretically predict the negative Poisson's ratio behaviour of developed braided structures and analyze the effects of parameters on their negative Poisson's ratio behaviour, an analytical model was established based on the geometry relationships existed in the structure. The accuracy of the model was validated by comparing its results with the experimental data obtained in the experimental study. With the model, the Poisson's ratio of structure at any given tensile strain could be calculated and thus could be used to evaluate the influence of parameters on the negative Poisson's ratio behaviour as well as optimize the developed braided structure for desired performance criteria.

## **1.4 Thesis outline**

Chapter 2 reviews the achievements and presents limitations and gaps of earlier work

in the relevant disciplinary areas so as to present the general understanding of background. This determines knowledge gaps and identifies research objectives and significances.

Chapter 3 presents the design and fabrication of novel braided structures with negative Poisson's ratio effect. Two approaches, i.e., wrapping or inserting extra stiff yarns onto the braided structure according to specific geometry designs and using both stiff and elastic yarns in the braided structure, were employed to fabricate two types of braided structures with negative Poisson's ratio effect. The geometry, deformation mechanism and manufacturing process of these structures are introduced and described in this chapter.

Chapter 4 presents a preliminary experimental study on the developed six auxetic braids. The experimental investigation on negative Poisson's ratio behaviour of them as well as on the effects of parameters on their negative Poisson's ratio behaviour are presented in this chapter.

Chapter 5 focuses on the theoretical analysis of the developed six auxetic braids. The analytical model established in this study in order to predict the Poisson's ratio of auxetic braided structure under extension were presented and described in this chapter. The effects of identified parameters on the Poisson's ratio of the structure were discussed using the results calculated from the established model.

Chapter 6 presents general conclusions, contributions, limitations and suggestions for future work based on this study.

## CHAPTER 2 LITERATURE REVIEW

### 2.1 Introduction

This chapter reviews the literature relevant to the objectives of the study. It firstly draws upon the literature dealing with Poisson's ratio in order to give an overview of its definition and its significance in the development of materials. Following that typical textile materials and structures with negative Poisson's ratio were surveyed. The geometry features, manufacturing process and auxetic behaviour of them were highlighted. Finally, the basic features of braiding technology and braided structures are also covered so that it can serve as the background knowledge of developing tubular braided structures with negative Poisson's ratio. The purpose of this chapter is to address the research gaps between the existing literature and the primary objectives of this study and to stress the significance of conducting such a study.

### 2.2 Poisson's ratio

#### 2.2.1 Definition of Poisson's ratio

Poisson's ratio (PR), named after Siméon Denis Poisson [15, 16], is the ratio between the transverse contraction strain and the longitudinal extension strain in an elastic loading condition. Considering the sign of strains, Poisson's ratio  $\nu = -\frac{\varepsilon_{transverse}}{\varepsilon_{longitudinal}}$ .

The engineering strain  $\varepsilon$  is the change in length  $\Delta L$  divided by the original length  $L$ ,  $\varepsilon = \frac{\Delta L}{L}$ . In practice, the Poisson's effect can be easily visualized by stretching a rubber band and observing the transverse deformation, which is contraction.

#### 2.2.2 Poisson's ratio and materials' properties

Poisson's ratio is intimately connected with the way structural elements are packed

and therefore Poisson's ratio is highly related to the elastic properties of the materials [17, 18]. Based on the elasticity theory [19-21], isotropic materials with properties range from 'rubbery' to 'dilatational', from 'elastic' to 'stiff' are all contained within the small narrow numerical bounds of the Poisson's ratio  $-1 \leq \nu \leq \frac{1}{2}$ . This means materials with different value of Poisson's ratio  $\nu$  can act a very differently mechanical behaviour under the stress or tension. For example, according to the Milton map illustrated in Figure 2.1 [22, 23], rubber and most liquids which have a Poisson's ratio  $\nu \rightarrow \frac{1}{2}$ , are extremely incompressible. Slightly reduced the value of Poisson's ratio to a value of  $\frac{1}{4}$ , materials can be compressed but still stiff, such as ceramics and glasses. In contrast with that polymers are compliant and yet share a similar value of  $\nu \approx \frac{1}{3}$ . If we further reduce the Poisson's ratio to a value of near  $-1$ , materials become extremely compressible. Thus, by studying the Poisson's ratio, an intuitive concept of the mechanical behaviour of materials when exposed to a loading can be gained. On the other hand, the physical significance of the Poisson's ratio is not only existed in its relationships with the elastic properties but also remained in its influence on other properties, including densification [24], connectivity [25], ductility [26, 27] and wave speeds. As a result, researcher has reconsidered the roles of Poisson's ratio recently and attempted to develop novel materials and structures with desired properties by tailoring the magnitude of the Poisson's ratio.

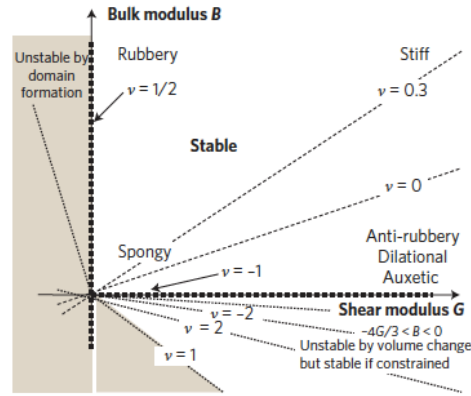


Figure 2.1 Interrelations between Poisson's ratio and elastic properties [22].

### 2.2.3 The positive side of being negative.

Poisson's ratio of any value within the thermodynamically admissible domain may be attained in materials and structures. Especially for those materials and structures with negative PR (termed auxetics [2]), they have gained increasingly scientific interest over the past three decades due to their counterintuitive behaviour under tension, i.e., they tend to be expanded when stretched and contract when compressed (Figure 2.2). At the same time, this behaviour has provided them with a unique synclastic curvature on out-of-plane flexure and a series of enhanced material properties, such as enhanced acoustic behaviour [3] and superior indentation resistance [3, 4], higher energy absorption [5] and increased shear stiffness [28], compared to conventional positive Poisson's ratio ones. Figure 2.3 illustrates the different reaction between non-auxetic materials and auxetic materials when an object was hitting on them. These special features have opened up broader commercial exploitation routes of auxetic materials and structures and auxetics may have potential applications in sportswear, filtration materials, artificial vascular, fasteners [29], etc. Therefore, tremendous efforts have been made in finding, fabricating and studying materials and structures with negative PR in the past 30 years [3-5, 7-9, 11, 12, 18, 23, 28-106]. In the following sections, the auxetic materials and structures in the textile field will be reviewed as the braid is

one of the textile structures manufactured from textile techniques.

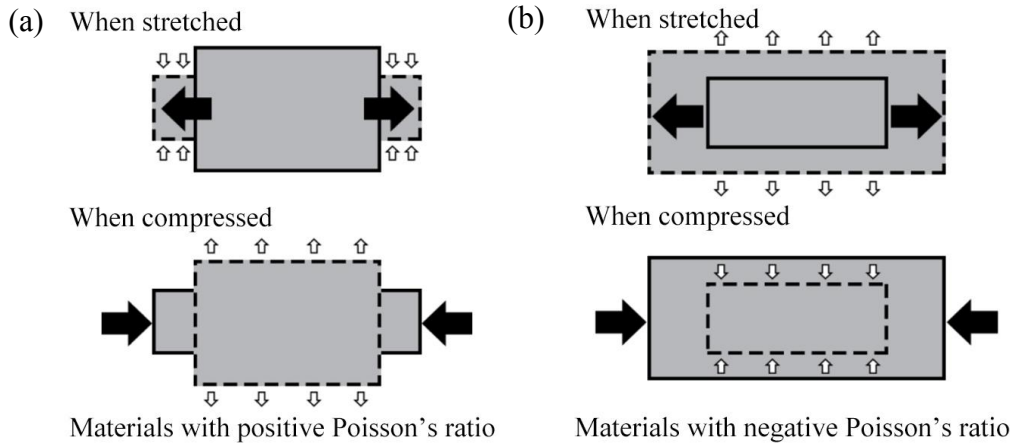


Figure 2.2 The schematics for the deformation of 2D materials under uni-longitudinal load: (a) materials with positive Poisson's ratio; (b) materials with negative PR.

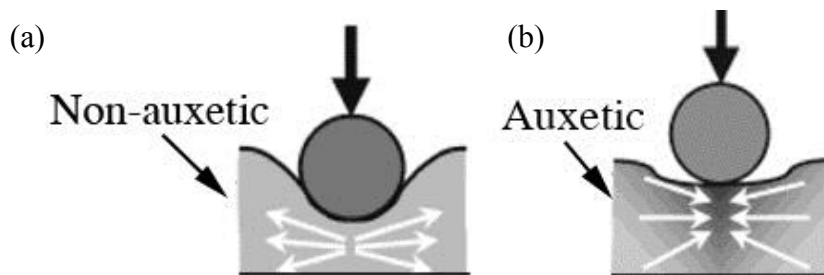


Figure 2.3 When an object was hitting on the material: (a) a non-auxetic material immediately flows away in the lateral direction; (b) an auxetic material flows into the region of the impact rather than flow away [99].

## 2.3 Textile materials and structures with negative PR

### 2.3.1 Auxetic fibers

The development of auxetic textile materials and structures started around fifteen years ago and began with the fundamental blocks of the textile, i.e., the fibers. In 2002, by using a continuous partial melt extrusion technique, Alderson et al. [96] firstly produced polypropylene fibers with a Poisson's ratio low to -0.6 (Figure 2.4a). After that, other auxetic polymeric fibers, such as auxetic polyester fibers and polyamide

fibers [41] were invented and developed using the same manufacturing and production method. Based on the video-extensometer and micro-tensile testing, the Poisson's ratios of them were found to be in a range of  $-0.15 \leq \nu \leq -0.75$ . Figure 2.4b compares the Poisson's ratio between auxetic polyester fibers and conventional positive Poisson's ratio polyester fibers.

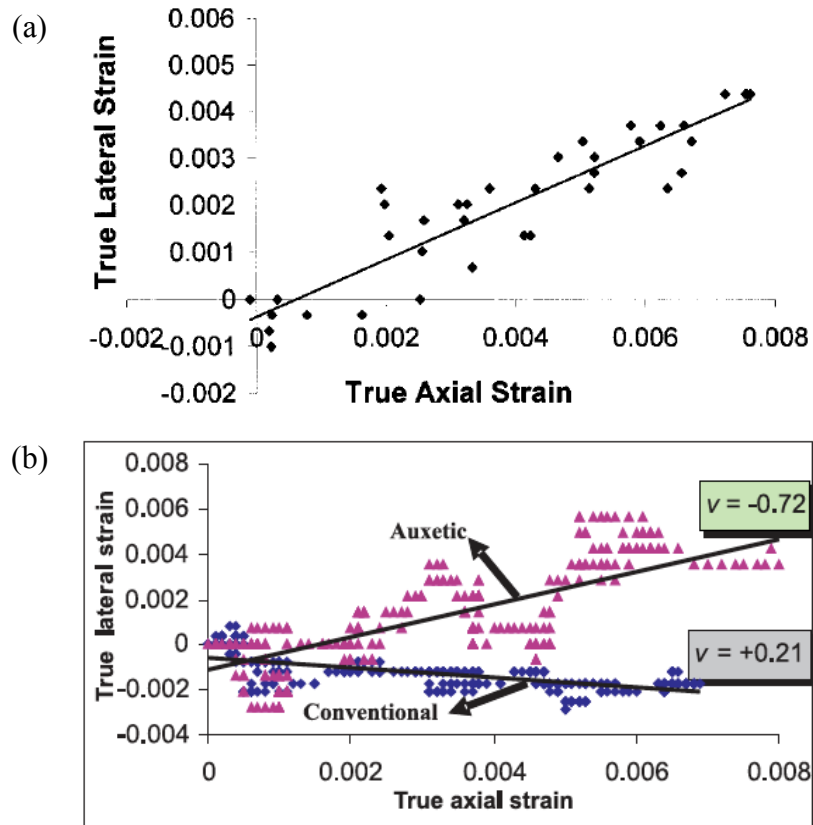


Figure 2.4 The Poisson's ratio of auxetic fibers: (a) auxetic polypropylene fibers; (b) auxetic polyester fibers and conventional positive Poisson's ratio polyester fibers.

According to the study conducted by Caddock and Evans [63], it was believed that the negative PR of these auxetic polymeric fibers originates from the nodule-fibril network structure existing in expanded polymeric powders. As shown in Figure 2.5a, this nodule-fibril network structure is formed by a semi-infinite regular array of rigid rectangular nodules interconnected by fibrils, of which highly ordered (i.e., crystalline) material are consisted. When stretched the hinging of fibril part will cause the nodule

translation, resulting in an opening of the structure and negative PR (Figure 2.5b). In this theory, it is important to obtain fibrils that are long enough to be able to work cooperatively with the nodules to produce the auxetic effect.

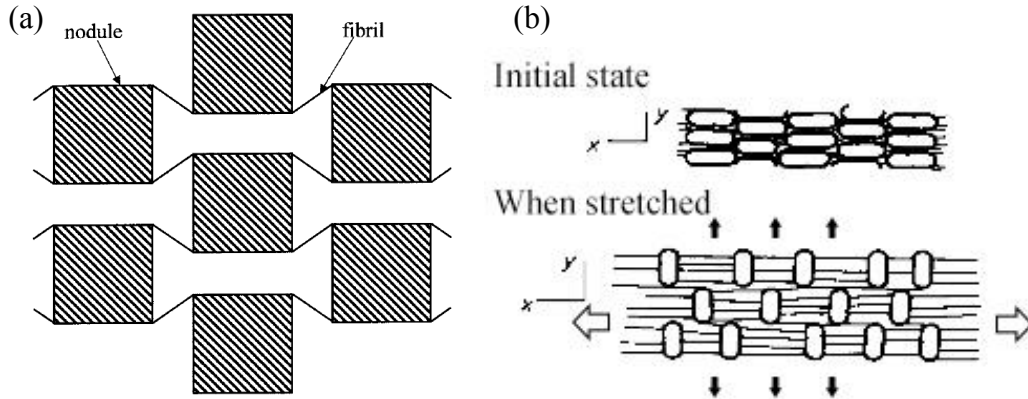


Figure 2.5 Nodule-fibril network structure in auxetic fibers: (a) schematic diagram of nodule-fibril model in the polypropylene polymer [96]; (b) expansion of nodule-fibril under tension [63].

On the other hand, Ravirala et al. develop an analytical rough particle model based on a structure of interlocking rigid hexagons in order to analyse the mechanism that is responsible for the auxetic manner and the negative PR of these fibers. As shown in Figure 2.6, the basic geometry in this theory is constructed by two kinds of the curved contact in trimers; one is the rectangular female keyway between two adjacent small discs and the other is a rectangular male key between three discs on the hexagon edge. When stretched, the rectangular female keyway is ‘soft’ and thus are likely to lead to trimer rotation and translation while the rectangular male key is ‘hard’ and thus can connect each part closely. The overall deformation mechanism of them then gives rise to the auxetic manner and a negative PR. Based on that analytical model, the Poisson’s ratio of these fibers can be expressed as

$$\nu_{xy} = \nu_{yx}^{-1} = -\frac{\cos \alpha (l_2 + l_1 \cos \alpha + a)}{l_1 \sin^2 \alpha + a \cos \alpha} \quad (2.1)$$

This Equation makes it clear that when  $0 < \alpha < 90^\circ$  an auxetic behaviour is displayed in auxetic fibers with possible interlocked hexagon structures.

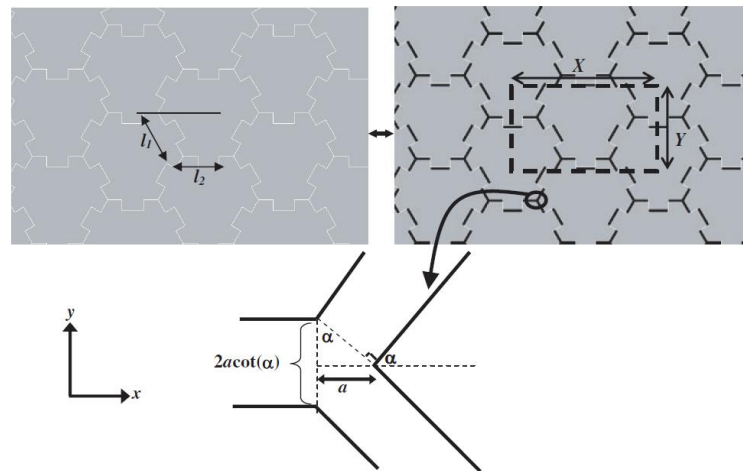


Figure 2.6 Fully densified (left) and expanded (right) hexagonal interlocked structures. The coordinate system, a unit cell (dashed box) and geometrical parameters are indicated.

Auxetic fibers are highly attractive as they can be fabricated into yarns and fabrics while the auxetic behaviour is maintained. These products then can be utilized in personal and sports protective applications [107] such as bulletproof vests, helmets and shin pads, biomedical applications [108] or medical application, such as smart wound-healing bandages, ligaments and sutures. Additionally, auxetic fibers could also play a significant role in the fiber-reinforced composite for enhanced properties, i.e., more resistance to pull the fiber out from the composites and thus preventing the failure at the fiber-matrix interface [109].

### 2.3.2 Auxetic yarns

The category of auxetic textile materials was later extended to yarns when Hook patented a novel helical auxetic yarn (HAY) exhibiting negative PR effect in 2006 [95]. As shown in Figure 2.7a, this yarn structure is constructed by a straight elastomeric core with a stiffer fiber helically wound around it. Upon tension, the stiff fiber which

is in a helical form in the initial state would straighten and in doing so displaces the core fiber into a crimped form, resulting in an expansion of the structure in the lateral direction (Figure 2.7b). If the diameter of the stiff fiber is smaller than that of the elastomeric core, an auxetic manner then will be displayed. This auxetic deformation then was proved by the mechanic tests which showed the maximum negative PR of this yarn structure was around -2.7 when using monofilament fibers with Poisson's ratios ranging from 0.38 to 1.95.

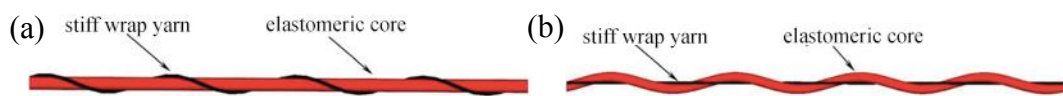


Figure 2.7 Helical auxetic yarn (HAY): (a) at an initial state; (b) at the maximum strain.

Because of its significant auxetic behaviour under tension, HAY has gained extensive scientific attention since it was reported. The geometrical parameters of it were defined by Sloan et al. [7], as shown in Figure 2.8. Five parameters, i.e., the initial diameters of the stiff wrap fiber and the elastomeric core,  $D_w$  and  $D_c$ ; the effective diameter of the yarn structure  $D$ , the initial wrap angle  $\theta$  and the cyclic pitch of the stiff fiber  $\lambda$ , were selected to define the circular cross-section of the structure and the cyclic frequency of the stiff wrap fiber. Among them, three parameters ( $D_w$ ,  $D_c$  and  $\theta$ ) were later found to have an influence on the auxetic behaviour of the HAY structure. Based on the study conducted by Zhang et. al [73], it is believed that a higher core/wrap diameter ration and a lower initial wrap angle can produce a larger maximum negative PR value in the HAY structure. On the other hand, by conducting a numerical study on HAY structure, Wright et. al [84] reported that the auxetic behaviour of this structure as well as its tensile properties were also highly related to the stiffness of used component fibers. In that manner, there existed a certain value of

stiffness ratios between used component fibers, below or above which could reduce the auxetic behaviour of the whole yarn structure. Figure 2.9 demonstrates a typical Poisson's ratio – strain curve of HAY structure.

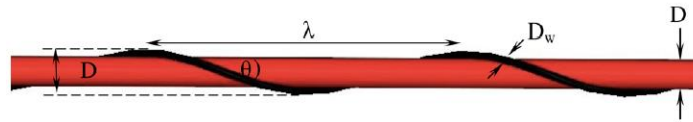


Figure 2.8 Geometric definitions of a helical auxetic yarn [7].

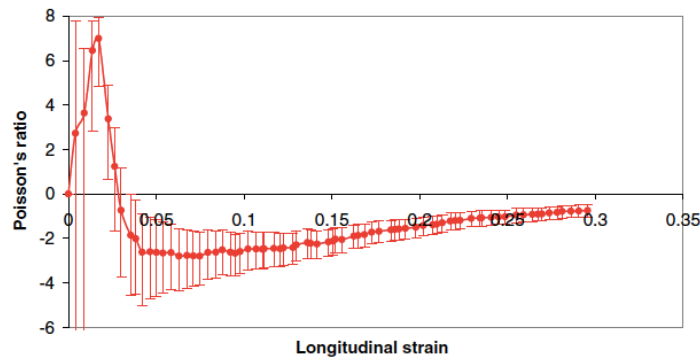


Figure 2.9 Poisson's ratio – strain curve of HAY structure with an initial wrap angle of 13° [7].

The successful of HAY structure well indicated that it is possible to manufacture auxetic yarns with components exhibiting a positive Poisson's ratio and inspired the development of other auxetic yarns structures.

Another auxetic yarn structure constructed by two positive Poisson's ratio components is the novel plied yarn with negative PR [31], firstly developed and reported by Ge et al. in 2016. As shown in Figure 2.10a, this yarn structure is formed by placing stiff yarns and soft yarns alternatively along the longitudinal direction and twisting them together. When stretched, the stiffer components which have relatively low longitudinal extension would tend to migrate into the inside of the yarn structure and thus pushing the softer components to move out (Figure 2.10b). This migration then increases the cross-sectional size of auxetic plied yarn structure, yielding a negative

PR. The magnitude of the negative PR of the structure then is influenced by the component diameter and the twist coefficient. When stiff yarns contact with each other in the center of the structure, the structure reaches its maximum cross-sectional size and after that the Poisson's ratio of the structure starts to increase. Compared with the HAY structure, the structure developed by Ge et al. has a more uniform auxetic behaviour under tension because of its improved regularity and stableness. Furthermore, the number of component yarns in this structure is not limited to a fixed value of four but can be six or eight or even more providing the number of each type of component yarns in this structure is even, demonstrating exceptional flexibility in structural design.

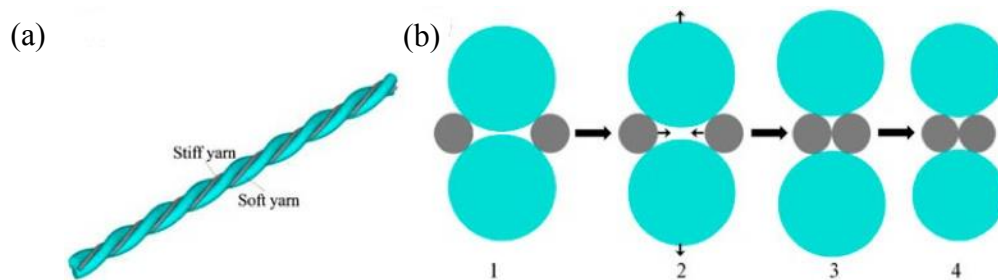


Figure 2.10 The novel plied yarn with negative PR: (a) geometry; (b) deformation mechanism responsible for auxetic behaviour [31].

In addition to the above two auxetic yarns, T.C Lim had developed an auxetic yarn structure that can exhibit positive and negative PR in two orthogonal planes. The structure is termed semi-auxetic yarn structure [77]. This structure is constructed by sewing an inextensible thin cord through an elastic fat cord in a triangular pattern, as shown in Figure 2.11a. The structural deformation shape of it under tension has two different types, as shown in Figure 2.11b. In its auxetic plane (which is the side view), the shape of the structure under tension is similar to a zigzag shape. In sharp contrast, the shape of the structure in its conventional positive Poisson's ratio plane (which is the front view) is contracted but remained same as a straight line. Varying the inserting

angles of inextensible thin cord would cause the change of shape deformation in both two planes and thus influencing the Poisson's ratio values in two planes. Compared to the auxetic yarns mentioned above, the use of semi-auxetic yarns allows very large magnitudes of positive and negative PR to be achieved at the same time and may find specific applications in practical use.

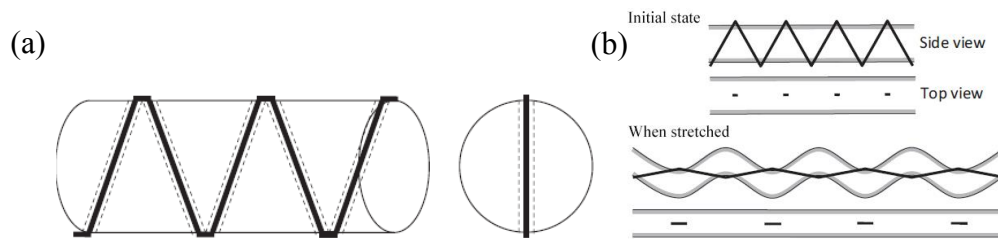


Figure 2.11 The semi-auxetic yarn structure: (a) geometry; (b) deformation mechanism responsible for auxetic behaviour [77].

### 2.3.3 Auxetic fabrics

As to auxetic fabrics, the first exploited technique is the knitting technology. By employing a method of unique unit cell geometry design, both weft-knitted and warp-knitted fabrics with negative PR have been successfully fabricated to date. In 2010, Liu et al. [8] firstly developed a folded knitted fabric based on an origami structure called Miura-origami. As shown in

Figure 2.12, this Miura-origami structure is created by arranging the face loops and back loops in a zigzag form, in which a rectangle outlines the smallest repeating unit of the pattern. To achieve that, a special knitting method called loop transfer technique is applied. Due to the imbalanced force distribution between the face loops and back loops, the fabric will curl and display an appearance as shown in Figure 2.13a. Upon stretch, the parallelogram shape in the repeating will change its inclined position related to the surface plane of the structure and the folded fabric will open (Figure 2.13b). Consequently, the dimension of the fabric is increased and a negative PR was

yielded in the fabric without changing the shape and size of the parallelograms. Totally, three types of fabric with different unit sizes, including 12 courses 12 wales (C12-W12), 12 courses 6 wales (C12-W6) and 6 courses 6 wales (C6-W6), were fabricated on a 14G STOLL flat knitting machine. Both the experiment and theoretical calculation confirmed that an auxetic behaviour was displayed in all fabrics. Figure 2.14 presents the Poisson's ratio-strain curves of all produced fabrics.

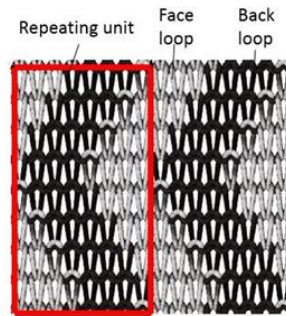


Figure 2.12 Fabrication method of auxetic knitted fabric with a zigzag arrangement

[8].

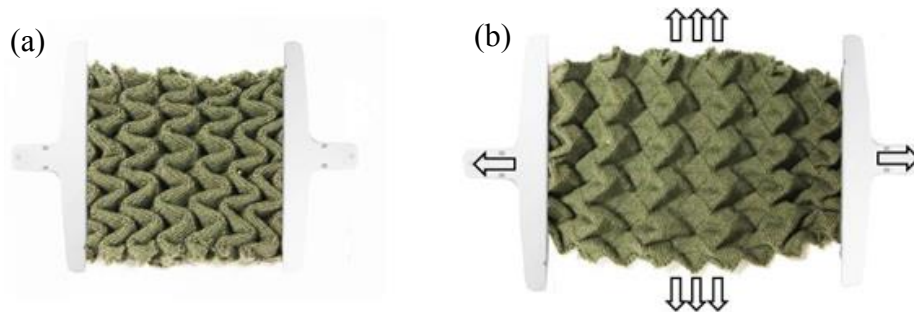


Figure 2.13 Auxetic knitted fabric with a zigzag arrangement: (a) initial state; (b)

when stretched [8].

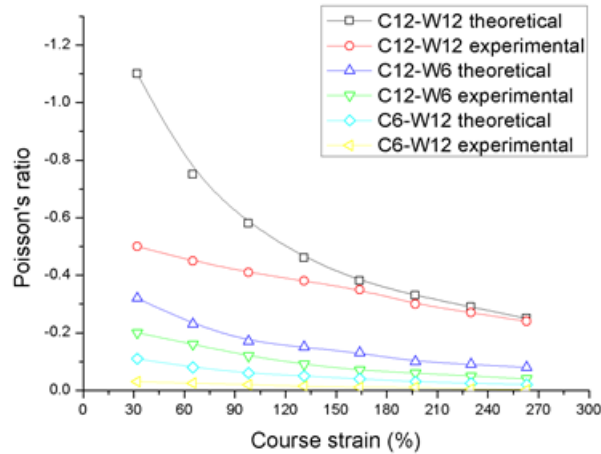


Figure 2.14 The Poisson's ratio-strain curves of produced auxetic knitted fabric with a zigzag arrangement [8].

Later on, by employing the same geometry design but a different fabric form, Boakye et al. [110] fabricated various weft knitted auxetic tubular fabrics using nylon, PES and cotton yarns. A negative PR was exhibited when fabrics were made of nylon and cotton yarns.

In addition to the zigzag arrangement of the knitted loops, Hu et al. [9] also produced folded auxetic fabrics with other two arrangements by using conventional yarns, i.e., with a rectangular arrangement (Figure 2.15a) and a horizontal and vertical stripes arrangement (Figure 2.15b). Same to the fabric knitted with the zigzag arrangement, produced two fabrics have a folded form at the initial state and are extended to a larger dimensional size when stretched (Figure 2.16). For fabric with a rectangular arrangement, this the expansion only occurs in the course direction and thus no negative PR effect was obtained in wale direction. Meanwhile, the fabric with a horizontal and vertical stripes arrangement has auxetic effect when it is stretched in both the course and wale directions.

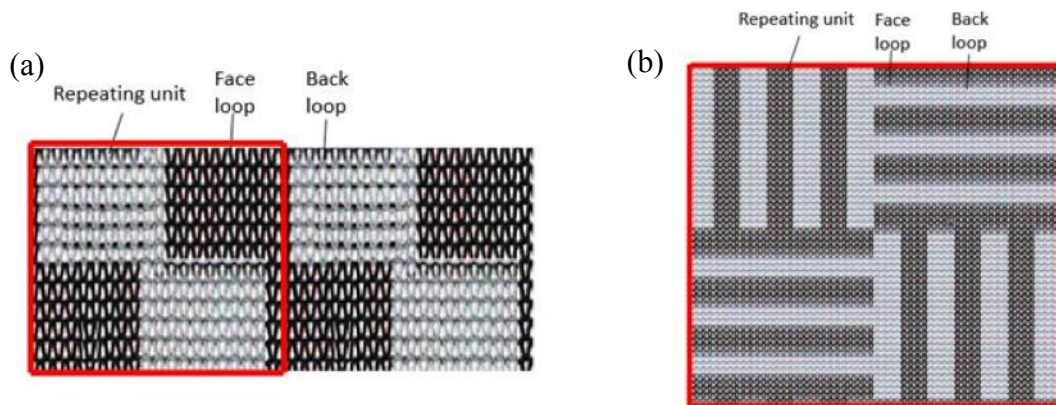


Figure 2.15 Fabrication method of auxetic knitted fabric: (a) with a rectangular arrangement; (b) with a horizontal and vertical stripes arrangement [9].

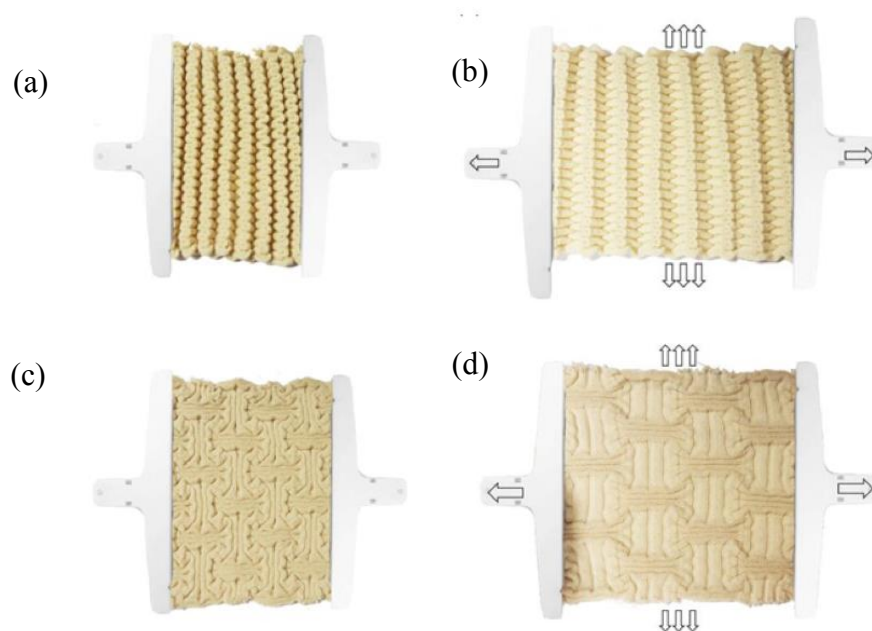


Figure 2.16 Auxetic knitted fabric with a rectangular arrangement: (a) initial state and (b) when stretched; Auxetic knitted fabric with a horizontal and vertical stripes arrangement: (c) initial state and (d) when stretched [9].

Other auxetic geometries, such as rotating rectangles, re-entrant hexagonal structure [9], double arrowhead [11, 111], etc. [10, 112, 113], had also been utilized by researchers to manufacture weft or warp knitted auxetic fabrics. The same approach, which is to arrange the loops in the repeating unit according to the selected auxetic geometry via a special knitting method, was used. The Poisson's ratio of them mainly

ranges between  $-0.1$  to  $-3.0$ . The primary advantage auxetic knitted fabrics are that they have superior shape fitting ability compared with the conventional positive Poisson's ratio fabric and thus are ideal for sportswear or maternity wears [78].

Differ from the knitting technology, the weaving technique has been employed in manufacturing auxetic woven fabrics in two ways. The first method is to utilize the auxetic yarns and interlaced them into a woven fabric. By using this method, both HAY and auxetic plied yarn structures mentioned above has been successfully made into auxetic woven fabrics [12, 14]. The photograph of auxetic woven fabrics made by them is presented in Figure 2.17. As these fabrics can be manufactured using simple woven patterns, i.e., plain weave, there a few technical barriers to produce them. However, since the auxetic behaviour of the fabric is inherited from used yarns and strongly influenced by the yarn arrangements, the magnitude of the negative PR of them are not high, which may limit their applications.

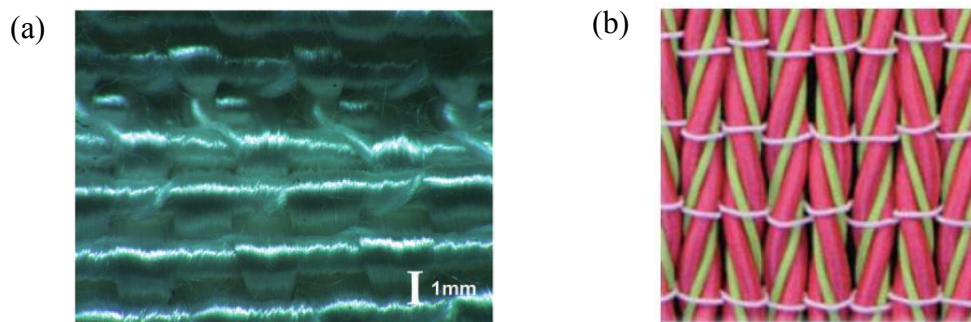


Figure 2.17 The photograph of auxetic woven fabrics: (a) made from HAY yarn [12]; (b) made from plied yarn with negative PR [14].

The second method is to utilize the conventional positive Poisson's ratio yarns and interlaced them in a specially designed woven pattern. Up to the present, one auxetic woven fabric has developed via this method and it was proposed by Adeel et al. in 2017 [13]. In this developed fabric, they used both elastic yarns and non-elastic yarn

with positive Poisson's ratio and interlaced them with combinations of loose and tight woven patterns so that a differential shrinkage effect was realized on the fabric smallest repeated units. This differential shrinkage phenomenon then would cause yarns to be arranged in a geometry shape which could yield negative PR. Figure 2.18 presents the fabric with a zigzag geometry shape. By using this approach, they have developed five types of auxetic woven fabrics with different geometry shapes, i.e., the fabric with parallel in-phase zig-zag folded geometrical shape, the fabric with oblique folded geometrical shape, the fabric with folded abrupt convexities geometrical shape and the fabric with rotating rectangle geometrical shape and the fabric with re-entrant hexagon. All of them presented an auxetic manner under tension with a maximum negative PR measured around  $-1$ . The Poisson's ratio versus longitudinal strain for all developed auxetic woven fabric is presented in Figure 2.19.

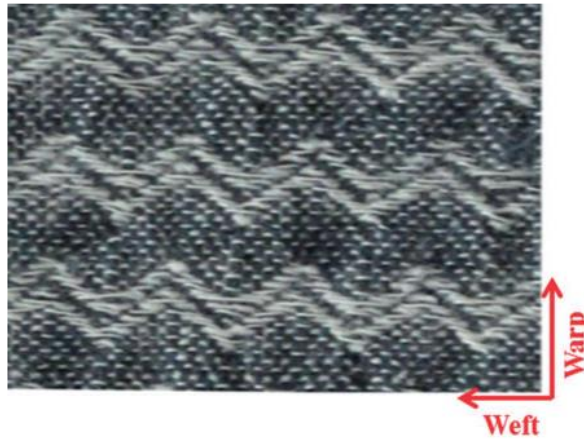


Figure 2.18 The auxetic woven fabric with a zigzag geometry shape [13].

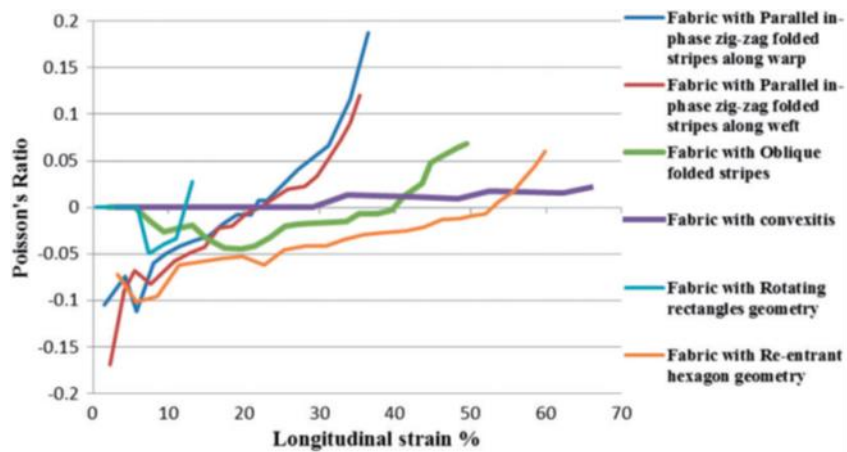


Figure 2.19 The Poisson's ratio versus longitudinal strain curve for developed auxetic woven fabrics with different geometry settings [13].

Besides the woven and knitting, non-woven technology was also exploited in developing auxetic textiles [75]. Figure 2.20 illustrates the approach employed by Verma et al. in order to induct out-of-plane auxetic behaviour in needle-punched nonwovens. The method they used is heat-compression protocol, which consists of treating the commercial non-woven fabrics with high compression in the thickness direction and heat-set process with a temperature chosen to be on the lower edge of the glass transition temperature of the component fibers. Through these two steps, it was believed that inclined fiber bundles were created along the fabric thickness directions (Figure 2.21) which are responsible for the auxetic manner of the fabric

when stretched. The negative PR of it can be as low as -7 according to the tests. Later on, Verma et al. [114] further examined the effect of temperature, pressure, and time on the magnitude of auxetic response in post manufacture-processed fabrics. The results showed that temperatures around and above the glass transition temperature, higher pressure and longer duration of treatment are likely to produce a larger auxetic effect in developed nonwoven fabrics.

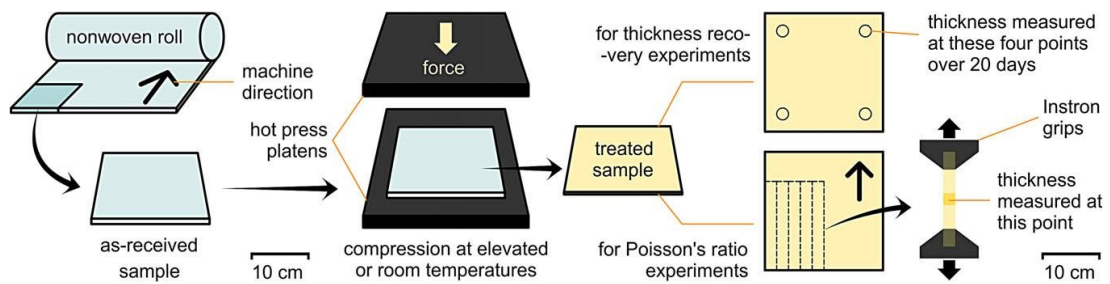


Figure 2.20 The approach of producing auxetic non-woven fabric [75].

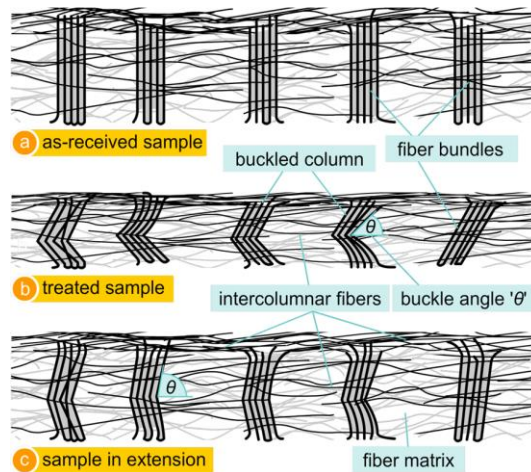


Figure 2.21 The schematic of buckled fibers responsible for producing auxetic behaviour in auxetic non-woven fabric [75].

Recently, Subramani et al. have attempted to exploit braiding technology in manufacturing the auxetics. The approach they used is to assemble braided rods with positive Poisson's ratio in an auxetic configuration so that the constructed composite could exhibit a negative PR when stretched. [70, 71, 79]. In order to prevent the possible deconstruction, epoxy resin and polyester filaments were utilized to glue the

braided rods together and to tie the cross-over points firmly. Up to the present, two types of auxetic composites with different auxetic configurations, one with a missing rib configuration and the other with a re-entrant honeycomb configuration, has been successfully manufactured by them. The photographs of these two types of auxetic composites are presented in Figure 2.22. It was reported that all produced auxetic structures, including five ‘missing rib’ types and three ‘re-entrant honeycomb’ types, had exhibited negative PR in the testing. The negative PR of these samples ranged from the lowest -0.5 to the highest -9.0. It was found that the structures with ‘re-entrant honeycomb’ types are likely to present a larger maximum negative PR compared with those with ‘missing rib’ types as the maximum value tested them was -9.0 and -5.2 respectively. The probable reason for that is the re-entrant honeycomb could result in a larger lateral deformation under tension and thus yielding a larger negative PR.

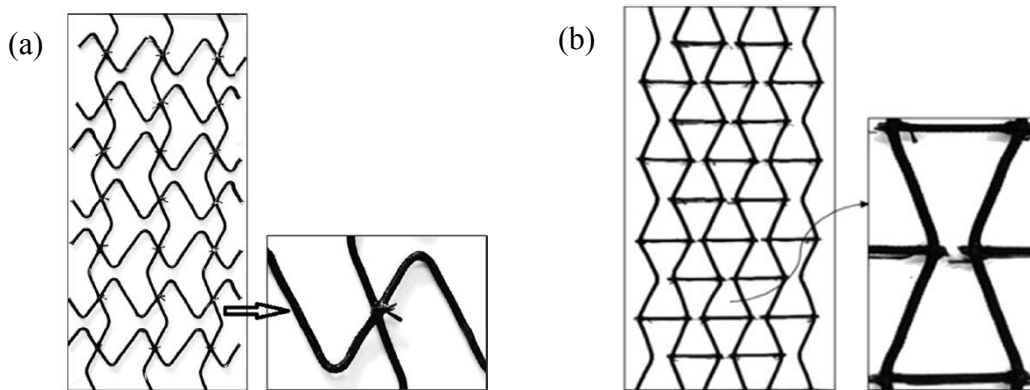


Figure 2.22 Auxetic composite based on non-auxetic braided rods: (a): with missing rib’ geometry [79]; (b) with ‘re-entrant honeycomb’ geometry [71].

### 2.3.4 Research gaps

With the above review, it can be seen that auxetic effect has been successfully achieved in fibers, yarns, both weft and warp knitted fabrics, woven and non-woven fabrics but not yet in braided fabrics. Despite the attempt of utilizing non-auxetic braided rods in

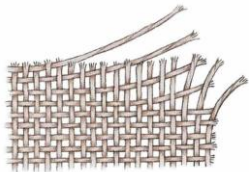
manufacturing an auxetic composite, no auxetic braided structures have been proposed and developed yet. The relevant research on the design and fabrication, the deformation behaviour, the properties and the influential parameters of braided structures with negative PR was lacking.

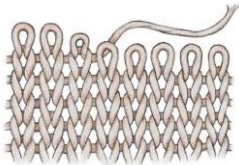
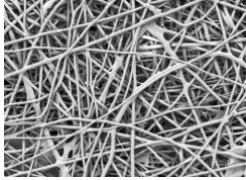
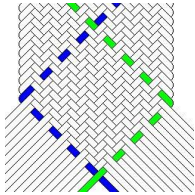
## 2.4 Braiding technology and braided structures

### 2.4.1 The definition of braiding

Braiding, an ancient textile manufacturing technology, has been existed for thousands of years [115, 116]. Traditionally, it has been used to produce items like ropes, shoelaces, and cables but also found great potential applications in the fields of medical, aerospace, transportation recently. According to the definition given by Encyclopedia Britannica , “braiding” in textiles can be described as a machine or hand method of interlacing three or more yarns or bias-cut cloth strips in such a way that they cross one another and are laid together in diagonal formation, forming a narrow strip of flat or tubular fabric. Compared with the other three classical textile processes, i.e., weaving, knitting and nonwoven, braiding is distinctive as it employs a fabric-processing method of intertwining instead of interlacing (for weaving), interloping (for knitting) and interlocking (for nonwoven fabrics). Table 2.1 compares the principle differences between these four textile processes and formed textile structures.

Table 2.1 Comparison of four textile processes.

Textile Process	Yarn direction	Formation techniques	Its structure
Weaving	Two sets of yarn (0° warp and 90° weft)	Interlacing	

Knitting	One set of yarn (0° warp or 90° weft)	Interloping	
Nonwoven	Randomly arranged fibers	Interlocking	
Braiding	Two sets of yarn (along with machine direction)	Intertwining	

#### 2.4.2 History of braiding technique

The oldest form of braiding was plaiting of human hair known as “Cornrow” [117]. A three-strand hair braiding process is presented in Figure 2.23 From A to F indicates the process to braid a three-strand hairstyle. In that hair plaiting, people picked up three groups of hair and interlaced them in zigzag forward through the overlapping mass of the others, resulting in an intertwined architecture which is typically braided structure. Later on, the same mechanism of hair plaiting was applied to the production of some useful tools, such as ropes and baskets, and braiding technology began to play an essential role in human life. At that time, the materials used in braided products were mainly depended on the indigenous plants and animals that are available in the local area and the hand-braiding dominated the braids production. Therefore, the structures of braided products cannot be very complex but simple while the quantity of these products is limited. This situation lasts a long period until the Industrial Revolution arrived. With the development of an amazingly broad and deep wealth of engineering inventions, complex braided structures such as lace braid [118], cord [119] and cables [120] can be produced on a large scale.

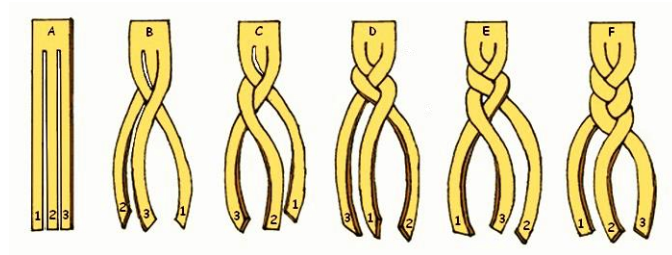


Figure 2.23 From A to F indicates the process to braid a three-strand hairstyle.

To these days, virtually any fiber with a reasonable degree of flexibility and surface lubricity can be economically braided. Typical fibers include aramid, carbon, polypropylene, ceramics, and fiberglass, as well as various natural and synthetic fibers and thermoplastics. The forms of braids are not limited to ropes or wires anymore but vary as reinforcement composite matrix for aircraft propellers, the covering for fuel pipes, and sutures used in medical surgery by using advanced braiding technologies.

### 2.4.3 Three primary braided structures in textile

In general, there are three kinds of braided textile structures are widely used in costumer and industrial markets, which are tubular braids, flat braids and 3D braids.

The tubular braided structure, also referred to as “round” or “circular” braid, is a fibrous cylindrical shell consisting of two sets of bias yarns. As shown in Figure 2.24a, these two sets of helical yarns in the structure are in opposite sense, one along the clockwise direction and the other along the counter-clockwise direction. Member yarns of the same set travel in concurrent paths and intersections only occur with members of the opposite set. In practice, ropes are typical products with a tubular braided structure.

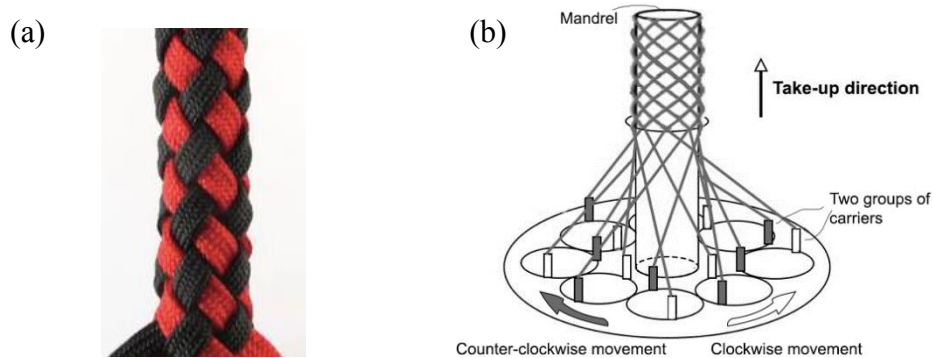


Figure 2.24 Tubular braid: (a) geometry; (b) the manufacturing process.

The specific technique used to produce tubular braided structures is called circular braiding technology. The principle of it is to arrange two groups of yarns around a closed serpentine circle and intertwining them in pairs. As shown in Figure 2.24b, two sets of yarns are placed on two groups of carriers and move along two serpentine tracks during the fabrication process, one move in a clockwise direction and the other moves in counter-clockwise. As carriers go over or under the others at the intersection area of the tracks, the interlacements between two sets of yarns are facilitated. After all carriers finish a complete circular movement, one geometry unit of the tubular braid can be obtained. In case of over braiding of profiles with carbon or glass fiber composites for, cables and high-pressure ropes, an extra mandrel will be added inside of the structure in order to support the formed tubular shape.

Differ from the tubular braids, flat braids are of ribbon-shaped braid structures, as shown in Figure 2.25a. The technology used to produce it is flat braiding technique. The major difference between flat braiding technique and circular braiding technique existed in the track they used. Unlike the spiral closed track in the circular braiding, flat braiding technique employs an open spiral track. This type of track requires intertwining sets of yarns reverse their movements at the edges and travel back in the

opposite direction, as shown in Figure 2.25b. As a result, the shape of the structure is not a closed circular shape but is a flat selvage shape.

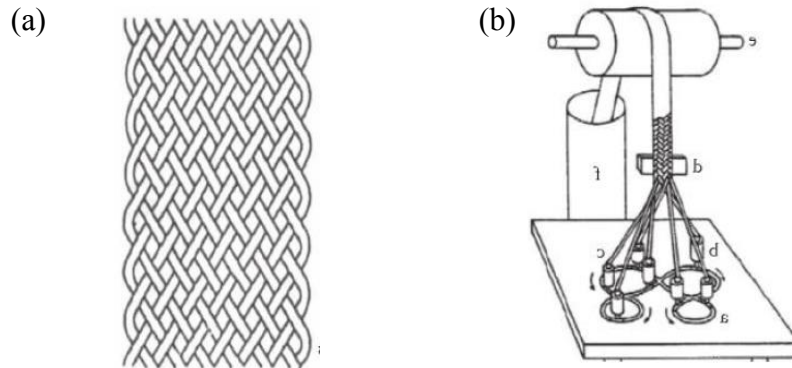


Figure 2.25 Flat braid: (a) geometry; (b) the manufacturing process [121].

For both tubular braid and flat braid, the special intertwining effect of yarns provides the structure with a unique deformation when longitudinally extended or compressed. When stretched, the structure is capable of substantial accommodation of strain because the initially inclined yarns are free to pivot to a position that is more parallel to the direction of the tension. As the braid extends, its diameter decreases until the fabric reaches a point of maximum packing density, called the tensile or extensive jamming point. Conversely, when compressed, the braid is forced to contract in length and its component yarns will re-align more perpendicular to the direction of the stress. During the process, the diameter of the braid would increase until reaches the compressive jam point. The extensive and compressive jamming are simple observances of the physical law of non-penetration of solids. This unique deformation has enabled tubular braid and flat braid to be used in applications where excellent strength at the extension is required; for example, the ropes and the shoelaces. Meanwhile, as the structure flat braids are denser and more durable compared with tubular braids, they are often used as a strong flexible connection between large components while tubular braids are widely used in shielding purpose.

In contrast to the mentioned two 2D braided structures, 3D braids are produced by a modified braiding machine with multiple concentric circular tracks [122]. The multiple concentric circular tracks consist of several inconstant tracks which could lead yarns to move through the braids thickness, resulting in interconnections of yarns in three directions. By virtue of it, 3D braids present an excellent toughness and an improved delamination resistance than 2D braids [121]. Therefore, 3D braids are widely used in fiber-reinforced composites and 3D integrals. Figure 2.26 presents the 3D braids used for reinforcement of the bicycle body and the rotary braiding method for producing 3D braids.

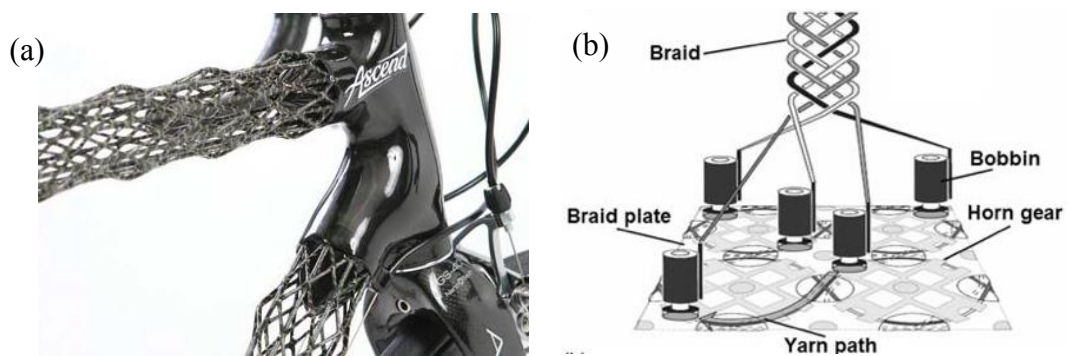


Figure 2.26 Three dimensional (3D) braids: (a) application in the reinforcement of bicycle body; (b) production process (rotary braiding method) [123].

#### 2.4.4 Braid geometry

Knowledge of the geometry of braid is critical to the structure and property analysis. Figure 2.27 demonstrates a typical braided geometry, which consists of braiding axis, stitch ( $S$ ), Line ( $L$ ) and braiding angle ( $\theta$ ).

As it can be seen from the Figure 2.27, the braid axis is a straight line along which braids was fabricated. In most cases, the braid axis is vertical to the horizontal plane

but can be parallel to the horizontal plane in producing some 3D braids. Stitch ( $S$ ) is a geometry term to characterize the length of one repeat of the structure along the braid axis. In contrast with that, Line ( $L$ ) characterizes the length of one repeat of the structure perpendicular to the braid axis. The number of it is same with the number of intertwining yarns in braided structure (in case of one carrier correspond with one yarn). By using these two parameters, another geometry parameter in braided structure can be derived, which is the angle between the yarns and braid axis called braiding angle. This parameter is critical important as it intuitively presents the features of the braid. As the value of it is highly related to preference systems, such as the radius of braiding platform, taking up speed, the speed of carrier movement, etc., this parameter is also widely used by engineers to change the machines settings for desired performance criteria.

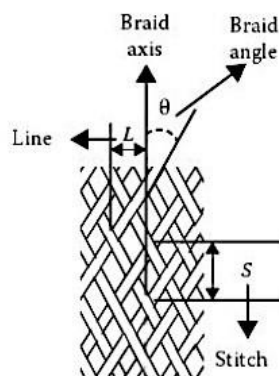


Figure 2.27 Geometry of braided structure [124].

#### 2.4.5 The advantage of auxetic braided structures

Braided fabrics have several unique features which distinguish themselves from other types of fabrics and make them popular. One of them is the unique network architecture formed by the diagonal interlacing of yarns. By virtue of this diagonally net effect, braided fabrics have exhibited improved dimensional stability, impact resistance, torsional integrity and energy

absorption compared with other types of textile fabrics [3]. In addition to that, as braiding is one of the most flexible and cost-efficient processes to fabricate a thicker, wider or stronger product from yarns or fibers, braided fabrics can be manufactured using various types of yarns with the least preparatory process [4], which offers a possibility to produce auxetic fabrics with different materials in a lower cost. Moreover, there exist numerous types of patterns and structures, including the mentioned tubular shape, flat shape and complex 3D shapes, which make the auxetic effect feasible on braided fabric through different structural designs. On the other hand, inducing auxetic behaviour in the braided structure is also useful and meaningful because it can provide an innovative and feasible approach to overcome the previous problems in braided fabrics; for example, the knot of non-auxetic braided sutures cast off easily in use. Finally, virtually any fiber with a reasonable degree of flexibility and surface lubricity can be economically braided which remove the technical barrier in the selection of component positive Poisson's ratio yarn when design and fabricate braided fabrics with negative PR.

## **2.5 Conclusions**

This chapter has reviewed the literature related to this study, including Poisson's ratio, auxetic materials and structures as well as the braiding technology and braided structure. It has been shown that being negative gives an improvement on mechanical properties of materials and has been successfully applied into a wide range of textile products recently, such as fibers, yarns, knitted and woven or nonwoven fabrics. Whereas the non-auxetic braided rods have been utilized in manufacturing auxetic structures, no braided structure with being auxetic itself has been reported yet. The relevant research on the design and fabrication, the deformation behaviour, the properties and the influential parameters of braided structures with negative PR still lack currently. Meanwhile, by reviewing the braiding technology and braided structures, it can be found that it is also possible to manufacture braids with negative

PR as different yarn combination and geometry construction can be used. Since braiding technology creates a textile structure that is thicker and stronger than the non-interlaced strands of yarn, auxetic braids are believed to be useful in practical use and may tackle the common problem existing in the conventional non-auxetic braids; for example, the problem of unsolid knot in medical sutures. In this connection, to conduct a study on production and characterization of the auxetic braided structure is highly demanded in both literature and industry.

In the following chapters, the research conducted on the design and fabrication of the novel braided structures with negative PR, investigation on their negative PR behaviour under tension and evaluation of the influence of different structural parameters on their negative PR behaviour in this study will be presented.

## **CHAPTER 3 DESIGN AND FABRICATE AUXETIC BRAIDED STRUCTURES**

### **3.1 Introduction**

This chapter presents the design and fabrication of six novel auxetic tubular braided structures by using two distinguish approaches, i.e., wrapping or inserting extra stiff yarns onto the braided structure and employing both stiff and elastic yarns to construct a braided structure. Both modified and conventional circular braiding techniques were exploited to manufacture six structures. The geometry of these structures, the deformation mechanism and their manufacturing process are introduced and described in the following sections.

### **3.2 Three auxetic braids developed using the first approach.**

#### **3.2.1 Geometry design and deformation mechanism**

The first three auxetic braids were designed and constructed via the approach of wrapping or inserting extra stiff yarns onto the tubular braided structure according to the special geometry. The idea of using this design and construction method originates in the structural features of tubular braid. Considering the tubular braided structure from a macro scale, it has a strip shape where the length is significantly larger than the width, resembling a typical shape of yarn. Based on it, the idea is that the geometries designed for producing auxetic yarns, such as the helical configuration in HAY structure [7] and trapezoidal configuration in semi-auxetic yarn structure [77], could also be applied to fabricate tubular braided structures with negative PR. Consequently, it was found that wrapping or inserting extra stiff yarn(s) onto the base braided structure is a feasible method to achieve these auxetic yarn geometries on tubular braids,

Figure 3.1 demonstrates the geometry designs of three auxetic tubular braided structures. As shown in Figure 3.1a, the first structure HL is designed based on a helical geometry and is constructed by helically wrapping an extra stiff yarn onto the tubular braided structure with a core yarn inside. By virtue of the interlacement between braiding yarns, the extra stiff yarn of it is fixed by two neighboring braiding yarns at every  $90^\circ$  and thus no need for the use of glues or resin, simplifying the manufacturing process. Here, a core yarn is added inside of the braided structure in order to prevent the irregular distortion of the structure and thus could help structure achieve negative PR behaviour when stretched. In contrast to the geometry design of the first structure, the second structure HC is designed based on the trapezoidal geometry, as shown in Figure 3.1b. In this structure, an extra stiff yarn is inserted into the base tubular braid along one direction and the path of stiff yarn is close to the trapezoidal wave when seeing from the front-view. Similar to the first structure, the extra stiff yarn in HC structure is also fixed by the interlacement effect between two neighboring braiding yarns. Modified from the structure HC, the structure FC is also designed based on the trapezoidal geometry but has two extra yarns inserted into the base tubular braid along two orthogonal directions, as shown in Figure 3.1c. In order to avoid the lateral displacement caused by one stiff yarn is offset by that caused by the other yarn, the insertion points of two extra yarns in structure FC are staggered. As a result, the path of two stiff yarns in structure FC resembles two trapezoidal waves with a phase difference of  $\frac{\pi}{2}$  when see from the front-view. For both HC structure and FC structure, no core yarn is added because the use of it will break the geometry shape of stiff yarns in the structure. On the other hand, for all three structures, the cyclic pitch of extra stiffer yarn along the braid axis is set as  $\lambda$  during the geometry design

process in order to unify the design parameter.

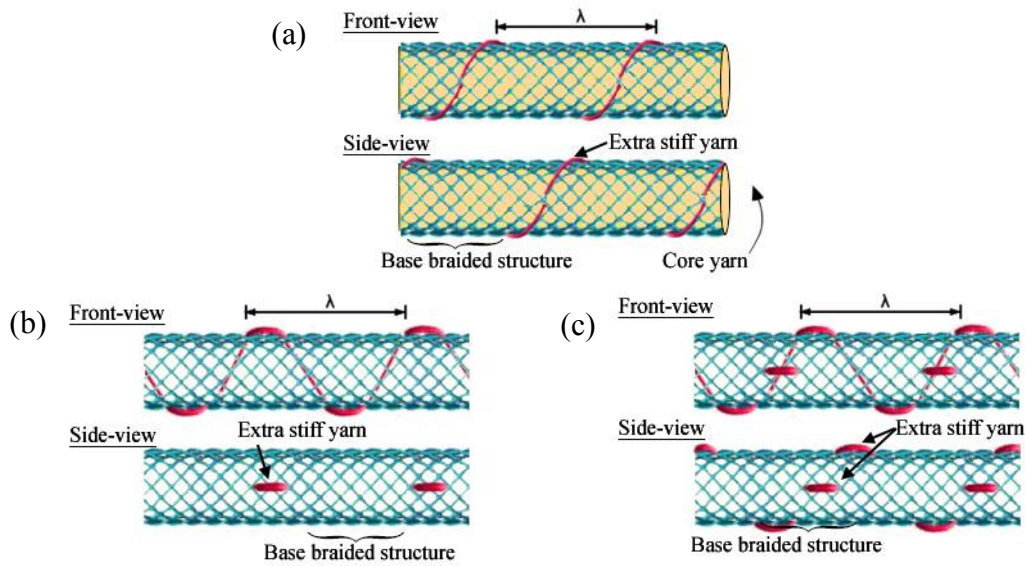


Figure 3.1 The auxetic tubular braided structures developed via wrapping or inserting extra stiff yarns: (a) HL; (b) HC; (c) FC.

Figure 3.2 demonstrates the auxetic behaviour of developed tubular braided structures HL. As it can be seen from the Figure 3.2, upon application of the stretching, the stiffer wrap yarn in structure HL would straighten and displace the base braided structure into a crimped form from the initial straight line. During that deformation process, a lateral expansion of the structure is caused and therefore cross-sectional size of the structure is increased, yielding a negative PR behaviour of the structure. The cross-sectional size of the structure then would further increase with the applying of the force until it reaches its maximum value. At that point, the extra stiff yarn is fully straightened along the center. If we continued the practice of stretching, the cross-sectional size of the structure would decrease because of the decrease in the component yarns diameters the reduction of the helical wave of braided structure.

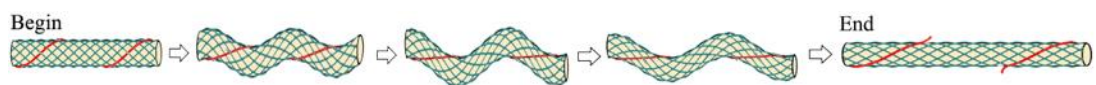


Figure 3.2 Auxetic behaviour of HL structures under tension.

Differ from the helical geometry, a trapezoidal geometry would result in another shape

deformation when stretched. As shown in Figure 3.3, in the direction where an extra stiff yarn is inserted, the shape of structure HC maintains its original shape as a straight line. Meanwhile, in the direction perpendicular to the insertion direction, the shape of structure HC is deformed to a typical zigzag shape leading to the expansion of the structure in this direction. As a result, the Poisson's ratio of structure HC measured in these two planes are expected to be positive and negative respectively, resulting in a conventional plane and an auxetic plane which are perpendicular to each other. On the other hand, as two stiff yarns are inserted alternatively into the base tubular braid along two orthogonal directions in structure FC, a double zigzag deformation in both two directions is presented in structure FC. However, the overall shape of the structure FC shall be closer to the helical shape due to the interaction between zigzag deformations in two orthogonal directions, as shown in Figure 3.4. Similar to the deformation mechanism of the structure HL, the cross-section sizes of structure HC and FC reach their maximum value when extra stiff yarn(s) is or are fully straightened along the center. Continue the stretching will decrease the cross-sectional sizes of structure HC and FC because of the decrease in the component yarns diameters the reduction of a zigzag wave of base braided structure.

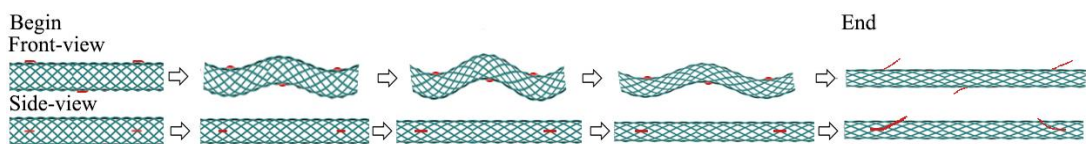


Figure 3.3 Auxetic behaviour of HC structure under tension.

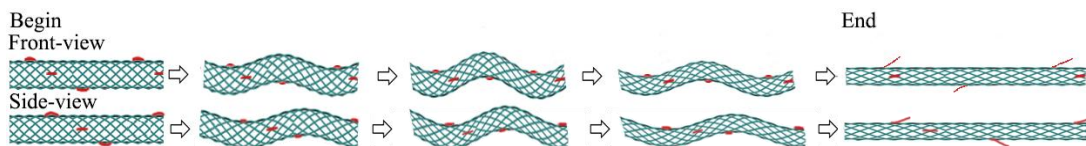


Figure 3.4 Auxetic behaviour of FC structure under tension.

Notice that there is also a reduction in the braiding angle among braiding yarns in all developed structures because the braiding yarns would become closer to each other due to the extension.

### 3.2.2 Fabrication process

To fabricate these auxetic braided structures, a special manufacturing process was developed based on the modification of a circular braiding technology. The whole manufacturing process can be realized on a conventional vertical circular braiding machine with a capability of 16 yarn carries, as shown in Figure 3.5.



Figure 3.5 The conventional vertical circular braiding machine utilized for manufacturing developed auxetic braided structures.

Figure 3.6 demonstrates the manufacturing process of structure HL. The whole process involves two steps, the formation of the base braided structure and the wrapping of the extra stiff yarn. At the initial process (Figure 3.6a), the stiff yarn is located outside of the braiding yarns at point A while the core yarn is placed in the central hole of the machine. The first step is then to form the base tubular braid around the core yarn by moving two groups of braiding yarns (eight yarns for each group) in opposite directions, one in the clockwise direction while the other group in the counter-clockwise direction. As a result, the braided structure is formed by diagonally intertwining between these two groups of braiding yarns. At the same time, the extra

stiff yarn also circularly moves from point A to point B around the base tubular braid to form a helical system (Figure 3.6b). The cyclic pitch of the stiff yarn ( $\lambda$ ) can be adjusted by changing its moving speed. The second step starts when the wrap yarn reaches point B. As shown in Figure 3.6c, in the second step, the wrap yarn will be fixed with the braiding yarns by first moving it from outside of the braiding yarns to the inside of the braiding yarns and then moving out after two neighboring braiding yarns around it making an interlacement. During the moving in and out, the movement of the braiding yarns stops. After the second step finishes, the next braiding process starts with the movement of the wrap yarn from point B to point C. Four braiding processes will be completed when the wrap yarn returns to point A and one geometry unit of the structure HL could be achieved.

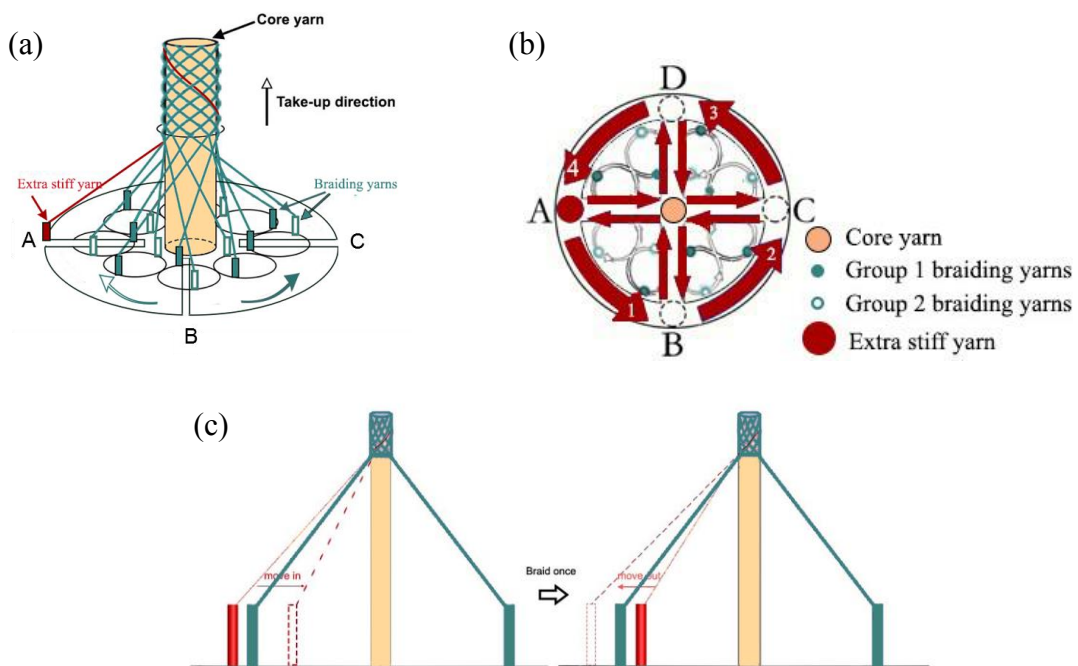


Figure 3.6 The manufacturing process for structure HL: (a) set-up of the braiding system; (b) the moving path of extra stiff yarn; (c) fixation of the stiff yarn.

Figure 3.7 demonstrates the manufacturing process of structure HC. Similar to that of the HL structure, the whole process of structure HC also involves two steps, the

formation of the base braided structure and the insertion of the extra stiff yarn. The formation process for the base braided structure is completed same as the mentioned above but the movement of extra stiff yarn is slightly different. In the first step, the stiff yarn is also located at point A and starts moving towards point C when all braiding yarns finish making an interlacement (Figure 3.7a). During the movement of stiff yarn from point A to C, the basic braiding process continues and the number of interlacements achieved during that time is determined by the required cyclic pitch of stiff yarn  $\lambda$  (Figure 3.7b). When stiff yarn reaches point C, the second step begins and all the braiding yarns would make another interlacement before the stiff yarn starts moving back towards to the point A. When the stiff yarn returns to point A, one geometry unit of the structure HC could be achieved.

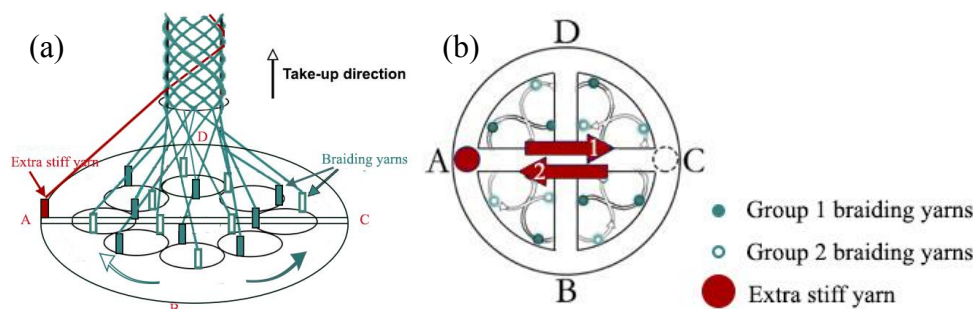


Figure 3.7 The manufacturing process for structure HC: (a) set-up of the braiding system; (b) the moving path of extra stiff yarn;

Figure 3.8 demonstrates the manufacturing process of structure FC. Modified from the manufacturing process of the structure HC, there are two stiff yarns moving along two orthogonal paths during the fabrication of the structure FC (Figure 3.8a). In the first step, the stiff yarn which is initially placed at point A would perform a movement to the point C. After it reaches the point C and one interlacement is made, it will stay a point C and starts the second step which is the stiff yarn which is initially placed at point B would perform a movement to the point D (Figure 3.8b). After the second stiff yarn reaches the point D and another interlacement was made between braiding yarns,

the reversed movement of two stiff yarns, i.e., the step 3 and step 4, begins. The process of during that period is same to the two steps mentioned above. Four steps will be completed when two stiff yarns return to the initial point A and B respectively. After that, one geometry unit of the structure FC could be achieved. Same to that of the structure HC, the basic braiding process continues during the movement of stiff yarns from point to point and the number of interlacements achieved during that time is determined by the required cyclic pitch of stiff yarn  $\lambda$ .

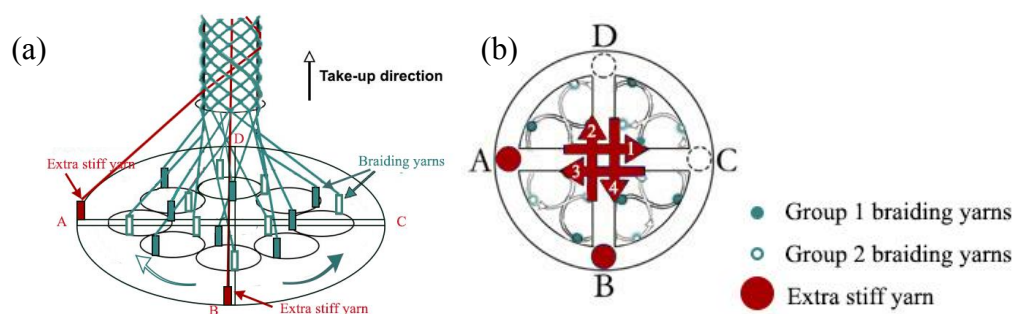


Figure 3.8 The manufacturing process for structure FC: (a) set-up of the braiding system; (b) the moving path of extra stiff yarn;

### 3.3 Other three auxetic braids developed using second approach.

#### 3.3.1 Geometry design and deformation mechanism

Differ from the first three braided structures, the braids in second group were designed and constructed via the approach of employing both stiff and elastic yarns in the tubular braided structure. This idea is inspired by the observation of the yarn path in the tubular braided structure, which is also in a helical shape. With that in mind, the thought is that elastic braiding yarn in the base braided structure may be replaced by stiffer yarn so that the stiffer yarn could straighten while the braided structure formed by the rest elastic braiding yarns could be laterally displaced, displaying a lateral expansion of the structure when stretched. In that case, a negative PR effect could be realized.

Based on the above idea, other three structures are designed and constructed. The geometry design and structural deformation of them are presented in Figure 3.9, Figure 3.10 and Figure 3.11 respectively. As shown in Figure 3.9a, the fourth structure R1 is constructed by covering a low modulus elastic core yarn with a braided sheath which is formed by one stiff braiding yarn and several low modulus elastic braiding yarns. Similar to the structural deformation of the HL structure, the R1 structure would also convert its shape from a straight line to a helical wave form (Figure 3.9b) when stretched because of the straightening of its one stiff yarn in braided sheath, yielding a negative PR effect.

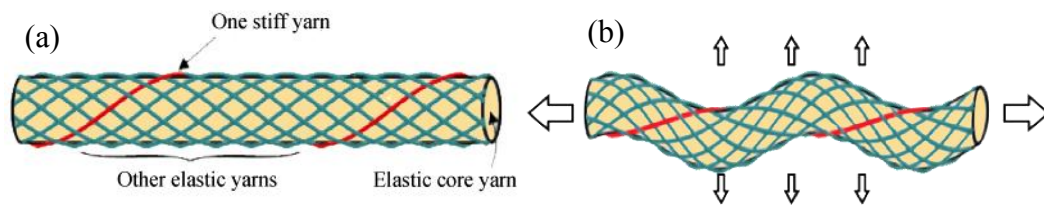


Figure 3.9 The auxetic tubular braided structure R1: (a) geometry; (b) auxetic deformation under tension.

Learning from the design process of the structure R1, another two structures R2 (Figure 3.10a) and R3 (Figure 3.11a) were developed using the same construction approach. In the geometry design of structure R2, two elastic braiding yarns moving in opposite directions are replaced by two extra stiffer yarn. Therefore, the path of the stiff yarn in the formed braided structure resembles a shape of alphabet 'X'. When stretched, despite the helical deformation caused by two stiff yarns are offset by each other, the intersecting points of two stiff would push the structure laterally and thus cause the expansion of the structure in lateral direction (Figure 3.10b). This expansion then could increase the cross-section size of the structure and yield the negative PR effect. As for the geometry design of structure R3, one more elastic braiding yarns was

replaced by extra stiffer yarn besides two elastic braiding yarns with opposite moving directions are replaced by two stiffer yarn. In that case, an extra helical deformation was caused by this third stiff yarn besides the mentioned lateral displacement mentioned above caused by other two stiff yarns when stretched, as shown in Figure 3.11b. It is designed that the third stiff yarn should be placed in the middle of other two stiff yarns in order to maximize the lateral expansion of the FC structure.

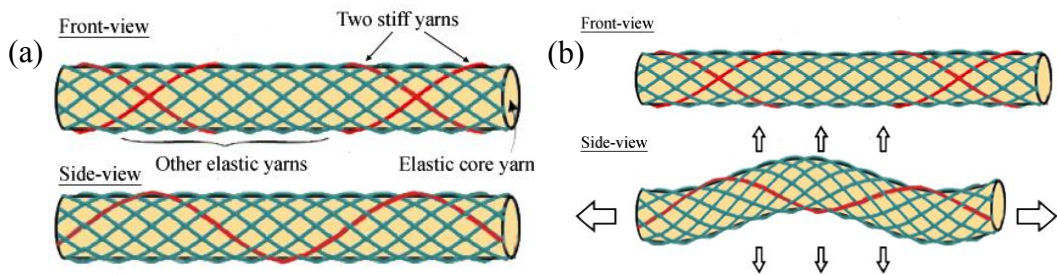


Figure 3.10 The auxetic tubular braided structure R2: (a) geometry; (b) auxetic deformation under tension.

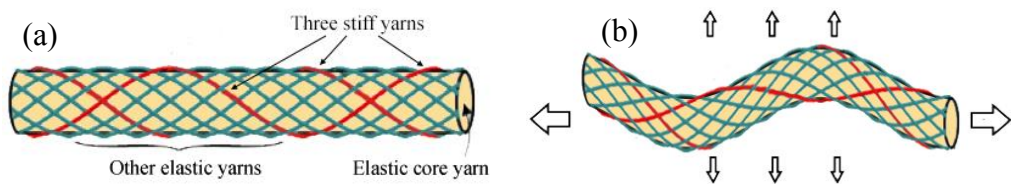


Figure 3.11 The auxetic tubular braided structure R3: (a) geometry; (b) auxetic deformation under tension.

### 3.3.2 Fabrication process

Since there is no additional wrapping process, three structures developed herein could be manufactured using a standard circular braiding technique. During the process, the same conventional vertical circular braiding machine which was shown in Figure 3.5 was used to fabricate three structures.

Figure 3.12 demonstrates the manufacturing process of structure R1. To manufacture

the structure R1, the stiff yarn was firstly mounted on one selected carrier while elastic yarns filled up the rest fifteen carries. The core yarn then was placed in the center hole of the machine. Upon rotating the machine, carriers are equally divided into two groups (8 carriers in each group) and perform two opposite circular movements as mentioned before. During the process, the stiff yarn and elastic yarns would be intertwined together to form the tubular braided structure and cover the core yarn. After all carriers finish a complete circular movement, one geometry unit of structure R1 is obtained. The same method but different yarn placement were used manufacture the structure R2 and R3. For structure R2, two stiff yarn was mounted on two selected carriers while elastic yarns filled up the rest fourteen carries, as shown in Figure 3.13. For structure R3, three stiff yarn was mounted on three selected carriers while elastic yarns filled up the rest thirteen carries, as shown in Figure 3.14. During the manufacturing process, clips with heavy weights were attached to stiffer yarns while clips with light weights were attached to the other elastic braiding yarns in order to tighten both two kinds of yarns at the same extent.

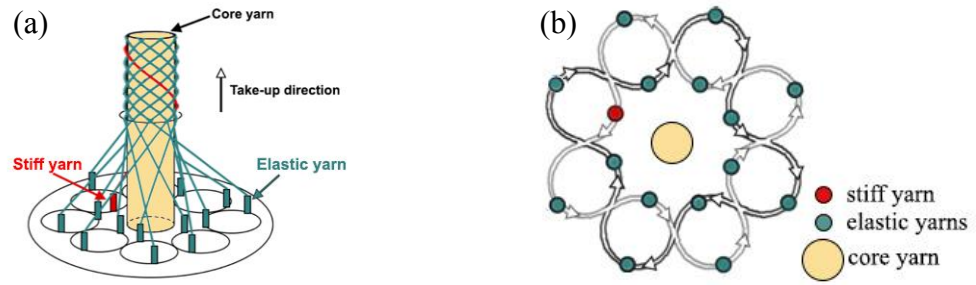


Figure 3.12 Structure R1: (a) the manufacturing process; (b) the yarn arrangement on 16 carriers.

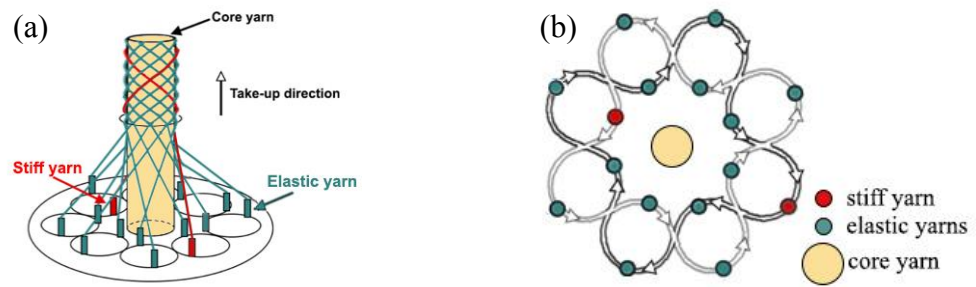


Figure 3.13 Structure R2: (a) the manufacturing process; (b) the yarn arrangement on 16 carriers.

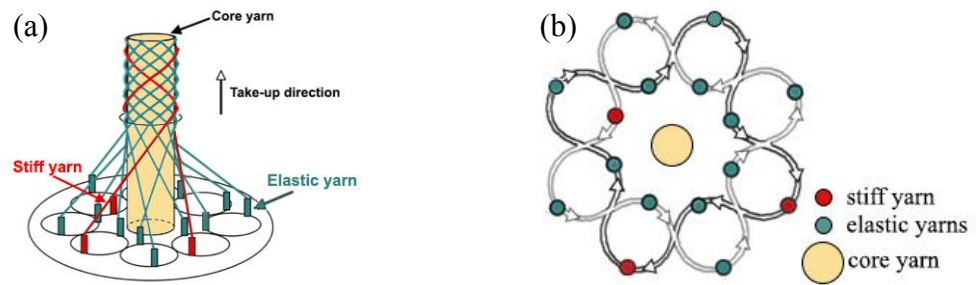


Figure 3.14 Structure R3: (a) the manufacturing process; (b) the yarn arrangement on 16 carriers.

### 3.4 Conclusions

In this chapter, the design and fabrication of six novel auxetic tubular braided structures were introduced. In general, six structures can be categorized into two

groups with three structures in each group. The first three structures were designed and constructed via wrapping or inserting extra stiff yarns onto the tubular braided structure and can be fabricated using a modified circular braiding technique. The other three structures in the second group were designed and constructed via employing both stiff and elastic yarns in the tubular braided structure and can be fabricated using a conventional circular braiding technique. By virtue of using components with different moduli, these structures could change its initial straight shape to a helical or trapezoidal shape and thus display a lateral size expansion under tension. As a result, all of them are designed to be structures with a negative PR effect when stretched.

# CHAPTER 4 EXPERIMENTAL ANALYSIS OF SIX AUXETIC BRAIDED STRUCTURES

## 4.1 Introduction

This chapter presents a preliminary experimental study on the negative PR effect of developed six auxetic tubular braided structures. A tensile testing system consists of an Instron 5544 Universal Testing Machine, a high-resolution CMOS camera and a computer were employed to test the Poisson's ratio of samples produced for six structures. Especially for two selected structures, i.e., HL and R1, different kinds of samples were produced and tested in order to evaluate the effects of different parameters on the negative PR effect of the structure.

## 4.2 Negative PR effect of six structures

### 4.2.1 Sample fabrication

Table 4.1 lists the component yarn materials used to construct two samples of each developed structure. Note that in the geometry design a core yarn is added in the structure HL, R1, R2 and R3. However, here, no core yarn is used in each sample of the structures in order to remove the effects of core yarn on the Poisson's ratio of the structure and thus compare the behaviour of these six structures more rigorously.

Table 4.1 Component yarn materials used to construct samples of the structures.

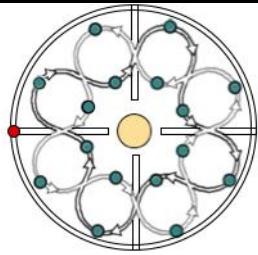
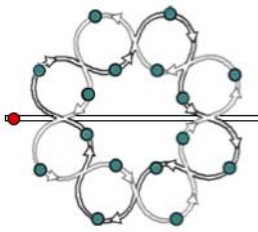
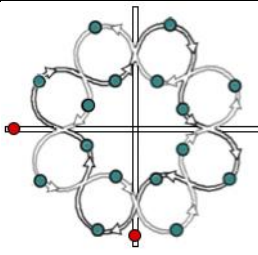
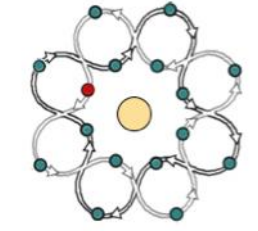
Name	Code	Yarn constituent	Diameter (mm)	Young's modulus (MPa)	Color
Stiff yarn	A	Polyester	0.82	320	blue
Braiding yarn	B	Polyester and Rubber	0.73	3.92	black

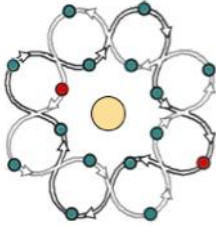
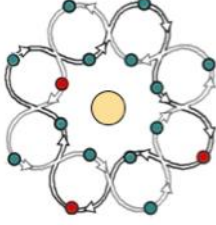
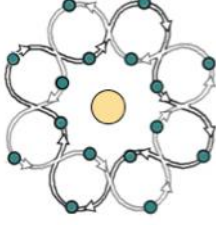
By using these component yarns, samples of each developed auxetic tubular braided structures were fabricated using the approaches mentioned in Chapter 3. For the

comparison, two samples of the conventional tubular braided structure with core yarn inside, N1, were also produced herein to indicate the conventional value of the Poisson's ratio of the braided structure when no auxetic geometry design is applied.

Table 4.2 presents the geometric features and photographs of produced samples.

Table 4.2 The details of samples for six auxetic tubular braided structures.

Structure	Sample code	Yarn combination	Component yarn arrangement	Photograph
			● A: stiff yarn ● B: elastic yarns ● C: core yarn	
HL	HL1	A+16B		
	HL2			
HC	HC1	A+16B		 (Front) (Side)
	HC2			
FC	FC1	2A+16B		
	FC2			
R1	R1a	A+15B		
	R1b			

R2	R2a	2A+14B		
	R2b			
R3	R3a	3A+13B		
	R3b			
N1	N1	16B		

#### 4.2.2 Poisson's ratio testing method

In order to assess the Poisson's ratio of auxetic yarns produced, a tensile testing system consists of an Instron 5544 Universal Testing Machine, a high-resolution CMOS camera and a computer (Figure 4.1a) was employed to measure the longitudinal and transverse strain of the sample. The longitudinal strain of the sample  $\varepsilon_l$  is provided by a tensile test which was conducted on the Instron 5944 tester (Instron Worldwide Headquarters, Norwood, Massachusetts, USA) using a 50N load cell. During the test, the sample was mounted vertically between the two clamps and secured manually using mechanical jaws of which the face size is 2.5 cm  $\times$  2.5cm. A special sample gauge length  $L_G=150\text{mm}$  was chosen according to the following condition.

$$L_G \geq 10\lambda \quad (4.1)$$

where  $\lambda$  is the cyclic pitch of stiff yarn in a helical arrangement. This condition is

adopted based on the numerical study by Wright et al. [84] to ensure a minimum number of wrap cycles within a specimen gauge length regardless of the yarn geometry. Tensile tests then were performed up to 30% loading strains for each sample or until the failure of the stiff yarn, whichever is earlier. The crosshead speed was set as 0.3 mm/s. The applied load and longitudinal tensile strain of samples  $\epsilon_l$  then were recorded using the Bluehill® Software (<http://www.instron.co.uk>) that is compatible with Instron testing system. Prior to data recording, samples were stretched cyclically to 0.01 strain at a rate of 0.1mm/s for several cycles as a ‘bedding in’ process to minimize the pretension induced during fixation of the samples on the jaws.

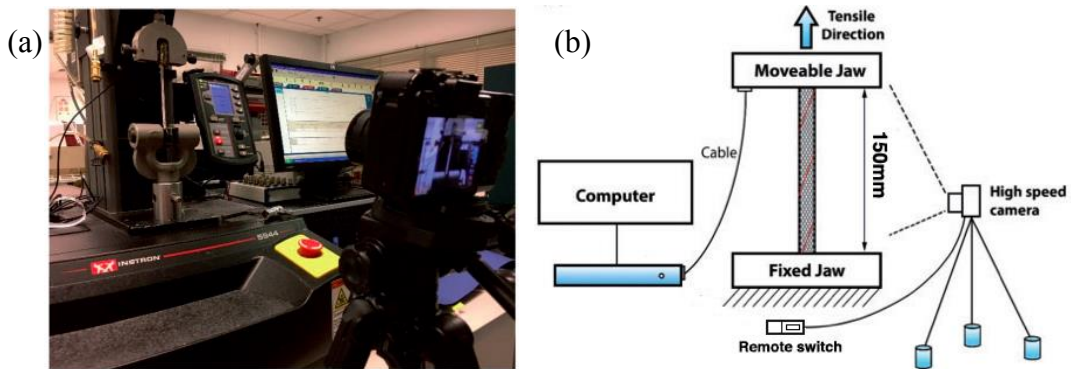


Figure 4.1 The tensile testing system used to calculate the Poisson’s ratio of developed structures: (a) schematic; (b) photograph.

The transversal strain then is calculated from the photographs of samples provided by the high-resolution CMOS camera and the computer. Following describes the method used herein. Firstly, by using the remote switch and the camera, a photograph of the tested sample was taken at every 1% longitudinal strain during the tensile test. These obtained photographs then were treated with a Digital Image Processing (DIP) technique in order to have more accurate results. During the treatment process, each captured photograph (Figure 4.2a) was binarized via the software Adobe Photograph CC and Matlab R2017a to remove the color noise. Threshold and line refill were also applied to the obtained binary image so that the edge of the sample could be

distinguished from the back ground (Figure 4.2b). As there is also yarn hairiness around the edge of samples, a syntax *bwareaopen* in Matlab R2017a was used to remove them and thus preventing inaccurate measurements. Finally, the effective transverse length of the tested sample was calculated by counting the pixels existing between the upper and lower boundaries in the treated image (Figure 4.2c). With the obtained transverse length, the transversal strain  $\varepsilon_t$  can be calculated by using Equation 4.2.

$$\varepsilon_t = \frac{H-H_0}{H_0} \quad (4.2)$$

where H and  $H_0$  are effective transverse lengths of the sample at the initial and stretched states, respectively. From here, the Poisson's ratio ( $\nu$ ) can be calculated with the longitudinal tensile strain  $\varepsilon_l$  read from the Instron 5944 tester and transverse strain  $\varepsilon_t$  obtained from the above as follows:

$$\nu = -\frac{\varepsilon_t}{\varepsilon_l} \quad (4.3)$$

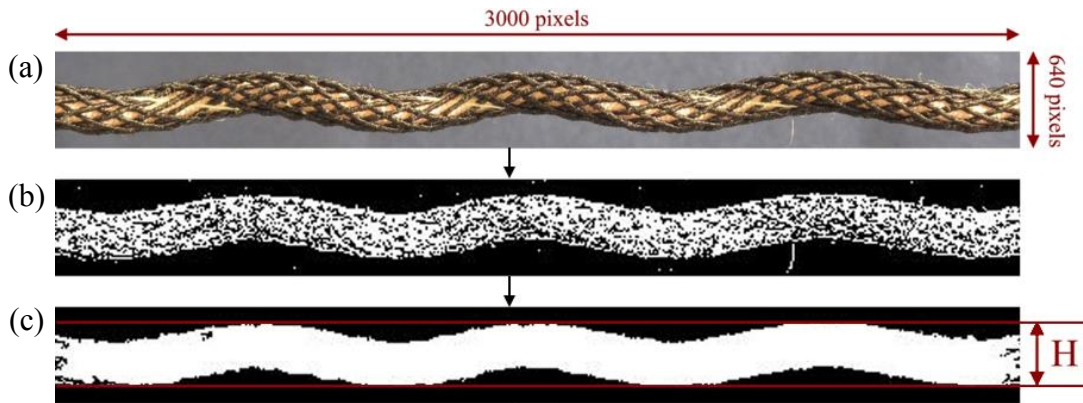


Figure 4.2 Digital Image Processing for yarn image obtained: (a) captured photograph; (b) binary and threshold image; (c) image for the calculation of effective transverse width of auxetic yarn.

The statistical approach used herein is the descriptive statistics. The tested data are analysed based on their central tendency and variability. For central tendency, it is

obtained from the arithmetic mean values of tested data set, which has the following mathematical expression:

$$\bar{x} = \frac{1}{n} \sum_{i=1}^n x_i = \frac{x_1 + x_2 + \dots + x_i}{n} \quad (4.4)$$

where  $x$  is the sample code for each structure and  $i$  is the serial number of parallel samples under this sample code. For variability, it is obtained from the standard deviation of tested data set, which has the following mathematical expression:

$$\sigma = \sqrt{\frac{1}{n} \sum_{i=1}^n (x_i - \bar{x})^2} \quad (4.5)$$

In figures, the central tendency of tested data set is presented as the curves while the variability of tested data set is indicated by the error bars.

### 4.2.3 Results and discussion

Based on the results obtained from the testing, two types of curves, i.e., the transverse length versus longitudinal length curve and Poisson's ratio-strain curve, were plotted for each developed auxetic tubular braided structure in this study. The first type of curve was used to evaluate the extent of the structure expansion when stretched while the latter curve was used to measure the Poisson's ratio yielded from this lateral expansion. With above two curves, the negative PR effect of developed six structures could be investigated. On the other hand, the experimental data of tubular braid N1 samples were also added in every curve so that the difference in Poisson's ratio between the developed auxetic braids and a conventional braid could be clearly shown. Following paragraphs present the experimental data and plotted two curves for each developed auxetic structure. Note that the curve plotted in each figure is the average value of the tested data of two samples.

Figure 4.3a and Figure 4.3b respectively present the transverse length–longitudinal length and Poisson's ratio-strain curves of structure HL. It can be seen that a lateral

expansion effect was exhibited in the structure HL when stretched, which in turn result in a negative PR effect.

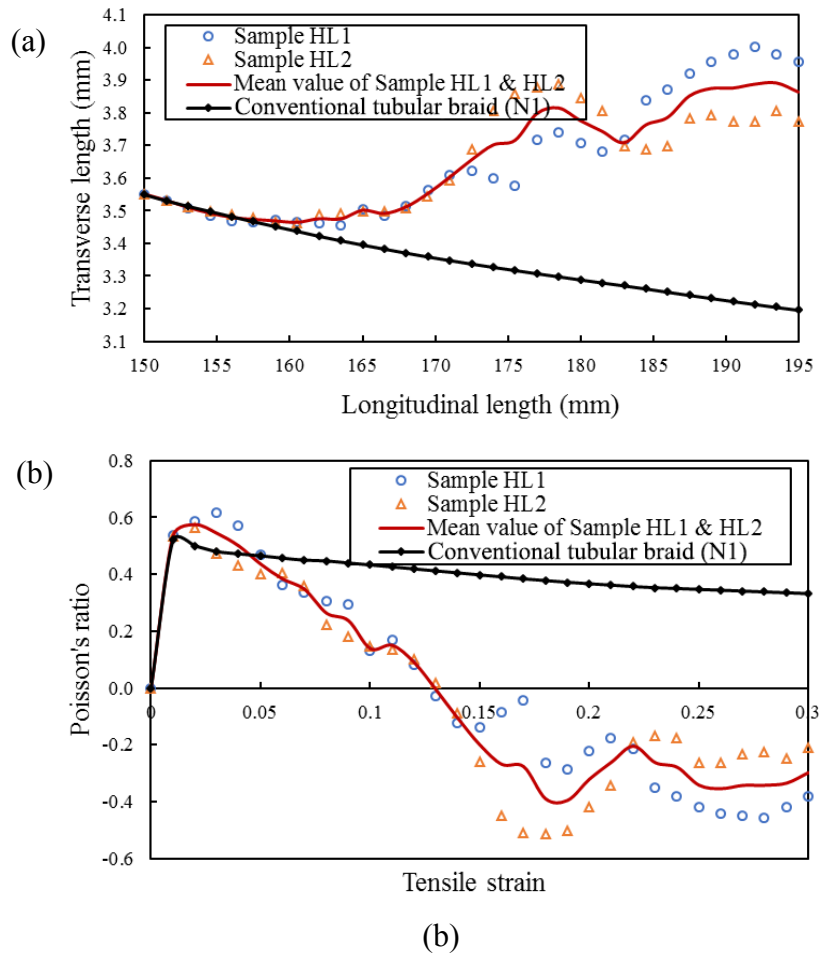
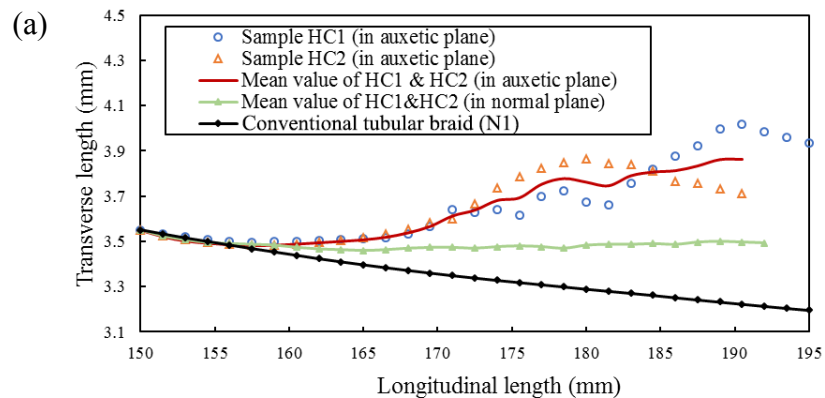


Figure 4.3 The negative PR effect of structure HL: (a) transverse length–longitudinal length curve; (b) Poisson's ratio–strain curve.

As shown in Figure 4.3a, upon application of stretching, the transverse length of the structure HL decreased firstly before the increase of it. This is mainly due to there exist voids between the stiff yarn and base tubular braid and thus the stiff yarn could not displace the structure laterally when it is slightly stretched, yielding a decrease in the size of the structure. In this period, since there is no lateral shape deformation, the size decrease rate as well as the Poisson's ratio of the structure HL (Figure 4.3b) is similar to those of the conventional positive Poisson's ratio braid N1. However, it can also be seen that the size of the structure HL increases rapidly after the initial decrease because

the shape of it changed from a straight form to a wave form at larger tensile strain. During that period, as a lateral expansion effect was exhibited, the Poisson's ratio of structure HL decreased noticeably from a positive value to a negative value and was able to maintain this behaviour until the end of the test. Comparatively, it can be seen that the Poisson's ratio of a conventional braid kept as a positive value during the whole tensile test.

Figure 4.4a and Figure 4.4b respectively present the transverse length–longitudinal length and Poisson's ratio-strain curves of structure HC. It can be seen that the uni-direction trapezoidal geometry provided structure HC with two orthogonal planes exhibiting different PR behaviours, negative PR in one plane and positive Poisson's ratio in the other plane.



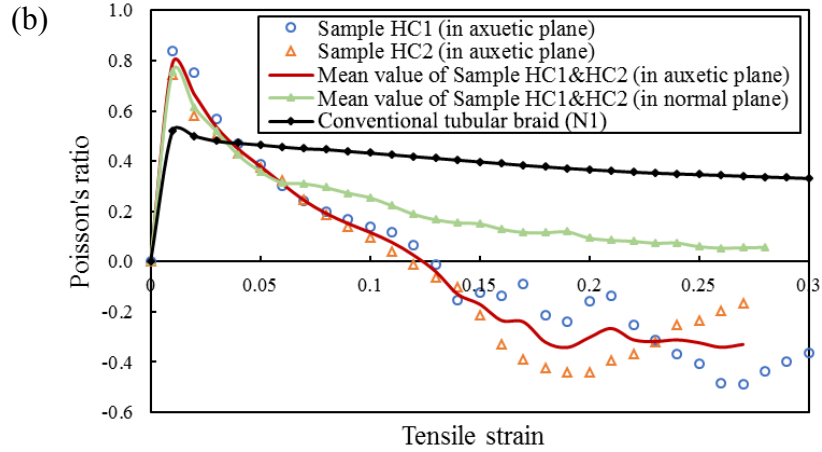


Figure 4.4 The negative PR effect of structure HC: (a) transverse length–longitudinal length curve; (b) Poisson’s ratio-strain curve.

As shown in Figure 4.4a, different size changes were displayed in the structure HC in its two orthogonal planes. In the plane that is parallel the inserting direction (termed auxetic plane), the size of the structure HC was able to increase to a larger value because the zigzag deformation generated when stretched. In the plane that is perpendicular to the inserting direction (termed normal plane), the size of the structure HC decreased upon the application of stretching because the stiff yarn could not displace the braid laterally but only flattened it. Since the size in the auxetic plane became larger than the initial value while the size in the conventional plane maintained smaller than the initial value, a negative PR and a positive Poisson’s ratio were exhibited in two planes respectively, as shown in Figure 4.4b. However, it is worth noting that the flattening effect caused by the stiff yarn could reduce the size decrease of the structure HC in its conventional plane. Therefore, a Poisson’s ratio which is comparatively smaller than that of the conventional braid at large tensile strain was exhibited in the normal plane of the structure HC.

Figure 4.5a and Figure 4.5b respectively present the transverse length–longitudinal length and Poisson’s ratio-strain curves of structure FC. It can be seen that by

employing a bi-direction trapezoidal geometry, structure FC exhibited an expansion effect in its lateral directions. However, the maximum negative PR of the structure FC is much smaller than that of the structure HC.

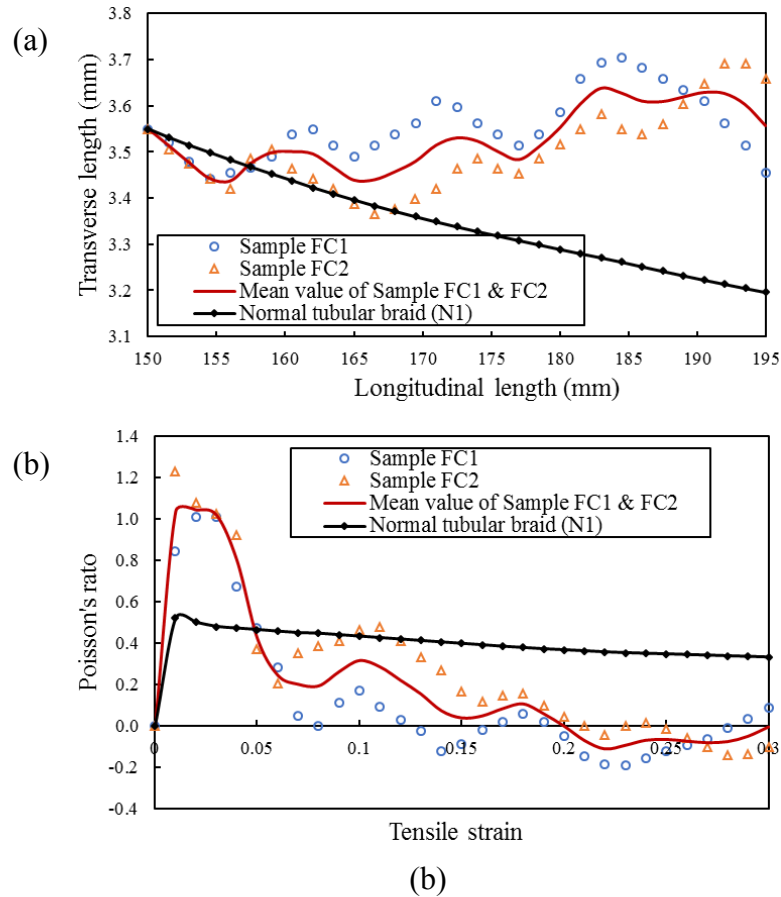


Figure 4.5 The negative PR effect of structure FC: (a) transverse length–longitudinal length curve; (b) Poisson's ratio–strain curve.

Firstly, it can be seen from the Figure 4.5a and Figure 4.5b that the structure FC exhibited an expansion effect in its lateral directions and a negative PR effect was able to be exhibited at large tensile strain levels. However, compared with the previous two structures and conventional braid, the size of the structure FC decreases more rapidly at small strain levels (Figure 4.5a) and the positive Poisson's ratio of it (Figure 4.5b) was much higher than that of the conventional braided structures. This is mainly due to the two stiff yarns in FC structure would squeeze the structure into a smaller diameter before they could display the structure laterally. On the other hand, it is

interesting to note that there is also a structural rotation besides the zigzag shape deformation when stretched. Seen from the Figure 4.6, this structural rotation is reflected by the movement of red point from the left side to the right side with the increase of the tensile strain. Since this rotation could not result in the lateral expansion, it may be the cause of the periodical decrease in the transverse length of the structure FC as shown in Figure 4.5a.

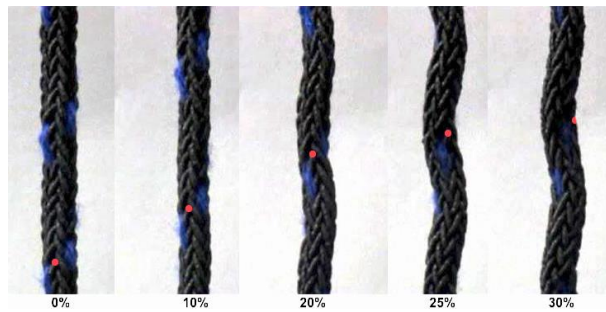
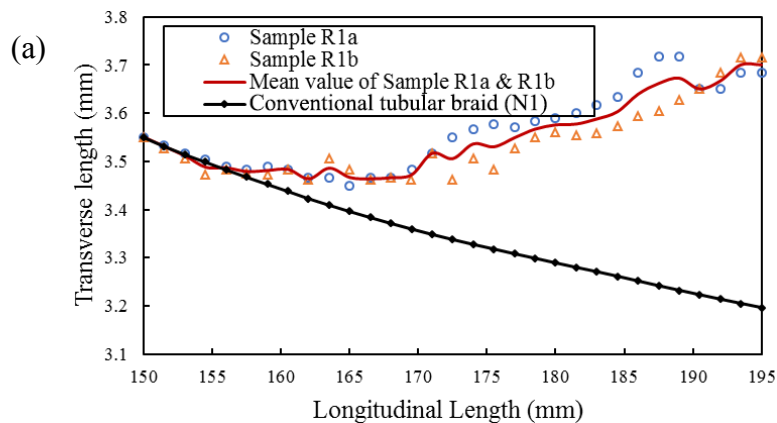


Figure 4.6 The photograph of Sample FC1 at critical tensile strains.

Figure 4.7a and Figure 4.7b respectively present the transverse length–longitudinal length and Poisson’s ratio–strain curves of structure R1. It can be seen that interlacing one stiff yarns with other elastic yarns could also result in a tubular braided structure with negative PR effect when stretched even though the maximum value of negative PR is reduced compared to that of the structure HL.



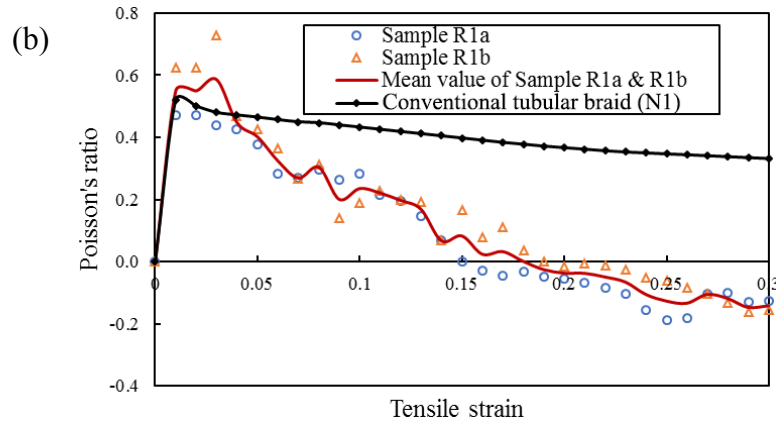


Figure 4.7 The negative PR effect of structure R1: (a) transverse length–longitudinal length curve; (b) Poisson’s ratio–strain curve.

As shown in the Figure 4.7a and Figure 4.7b, the change of size and Poisson’s ratio of structure R1 presented a trend similar to that of the structure H1 and a negative PR effect of it was able to activate at a tensile strain of 17%. However, compared to that of the structure HL (Figure 4.3b), this activation strain is much larger. This is because in R1 structure the stiff yarn is interlaced with other elastic yarns and the path of it in the initial state is in a crimped shape, as shown in Figure 4.8a. Upon the application of the stretching, the stiff yarn needs to change its shape from the crimp to the helical (Figure 4.8b) so that it could displace the braided structure laterally. This later displacement then results in the later activation of the auxetic behaviour as well as the smaller maximum negative PR.

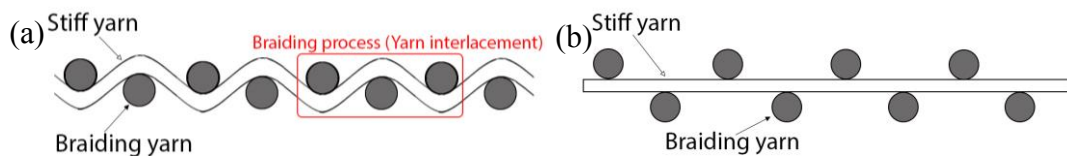


Figure 4.8 The path of stiff yarn in structure R1 when rolled out into a flat surface: (a) crimp shape at an initial state; (b) helical shape when slightly stretched.

Figure 4.9a and Figure 4.9b respectively show the transverse length–longitudinal length and Poisson’s ratio–strain curves of structure R2. It can be seen that similar to

the structure HC, structure R2 also has two orthogonal planes which respectively presents a negative Poisson's ratio and positive Poisson's ratio. In its auxetic plane, structure R2 presents a larger maximum negative PR effect compared to the structure R1.

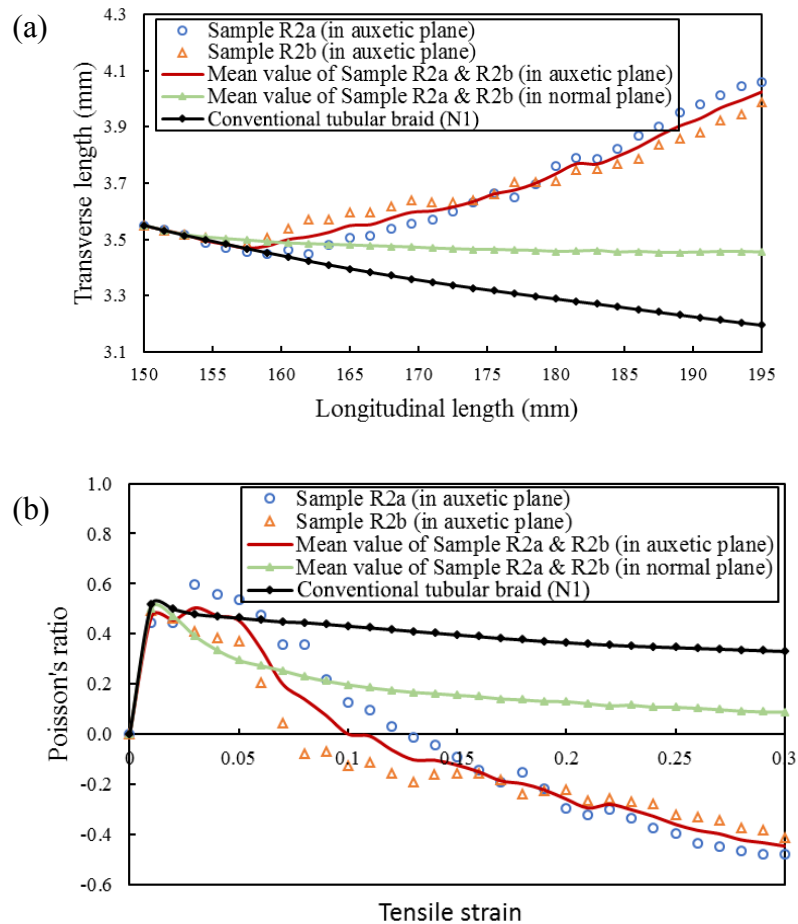
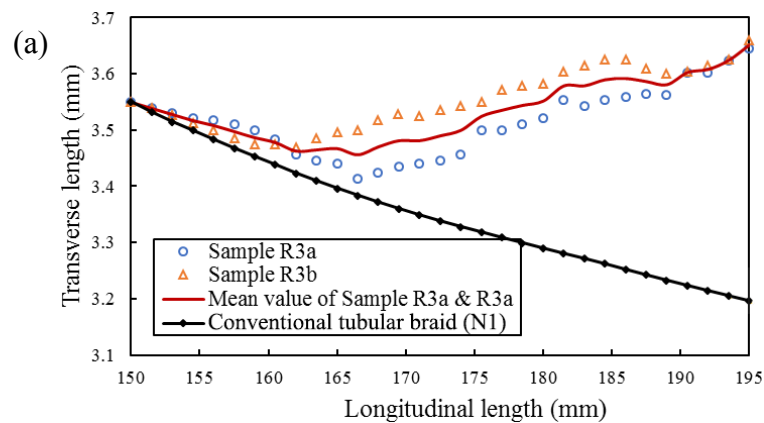


Figure 4.9 The negative PR effect of structure R2: (a) transverse length–longitudinal length curve; (b) Poisson's ratio–strain curve.

By employing two stiff yarns, the structure R2 presented a different tensile behaviour compared to the structure R1. Different size changes (Figure 4.9a) and Poisson's ratio value (Figure 4.9b) of structure R2 were exhibited when measured in a different plane. When measured from the front-view plane as shown in Figure 3.10 (termed normal plane here), the transverse length of the structure diminished linearly to its minimum value because the helical deformation caused by two stiff yarn are offset by each other

and thus presented a positive Poisson's ratio. When measured from the side-view plane as shown in Figure 3.10 (termed auxetic plane here), the transverse length of the structure was able to increase to a large value because two stiff yarns are pushing the structure laterally at intersecting points which causes a zigzag shape deformation. This zigzag shape then results in the lateral expansion of the FC structure and its transverse length increase. Apart from the above, it is interesting to note that the trend in transverse length and Poisson's ratio value change of structure R2 is similar to that of the structure HC (Figure 4.4b). This is mainly because the shape deformations of these two structures are similar to each other.

Figure 4.10a and Figure 4.10b respectively demonstrate the transverse length–longitudinal length and Poisson's ratio–strain curves of structure R3. It can be seen that adding one more yarn on the basis on the structure R2 could result in a structure expansion in later directions while the overall negative PR effect is reduced.



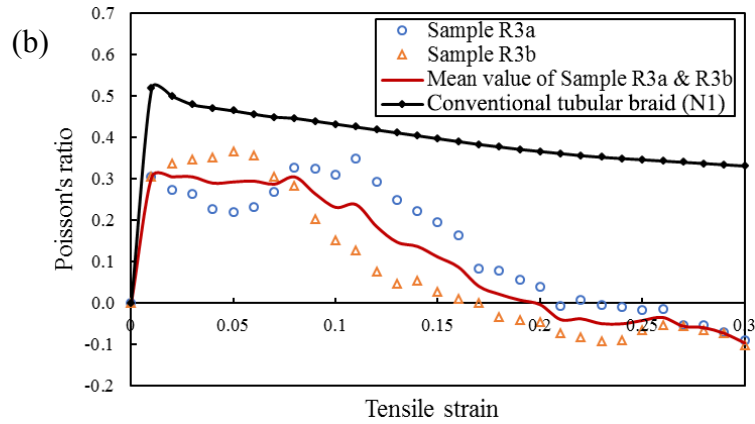
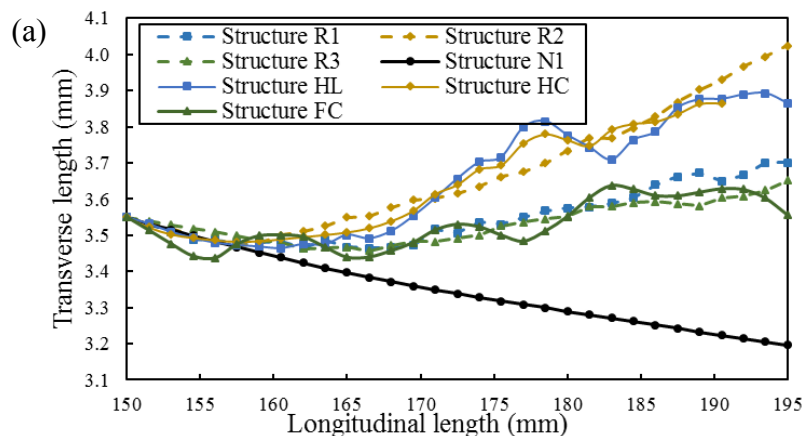


Figure 4.10 The negative PR effect of structure R3: (a) transverse length–longitudinal length curve; (b) Poisson's ratio-strain curve.

As shown in Figure 4.10a, a common two-stage trend of transverse length change was demonstrated in the structure R3, i.e., the transverse length of it decreased firstly before the increase. However, this change is small, yielding a smaller positive Poisson's ratio at lower tensile strains and negative PR at higher tensile strains (Figure 4.10b). This can be attributed to the fact that the employment of three stiff yarns restricts the shape deformation of structure R3 under tension. Therefore, the lateral expansion of it is small and the negative PR effect becomes less evident.

At last, in order to clearly show the negative PR effect of all developed structures. The transverse length–longitudinal length and Poisson's ratio-strain curves includes all structure were plotted and presented in Figure 4.11.



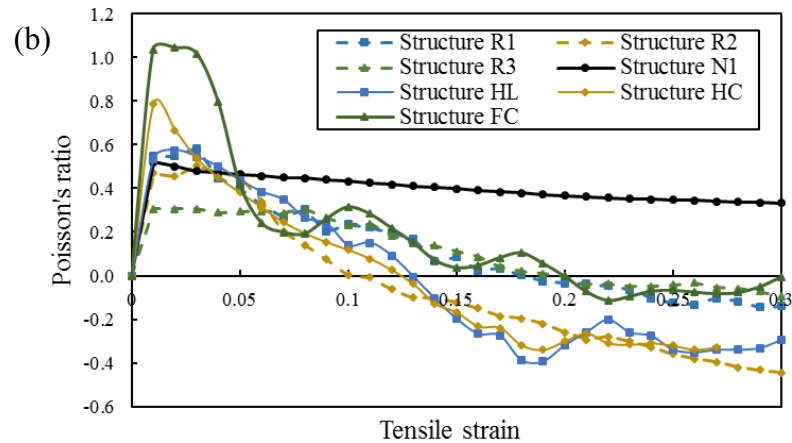


Figure 4.11 The negative PR effect of all produced structures: (a) transverse length–longitudinal length curve; (b) Poisson’s ratio-strain curve.

From the Figure 4.11a and Figure 4.11b, it can be found that three structures, i.e., the structure HL, the structure HC and structure R2, presented a larger maximum negative PR value, earlier auxetic behaviour activation strain as well as smaller strain when the maximum negative PR value occurs compared to other three structures. For HL structure, it is mainly because there is less interlacement between stiff yarn and other elastic braiding yarn compared to R1 and R2 and R3 and thus the stiff yarn has less crimp shape in the initial state. As a result, its auxetic behavior is early activated. In the meantime, since the stiff yarn is wrapped on the outside of the braiding yarns, straightening of stiff yarn could displace the whole structure to large deformation, yielding a larger negative PR.

### 4.3 Effects of parameters on the negative PR effect

Due to the limitation of the study period, it is impossible to analyze the influence of parameters on the Poisson’s ratio for every developed structure. Thus, in this study, two representative structures manufactured by two different approaches, i.e., by wrapping or inserting extra stiff yarns to the braided structure and by employing both stiff yarn and elastic yarns in braided structure, were selected to analysis objects for

the influence of structural parameters on the Poisson's ratio. The selected two structures herein were structure HL and structure R1 as they have the same geometry design but different design approaches and manufacturing processes.

In order to vary the structural parameter settings of samples of these two structures, six types of component yarns were used. The details of them are listed in Table 6.1. In order to distinguish component yarns with each other when construct sample with different parameter settings, yarns with various colours were employed. By using these component yarns and the fabrication method mentioned in previous chapters, samples with different structural parameter settings for structures HL and R1 were manufactured.

Table 4.3 The details of used component yarns for samples with different parameters.

Component	Code	Yarn constituent	Diameter (mm)	Young's modulus (MPa)	Poisson's ratio	Color
Stiff yarn	D	Polyester	0.18	892	0.50	white/red/black
Elastic yarns	E1	Polyester and rubber	0.73	4.10	0.47	white/black
	E2	Polyester and rubber	0.40	4.10	0.47	black
	E3	Cotton and spandex	0.20	5.75	0.52	white
Core yarn	F1	Polyester and rubber	2.20	4.23	0.32	pink
	F2	Polyester and rubber	1.45	4.23	0.32	green

### 4.3.1 Sample fabrication

Table 4.4 presents the details of samples with various parameter settings for structures HL. The initial braiding angle is defined by the angle formed between the central longitudinal line of the braided structure and axis of the braiding yarn. The initial wrap angle is defined by the angle formed between the central longitudinal line of the braided structure and axis of the stiff yarn. Both of two parameters can be adjusted by changing the stiff yarn wrapping speed, elastic braiding yarn spindle speed and braid take-up speed accordingly. Overall, the fabricated samples can be split into three groups according to the considered influence of different parameters. The first group includes samples X-1, X-2 and X-3 which are produced with the same braiding yarn, the same core yarn and the same initial braiding angle but with different initial wrap angles. The second group includes samples X-1, X-4 and X-5, which are produced with the same braiding yarn, the same core yarn and the same initial wrap angle but with different initial braiding angles. The third group includes X-6 and X-7, which are produced with the same initial braiding angle, the same initial wrap angle, the same core yarn, but with different diameters of braiding yarns. In this group, the change of the braiding yarn diameter also results in the change of structure size. For all the samples, the stiff wrap yarn is kept unchanged. Note that five parallel samples were manufactured for each sample code listed in Table 4.4.

Table 4.4 The details of samples with various parameter settings for structures HL.

Sample code	Component yarns	Diameter (mm)	Initial wrap and braiding angle (degree)	Photograph
X-1	D+16E1+F1	4.5	21.7 and 20.6	
X-2	D+16E1+F1	4.5	17.5 and 20.6	

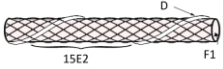
X-3	D+16E1+F1	4.5	12.1 and 20.6	
X-4	D+16E1+F1	4.5	21.7 and 24.5	
X-5	D+16E1+F1	4.5	21.7 and 35.7	
X-6	D+16E1+F2	3.2	21.7 and 35.7	
X-7	D+16E2+F2	2.3	21.7 and 35.7	

Note that three parallel samples were manufactured for each sample code listed in Table 4.5.

Table 4.5 presents the details of samples with various parameter settings for structures R1. As the influence of initial braiding angle was unable to be considered here for R1 structure due to the limitation of used braiding machines, we investigate the effect of adding one stiff yarn for the R1 structure. This may cause the samples presented here slightly different from the R1 structure design, i.e., the samples Y-2, Y-3 and Y-4 have two stiff yarns in structure while for a typical R1 has only one stiff yarn in structure. However, we believe Y-2, Y-3 and Y-4 are part of the R1 design because the main geometry feature of the R1 is that the stiff yarn is in a helical path in one direction. In that case, Y2, Y3 and Y4 can be regarded as the R1 structure with different stiff yarn cyclic pitch. Y-2, Y-3 and Y-4 cannot be categorized into R2 type structure because in R2 structure one stiff yarn is placed in ‘S’ direction while the other stiff yarn is placed in ‘Z’ direction. In general, samples of structure can be split into three groups according to the considered influence of different parameters. The first group includes samples Y-1 and Y-2, which are produced with a different number of stiff wrap yarn.

The second group includes samples Y-2, Y-3 and Y-4, which are produced with a different arrangement of stiff yarns. The last group includes Y-1, Y-6 and Y-7, which are produced with different diameters of component yarns. The influence of initial braiding angle and initial wrap angle were not considered here due to the limitation of used braiding machines. Thus, for all the fabricated samples including the HAY, both angles were kept unchanged as  $35.7^\circ$  in order to facilitate the analysis. Note that three parallel samples were manufactured for each sample code listed in Table 4.5.

Table 4.5 The details of samples with various parameter settings for structures R1.

Sample code	Component yarns	Diameter (mm)	Initial braiding angle (degree)	Illustration	Photograph
Y-1	D+15E2+F1	3.1	35.7		
Y-2	2D+14E2+F1	3.1			
Y-3	2D+14E2+F1	3.1			
Y-4	2D+14E2+F1	3.1			
Y-5	D+15E3+F1	2.3			
Y-6	D+15E3+F2	1.8			

#### 4.3.2 Poisson's ratio testing method

The testing method mentioned in Section 4.2.2 was used here to assess the Poisson's ratio of produced samples for structure HL and R1. However, the whole testing was

performed up to a tensile strain of 0.5 and 0.25 for samples of structure HL and R1 respectively because of the different length of stiff yarn in the structure. Meanwhile, it is worth noting that the tested data for HL and R1 in Section 4.2.3 and Section 4.3.2 present a huge difference regarding the negative PR value because of following reasons:

(1) The data presented in Section 4.2.3 figures are obtained from samples which have large stiff yarn diameter and have no core yarn inside. Countering that, the data presented in Section 4.3.2 figures are obtained from samples which have small diameter stiff yarn and have core yarn inside. Based on the previous studies in auxetic yarns and our experimental study, the adding of core yarn and the use of smaller stiff yarn diameter will lead to a larger maximum negative PR of structure. Therefore, the experimental results in section 4.3.2 are inconsistent with that in section 4.2.3. For example, the samples of structure R1 presented a maximum negative PR value of -0.1 in Figure 4.7b but -1 in Figure 4.15.

(2) In the meantime, the huge difference in experimental results of Figure 4.3b and Figure 4.12 are also resulted from the fact that the samples presented in Fig. 4.12 is pre-tightened before the testing. The pre-tension can make these samples present an earlier activation of the auxetic effect and larger negative PR value when compared to samples which are not pre-tightened.

### **4.3.3 Experimental results and discussion for HL structure**

The initial wrap angle is the first structural parameter that can be employed to tailor the Poisson's ratio of auxetic tubular braided structures. The Poisson's ratio-strain curves of three different types of auxetic braids HL made with the same braiding yarns,

the same core yarn and the same initial braiding angle, but with different initial wrap angles are shown in Figure 4.12. It can be seen that the initial wrap angle has obvious effects on negative PR effect of the structure HL.

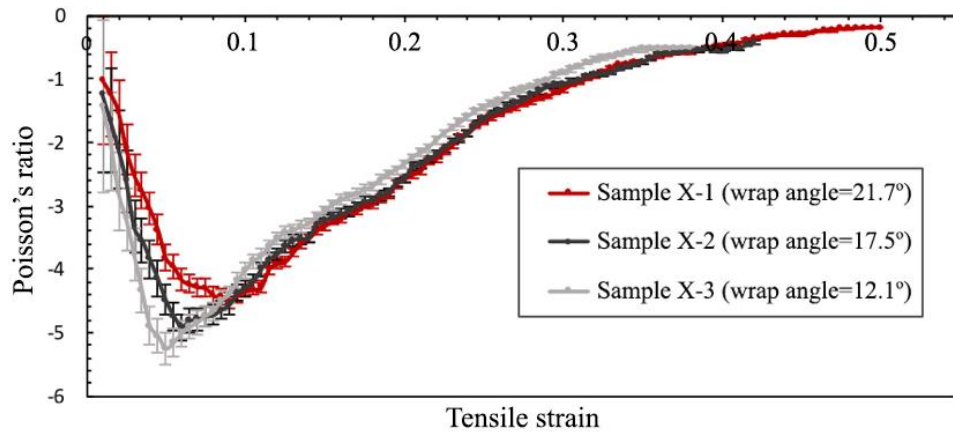


Figure 4.12 Poisson's-strain curves for samples of HL with different initial wrap angles.

As shown in Figure 4.12, the effect of the initial wrap angle on Poisson's ratio is clearly observed in the first stage of the stretching process. It can be seen that the maximum negative PR of the structure increases with the decrease of the initial wrap angle, but the tensile strain to reach the maximum negative PR value decreases with the decrease of the initial wrap angle. As the shape change of the structure HL from a straight form to a wave form mainly comes from the straightening of the extra stiff yarn, it is conventional that lower initial wrap angle can cause the early activation of shape change in structure and thereby result in a better auxetic behaviour as well as the larger maximum negative PR value. These results showed good agreement with previous findings on the effects of wrap angle on HAY structures [22, 23, 25], which has a similar helical arrangement as mentioned. However, these assumptions may become untrue under certain conditions as having been pointed out by Faisal et al. [26]. By employing the Finite Element Analysis method, they found a wrap angle of around  $7^\circ$  is an optimum choice for obtaining the maximum auxetic effect in an auxetic structure

based on a helical geometry. The angle below  $7^\circ$  would not strengthen the auxetic performance of the structure but hinder it. On the other hand, lower wrap angle makes the length of extra stiff yarn in the structure shorter, therefore making it easily straightened at a lower tensile strain and resulting in an earlier activation of the negative PR. From Figure 4.12, it can also be seen that the effect of the initial wrap angle on Poisson's ratio becomes in-evident after the maximum negative PR point. This is mainly because the stiff yarn is straightened along the center line of the structure and thus could not cause the further lateral expansion of the structure, i.e., the increase of the cross-sectional size of the structure.

Another critical structural parameter selected for analysis in developed structure HL is the initial braiding angle. Figure 4.13 illustrates the Poisson's ratio-strain curves of three different types of auxetic braids HL made with the same braiding yarns, the same core yarn and the same initial wrap angle, but with different initial braiding angles, respectively. It can be seen that the effects of the initial braiding angle are not as evident as those of the initial wrap angle.

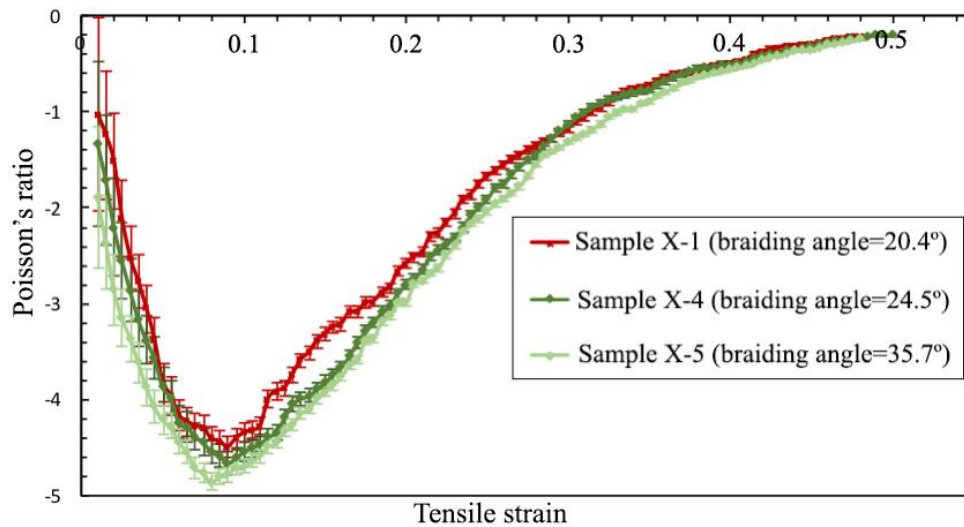


Figure 4.13 Poisson's-strain curves for samples of HL with different initial braiding angles.

As shown in Figure 4.13, the maximum negative PR of the auxetic tubular braided structure HL is slightly increased with the increase of the initial braiding angle in the whole stretching process. This phenomenon can be explained by the fact that with the increase of the initial braiding angle, the base braid gets easier extended. This means its Young's modulus gets decreased with the increase of the initial braiding angle. As a result, the lower modulus makes the base braid to be easier bent and thus could deform into a helical wave with higher amplitude under the straightening of the stiff yarn, leading to larger expansion in the lateral direction as well as a larger increase in the cross-sectional size. Therefore, a larger value of negative PR is presented in the structure with larger initial braiding angle than the structure with the smaller initial braiding angle.

The last structural parameter selected here for the analysis is the braiding yarn diameter. Figure 4.14 illustrates the Poisson's ratio-strain curves of the auxetic braids HL made with the same initial braiding angle, the same initial wrap angle and the same core

yarn, but with different braiding yarn diameters, respectively. It can be seen that the braiding yarn diameter has obvious effects on the Poisson's ratio.

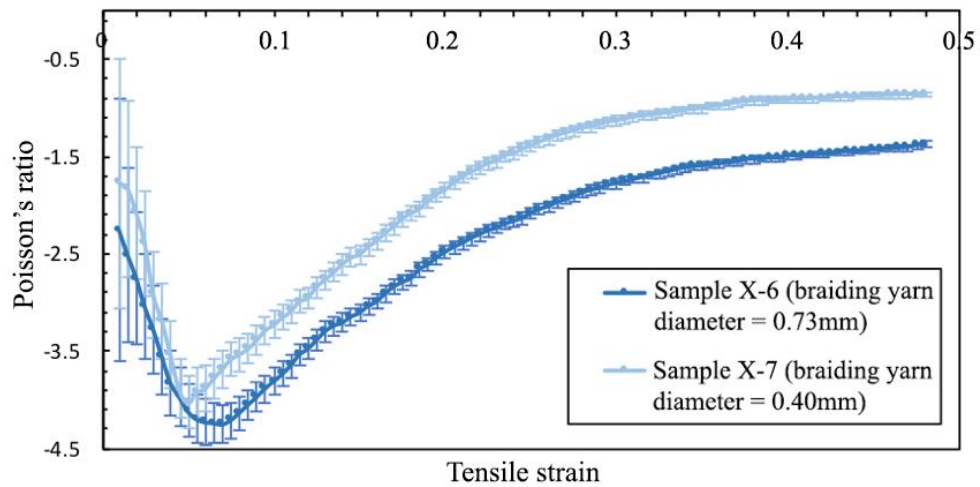


Figure 4.14 Poisson's-strain curves for samples of HL with different braiding yarn diameters.

As shown in Figure 4.14, the effect of braiding yarn diameter on the Poisson's ratio is not very evident in the initial stage of the stretching process. This is because the structure has a similar shape change when the initial wrap angle is maintained as the same. However, it can also be seen that the maximum value of negative PR of the structure increases with the increase of the braiding yarn diameter. The possible reason is that the auxetic braid with large braiding yarn diameter also has a larger braid diameter and thus the cross-sectional contour size increase in the structure is more significant than auxetic braid with small braiding yarn diameter. Also due to the same reason, the negative PR effect of the auxetic braid with larger braiding yarn diameter is kept higher than that of the auxetic braid with smaller braiding yarn diameter from the maximum negative PR point to the fail of the structure.

At last, it is worth noting that it is interesting to note that all produced HL sample here did not present a positive Poisson's value at the beginning of the traction does not

present as it is the case for other samples in this study. The primary reason is that knots were employed to secure the ends of samples before they were taken down from the braiding machine. This fixation process not only avoided the possible slippage of the stiff yarn, but also caused it pre-straightened. Though this straightening effect was small and could not be observed with eyes, it would lead to instantly decrease of the Poisson's ratio of braids at the beginning of the traction and thus no positive Poisson's ratio was presented.

#### 4.3.4 Experimental results and discussion for R1 structure

As the wrap angle and braiding angle is fixed for the structure R1 due to the limitation of the machine, the first parameter analyzed here is the influence of stiff yarn numbers because the use of stiff yarn is the primary reason that triggers auxetic effect and influences the Poisson's ratio in developed auxetic tubular braided structures. The Poisson's ratio-strain curves for samples of structure R1 with different numbers of stiff yarns are compared in Figure 4.15. It can be seen that the number of stiff yarns has an obvious influence on the Poisson's ratio of the structure.

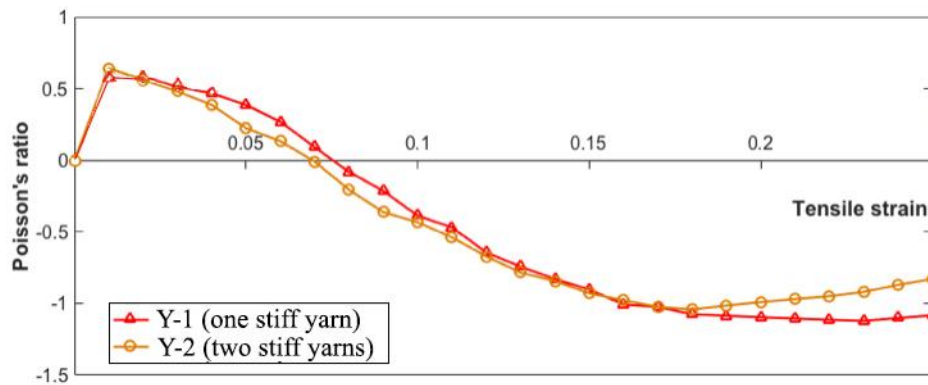


Figure 4.15 Poisson's-strain curves for R1 samples with a different number of stiff yarns.

As shown in Figure 4.15, the R1 structure with two adjacent stiff yarn presents an earlier activation of auxetic effect but smaller maximum negative PR compared to the

structure with one stiff yarn. This is because the increase in the transverse width of the structure is related to the overall lateral displacement of the core caused by all stiff yarns in the structure. When two adjacent stiff yarns are used in the structure like Y-2, the core is easier to be displaced laterally at initial action of the stiff yarns, resulting in an earlier activation of an auxetic effect than the structure with one stiff yarn like Y-1.

From the above analysis, it is found that the additional stiff yarn will influence the Poisson's ratio of the R1 structure. However, this influence may vary because the two stiff yarns in R1 structure can be arranged to different positions and the distance between them can be changed. To analyze the influence of this parameter, the auxetic effect and Poisson's ratio of R1 samples consisting of two stiff yarns with different distance were investigated. Figure 4.16 presents the Poisson's ratio - strain curves of three R1 sample with different arrangements of two stiff yarns. It can be found that the distance between two stiff yarns has a significant influence on the auxetic behaviour of the structure.

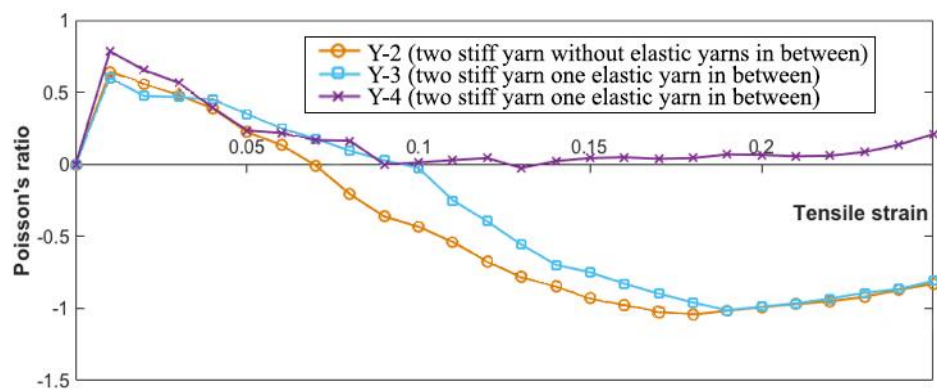


Figure 4.16 Poisson's-strain curves for R1 samples with two stiff yarns in the different distance.

From Figure 4.16, it can be found that the auxetic effect of R1 is weakened by increasing the distance between two stiff yarns. This phenomenon can be explained by

constructive and destructive interference between two waves. As the stiff yarn is helically wrapped onto the core in the R1 structure, the deformation of the core caused by the stiff yarn in the plane is in a wave shape. In case there are two stiff yarns in the structure, the overall deformation of the core under extension becomes a resulting wave of two wave shapes caused by each stiff yarn individually. Thus, as the increase in distance between two stiff yarns increases the phase difference between two waves, the lateral displacement of the core caused by them is smaller than that caused by each stiff yarn. As a result, the auxetic effect of the structure is weakened and a smaller negative PR effect is displayed. Especially, when two stiff yarns are wrapped onto the core with a phase difference of  $\pi$  (like Y-4 sample), the auxetic effect of the R1 structure is eliminated. This is because the wave shape (or lateral displacement) of the core caused by one stiff yarn is opposite to that caused by the other stiff yarn. Table 4.6 presents the photographs of three samples with different distance between two stiff yarns at different critical tensile strains, from which it can be seen that the overall deformation of the structure under extension is influenced by the position of two stiff yarns.

Table 4.6 The photographs of three samples of the R1 structure at different critical tensile strains.

Tensile strain	5%	15%	25%
Y-2	 $\nu = 0.22$	 $\nu = -0.92$	 $\nu = -0.80$
Y-3	 $\nu = 0.35$	 $\nu = -0.75$	 $\nu = -0.81$
Y-4	 $\nu = 0.23$	 $\nu = 0.04$	 $\nu = 0.21$

From the analysis on the structure HL, it is known that the diameter of elastic braiding yarns could influence the Poisson's ratio of the structure under tension. To further evaluate the influence of component yarn diameter, the Poisson's ratio-strain curves of three different types of R1 made with the same stiff yarn, but with different elastic yarns and core yarns are compared in Figure 4.17

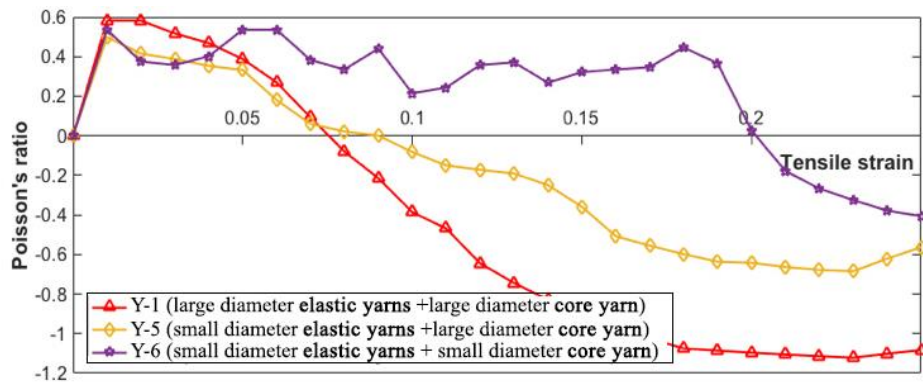


Figure 4.17 Poisson's-strain curves for R1 samples with two stiff yarns with the same stiff yarn, but with different elastic yarns and core yarns.

By comparing curves of Y-1 and Y-5 in Figure 4.17 Poisson's-strain curves for R1 samples with two stiff yarns with the same stiff yarn, but with different elastic yarns and core yarns., it can be found the effect of elastic yarn diameter is evident at both small and large strains. R1 structure with larger elastic yarn diameter exhibits a higher positive Poisson's ratio at small tensile strains. This can be attributed to the fact that the major deformation of the R1 structure at small tensile strains is the reduction in the cross-section size, which is resulted from the diameter decrease in single yarn components. As the Poisson's ratio of elastic yarns used here is higher than that of the core, the use of larger elastic yarn diameter also causes a larger reduction in the cross-section size of the R1 structure and thus yielding a higher positive Poisson's ratio. This situation, however, is inverted after the tensile strain exceeds 8%. The R1 structure which has larger elastic yarn diameter triggers its auxetic effect earlier and presents a

larger maximum negative PR than that of R1 structure with smaller elastic yarn diameter. This result can be attributed to the phenomenon as explained before, that is, the employment of elastic yarn reduces the value difference between the initial diameter of the core and the initial transverse width of the R1 structure. As the larger elastic yarn diameter leads to a larger reduction in that difference, an earlier activation of auxetic behaviour is presented. At the same time, this early activation of auxetic effect also leads to a larger maximum negative PR under the same degree of structural deformation. The other reason is the R1 with larger braiding elastic yarn diameter also has a larger braid diameter and thus the cross-sectional contour size increases in the R1 structure is more significant. Because of these reasons, the negative PR effect of the R1 with larger elastic yarn diameter is activated earlier and kept larger than that of the R1 with smaller braiding yarn diameter to a tensile strain of 25%.

By comparing curves of Y-5 and Y-6 in Figure 4.17, it can also be seen that the auxetic effect of the R1 is significantly influenced by the core diameter. An earlier activation of the auxetic effect as well as a larger maximum negative PR is exhibited in R1 structure with larger core diameter. This phenomenon is consistent with the findings in a helical auxetic yarn system [39], where a higher core/stiff diameter ratio provides a better auxetic performance. The main reason for this phenomenon is that R1 structure with larger core diameter also has a larger lateral displacement under extension and therefore presenting a higher maximum negative PR. Meanwhile, the increase in diameter of the core simultaneously increases the diameter ratio between core/elastic yarns so that the effect of elastic yarn on the transverse width of the structure is weakened. As a result, the decrease in the transverse width at small strains of the R1 structure with larger core diameter is smaller, thus presenting an earlier decrease in the Poisson's ratio.

#### 4.4 Conclusions

In this chapter, a preliminary experimental study was conducted to investigate the negative PR effect of developed six auxetic tubular braids and the effects of different structural and material parameters. Based on the results gained from the testing, following conclusions are drawn for the negative PR effect of developed six auxetic tubular braids:

- All developed six tubular braids presented a negative PR effect when stretched. Among them, two structures, i.e., the HC structure and R2 structure exhibited different Poisson's ratio values in different planes, negative in one plane and positive in its orthogonal plane.
- Structures with core yarn inside have a lower positive Poisson's ratio at small tensile strains compared to those without core yarn inside.
- For all produced structure, the transverse length of them decreased first before it increased.

On the other hand, following conclusions are drawn for the effects of different structural and material parameters on the negative PR effect of the structure:

- All selected three structural parameters, i.e., the initial wrap angle, the initial braiding angle and the braiding yarn diameter have influences on the negative PR effect of the auxetic tubular braided structure HL. Overall, the HL structure with a lower initial wrap angle, a higher initial braiding angle and a larger braiding yarn diameter has a better auxetic performance under tension.
- All selected three structural parameters, i.e., the stiff yarn number, the distance between two stiff yarns in the structure and the component yarn diameter have influences on the negative PR effect of the auxetic tubular braided structure

R1. Overall, the R1 structure with larger elastic yarn diameter, larger core diameter has a better auxetic performance.

## **CHAPTER 5 THEORETICAL ANALYSIS OF THE AUXETIC BRAIDED STRUCTURE**

### **5.1 Introduction**

This chapter presents the theoretical analysis of the developed two auxetic braided structures, i.e., HL and R1, which have similar shape deformation mechanism under tension. An analytical model which can be used to predict the Poisson's ratio of structure under axial extension is developed based on the existed geometric relationships. The developed model is first compared with the experimental data obtained in Chapter 4 in order to validate its accuracy. Using the results calculated from the established model, the effects of identified parameters on the Poisson's ratio of the structure then was discussed.

### **5.2 Analytical modelling**

#### **5.2.1 Uniaxial extension structural deformation analysis**

As presented in the Section 3.2.1 and Section 3.3.1, the unique geometry designs of structure HL and structure R1 had provided them with a special helical shape deformation when longitudinally extended. In detail, this structural deformation can be divided into two stages and can be described as follows.

The first stage starts with the initial and ends when the structure reaches its largest contour cross-sectional width. As shown in Figure 5.1, in this stage the stiff yarn straightens upon application of a longitudinal tensile strain and in doing so displaces the braiding yarns and the core yarn laterally. The whole structure which is of straight tubular shape in the initial state is then converted into a wave shape when stretched. During that process, the helical radius of the stiff yarn decreases with the continued

applying of stretching. Meanwhile, the helical radius of the core yarn and braiding yarns increases. The cross-sectional contour size of the whole structure then reaches its maximum value when the stiff yarn becomes straight along the center line of the whole structure.

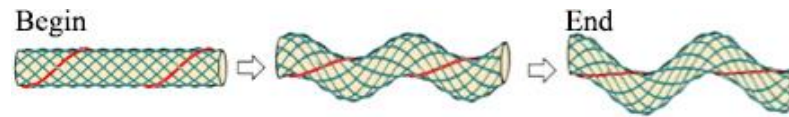


Figure 5.1 The deformation of the structure in the first stage.

The second stage starts from the end of the first stage and ends with the failure of the stiff wrap yarn. As shown in Figure 5.2, in this stage the stiff yarn cannot displace the core yarn and braiding yarns laterally to further extent as it is completely extended to a straight line along the center line. Because of that, the effective diameter of the structure (which is equal to the minimum diameter of a tubular that can contain the whole structure inside) decreases with the increased tensile strain due to the decrease of the cross-sectional size of the three component yarns as well as the reduction of the helical wave shape of the braided structure. This situation continues until the stiff yarn fails eventually due to excessive stretching. At that time, the whole structure immediately converts back into a straight shape.

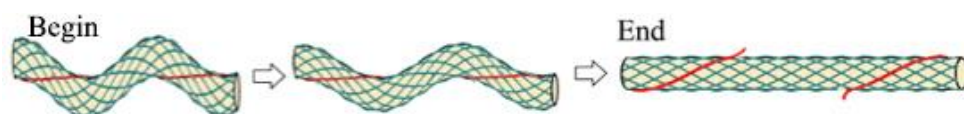


Figure 5.2 The deformation of the structure HL in the second stage.

### 5.2.2 Basic assumptions

From above, it can be seen that the deformation of two structures during the tensile process presented a typical helical shape change. There, an analytical model which is similar to that of the helical auxetic yarn [125] can be established and used to

theoretically predict the overall Poisson's ratio behaviour of two structures with following assumptions.

(1) The Poisson's ratio of all component yarns is constant during the whole tensile process.

(2) The cross-section of component yarns has a perfectly regular shape during the whole tensile process.

(3) The interactions force and the relative slippage effect between three component yarns are neglected.

(4) The crimp of the stiff yarn in both HL and R1 structure is neglected and thus the shape of it before the tensile process is a perfect helical shape.

(5) From the experimental results presented in Section 4.3.4, it can be found that the effects of the initial braiding angle on the negative PR effect of the structure are not evident. Based on that finding, the braiding angle is assumed to be kept unchanged during the whole tensile process in this analytical model.

(6) In the first stage, there are only shape changes in the stiff yarn, i.e., from a helical to a straight line, and thus it has no longitudinal extension. As a result, the diameter of it is constant. Meanwhile, the diameter of the braiding yarns and the core yarn decreases due to the elongation and helical shape change. In the third stage, the stiff yarn becomes straight along the center line of the whole structure and thus the continued stretching will cause it extended and contract. Meanwhile, the diameter of the braiding yarns and the core yarn continues decreasing because of the further stretching.

Based on the above assumptions, mathematic formulations where Poisson's ratio of the structure is represented its seven parameters, namely the initial helical angle of stiff wrap yarn  $\beta_0$ ; the Poisson's ratio of component yarns, including  $\nu_w$  for the stiff

yarn,  $\nu_b$  for braiding yarns and  $\nu_c$  for the core yarn; and the initial diameter of the component yarns, including  $D_w$  for stiff yarn,  $D_b$  for braiding yarns and  $D_c$  for the core yarn, had been devised in this analytical model. The detailed derivation process is presented as follows.

### 5.2.3 The Poisson's ratio of structure in the first stage.

Based on the Poisson's law, the Poisson's ratio of the whole structure can be expressed as;

$$\nu = -\varepsilon_t \times \frac{1}{\varepsilon_l} = -\frac{H-H_0}{H_0} \times \frac{1}{\varepsilon_l} \quad (5.1)$$

where  $\varepsilon_t, \varepsilon_l$  are the transverse and longitudinal strains of whole auxetic structure respectively while  $H_0$  and  $H$  are the maximum transverse length of whole auxetic structure at zero strain and  $\varepsilon_l$  strain respectively. Therefore, in order to establish the geometrical relationship between Poisson's ratio of the structure and its seven parameters, it is necessary to represent the  $H_0$  and  $H$  with selected seven parameters and longitudinal strain of the whole auxetic structure  $\varepsilon_l$ .

To represent the  $H_0$  with selected structural parameters, one cycle of the structure is taken, as shown in Figure 5.3. Based on the assumption (3) that interactions force between three components yarns are neglected, the maximum transverse length of the hole auxetic structure at zero strain can be presented as:

$$H_0 = D_{c0} + 4D_{b0} + 2D_{w0} \quad (5.2)$$

where  $D_{c0}, D_{b0}$  and  $D_{w0}$  are the initial diameters of core yarn, braiding yarns and stiff yarn respectively. As for  $H$ , it is determined differently in the first stage according to the different value longitudinal strain  $\varepsilon_l$ . When  $\varepsilon_l$  is small, as the stiff yarn is

placed outside of the base braid, the transverse length of the whole auxetic structure is determined by the outer edge of the stiff wrap yarn as follows;

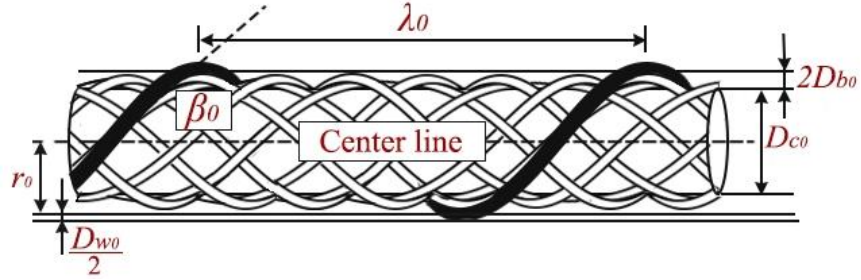


Figure 5.3 One geometry cycle of the structure in the initial state.

$$H = 2r + D_w \quad (5.3)$$

where  $r$  and  $D_w$  are the helical radius and diameter of the stiff wrap yarn at  $\varepsilon_l$  strain respectively. However, the situation reversed when  $\varepsilon_l$  becomes large. The stiff yarn which are placed outside of the base braid moves into the inner place with the increase of the  $\varepsilon_l$  and the base braid gradually expands into the outer place. Thus, the cross-sectional width of the whole auxetic structure becomes being determined by the outer edge of the base braid. Based on the assumption (3) and (5), core yarn and braiding yarn share a same helical radius. Thus, the  $H$  can be obtained in the Equation (5.4);

$$H = 2R + D_c + 4D_b \quad (5.4)$$

where  $R$  is the helical radius of core yarn and braiding yarn while  $D_c$  and  $D_b$  are the diameter of the core yarn and braiding yarn at  $\varepsilon_l$  strain respectively. The cross-sectional width of the whole auxetic structure at any given stain in the first stage then should be the larger value obtained from Equation (5.3) and Equation (5.4), which is given as follows;

$$H = \text{Max} (2r + D_w, 2R + D_c + 4D_b) \quad (5.5)$$

Since the diameter of the stiff yarn is kept unchanged in the first stage;

$$D_w = D_{w0} \quad (5.6)$$

It is required to present  $r$ ,  $R$ ,  $D_c$  and  $D_b$  with seven known structural parameters. Since there is no elongation in the length of stiff yarn per pitch in the first stage, the  $r$  then can be calculated by rolling out one cycle of the structure at zero stain and at  $\varepsilon_l$  into a flat surface, as shown in Figure 5.4.

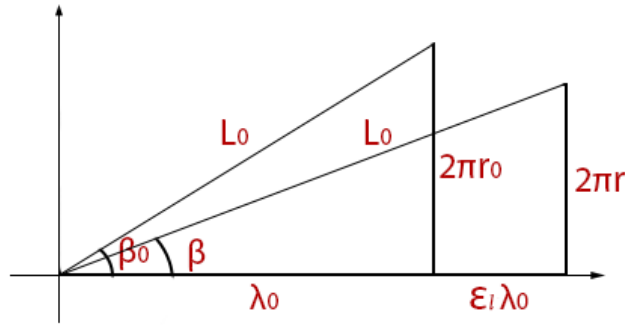


Figure 5.4 Trigonometric relationship exists between  $r$  and  $\varepsilon_l$ .

Based on the triangle relationship between  $r$  and  $\varepsilon_l$  in Figure 5.4, we have;

$$r = \frac{L_0 \sin \beta}{2\pi} = \frac{r_0 \sqrt{1 - (1 + \varepsilon_l)^2 \cos^2 \beta_0}}{\sin \beta_0} \quad (5.7)$$

From Figure 5.3, it can be known that the initial helical radius of the stiff yarn  $r_0$  is:

$$r_0 = \frac{(D_{c0} + 4D_{b0} + D_{w0}) \sqrt{1 - (1 + \varepsilon_l)^2 \cos^2 \beta_0}}{2 \sin \beta_0} \quad (5.8)$$

By substituting Equation (5.8) into Equation (5.7), the  $r$  can be represented by known structural parameters as:

$$r = \frac{(D_{c0} + 4D_{b0} + D_{w0}) \sqrt{1 - (1 + \varepsilon_l)^2 \cos^2 \beta_0}}{2 \sin \beta_0} \quad (5.9)$$

In order to present  $R$ ,  $D_c$  and  $D_b$  with known structural parameters, a cross section of the structure when the structure is deformed into a helical shape is presented in the Figure 5.5. With the relationship between  $\beta$  and the helical radius of the stiff wrap yarn  $r$ , the helical radius of the base braided structure  $R$  can be calculated as follows:

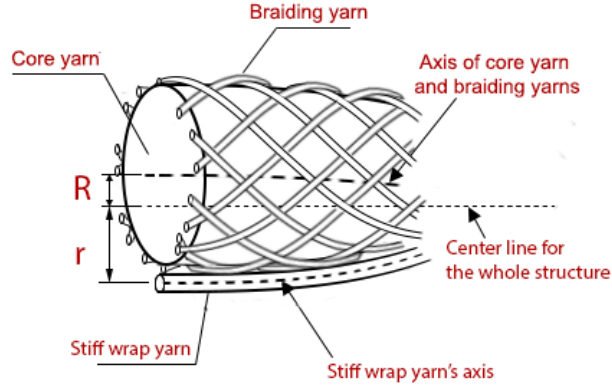


Figure 5.5 The cross-section of the structure when the structure is deformed into a helical shape.

$$R = \frac{(D_c + 4D_b + D_w)}{2} - r = \frac{(D_c + 4D_b + D_{w0})}{2} - \frac{(D_{c0} + 4D_{b0} + D_{w0})\sqrt{1 - (1 + \epsilon_l)^2 \cos^2 \beta_0}}{2 \sin \beta_0} \quad (5.10)$$

According to the Poisson's law, the diameter of the core yarn  $D_b$  is;

$$D_c = D_{c0}(1 - \nu_c \epsilon_c) \quad (5.11)$$

Base on the assumption (3) and (5), it can be known that braiding yarn has a same longitudinal strain of the core yarn. Thus, the diameter of braiding yarn is:

$$D_b = D_{b0}(1 - \nu_b \epsilon_c) \quad (5.12)$$

The  $\epsilon_c$  then can be obtained by the triangle relationship between the helical radius of the core yarn and the longitudinal strain of the whole structure in the Figure 5.6 as:

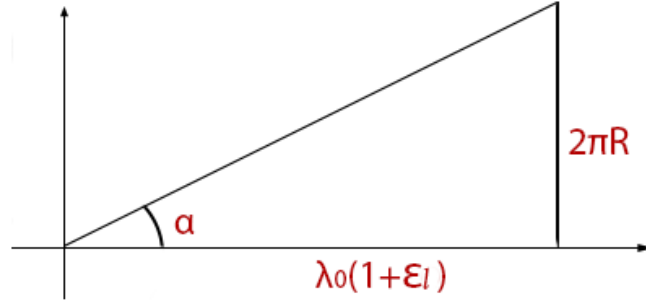


Figure 5.6 The triangle relationship between the helical radius of the core yarn and the longitudinal strain of the whole structure.

$$\varepsilon_b = \frac{\sqrt{(2\pi R)^2 + \lambda_0^2 (1 + \varepsilon_l)^2} - \lambda_0}{\lambda_0} \quad (5.13)$$

According to Figure 5.3 and Figure 5.4,  $\lambda_0$  and  $\beta_0$  have the following relations:

$$\lambda_0 = \frac{\pi(D_{c0} + 4D_{b0} + D_{w0})}{\tan \beta_0} \quad (5.14)$$

By substituting Equations (5.11) to (5.14) into Equation (5.10), the helical radius of the core yarn and braiding yarns in the first stage can be represented with selected parameters as;

$$R = \frac{D_{c0} \left( 1 + \nu_c - \frac{\nu_c \sqrt{(2\pi R \tan \beta_0)^2 + \pi^2 (D_{c0} + 4D_{b0} + D_{w0})^2 (1 + \varepsilon_l)^2}}{\pi (D_{c0} + 4D_{b0} + D_{w0})} \right)}{2} + 2D_{b0} \left( 1 + \nu_c - \frac{\nu_b \sqrt{(2\pi R \tan \beta_0)^2 + \pi^2 (D_{c0} + 4D_{b0} + D_{w0})^2 (1 + \varepsilon_l)^2}}{\pi (D_{c0} + 4D_{b0} + D_{w0})} \right) + \frac{D_{w0}}{2} - \frac{(D_{c0} + 4D_{b0} + D_{w0}) \sqrt{1 - (1 + \varepsilon_l)^2 \cos^2 \beta_0}}{2 \sin \beta_0} \quad (5.15)$$

It can be seen from Equation (5.15) that the  $R$  of the base braid can be solved because there is only one unknown parameter and  $R$  varies from the longitudinal strain  $\varepsilon_l$  of the whole structure when stretched. With the Equation (5.1), (5.5), (5.6), (5.9) and (5.15), the Poisson's ratio of the structure in the first stage then can be expressed as follows;

$$v = \text{Max}(v_1, v_2) \begin{cases} v_1 = -\frac{(D_{c0}+4D_{b0}+D_{w0})\sqrt{1-(1+\varepsilon)^2 \cos^2 \beta_0} - \sin \beta_0 (D_{c0}+4D_{b0}+2D_{w0})}{\varepsilon_1 \sin \beta_0 (D_{c0}+4D_{b0}+2D_{w0})} \\ v_2 = -\frac{\left\{ D_{c0} \left[ \frac{\sqrt{(2\pi R \tan \beta_0)^2 + \pi^2 (D_{c0}+4D_{b0}+D_{w0})^2 (1+\varepsilon)^2}}{\pi(D_{c0}+4D_{b0}+D_{w0})} \right] + D_{b0} \left[ \frac{\sqrt{(2\pi R \tan \beta_0)^2 + \pi^2 (D_{c0}+4D_{b0}+D_{w0})^2 (1+\varepsilon)^2}}{\pi(D_{c0}+4D_{b0}+D_{w0})} \right] - D_{w0} \right\} \frac{(D_{c0}+4D_{b0}+D_{w0})\sqrt{1-(1+\varepsilon)^2 \cos^2 \beta_0}}{\sin \beta_0}}{\varepsilon_1 (D_{c0}+4D_{b0}+2D_{w0})} \end{cases} \quad (5.16)$$

Meanwhile, based on the assumption that the stiff yarn has no elongation in the first stage and it becomes straight at the end, the longitudinal strain of the structure at the end of the first stage  $\varepsilon_{cri}$  can be calculated from the Figure 5.4 as:

$$\varepsilon_{cri} = \frac{L_0 - \lambda_0}{\lambda_0} = \frac{1}{\cos \beta} - 1 \quad (5.17)$$

#### 5.2.4 The Poisson's ratio of structure in the second stage.

Differ from the situation in the first stage, the maximum transverse length of whole structure in the second stage is always determined by the outer edge of the braiding yarns because the stiff yarn becomes straight along the center line. Base on the Equation (5.1), (5.2) and (5.4), the Poisson's ratio of the structure in the second stage then is:

$$\nu = \frac{2R+D_c+4D_b-H_0}{H_0} \times \frac{1}{\varepsilon_x} = \frac{2R+D_c+4D_b-D_{c0}-4D_{b0}-2D_{w0}}{\varepsilon_x(D_{c0}+4D_{b0}+2D_{w0})} \quad (5.18)$$

Based on the Equation (5.18), it is required to represent  $R$ ,  $D_c$  and  $D_b$  with known structural parameters. In the second stage, as there is no separation between the components, the helical radius of core yarn and braiding yarns can be expressed as follows.

$$R = \frac{(D_w+D_c+4D_b)}{2} \quad (5.19)$$

As all three component yarns have a radial contraction in this stage, their diameter has the following formula according to the Poisson's law;

$$\begin{cases} D_c = D_{c0}(1 - \nu_c \varepsilon_c) \\ D_c = D_{b0}(1 - \nu_b \varepsilon_b) \\ D_w = D_{w0}(1 - \nu_w \varepsilon_w) \end{cases} \quad (5.20)$$

Compared with its original length  $\lambda_0$ , the longitudinal strain of the core yarn  $\varepsilon_c$  can be obtained from Figure 5.7.

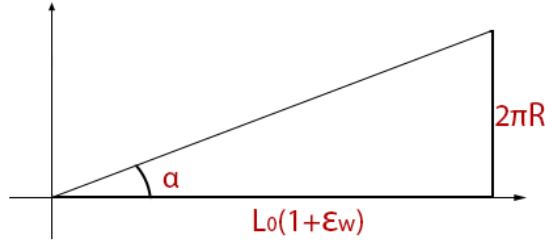


Figure 5.7 The triangle relationship between the helical radius of the core yarn and the longitudinal strain of the stiff yarn.

$$\varepsilon_c = \frac{\sqrt{(2\pi R)^2 + L_0^2(1 + \varepsilon_w)^2} - \lambda_0}{\lambda_0} \quad (5.21)$$

Based on the assumption, the longitudinal strain of braiding yarns is equal to that of core yarn, thus;

$$\varepsilon_b = \varepsilon_c = \frac{\sqrt{(2\pi R)^2 + L_0^2(1 + \varepsilon_w)^2} - \lambda_0}{\lambda_0} \quad (5.22)$$

As it is assumed that the stiff yarn in the second stage is completely straight along the center line, the longitudinal strain of stiff yarn  $\varepsilon_w$  can be obtained according to its relationship with the longitudinal strain of the whole auxetic structure  $\varepsilon_l$ , which is:

$$L_0(1 + \varepsilon_w) = \lambda_0(1 + \varepsilon_l) \quad (5.23)$$

Based on the relationships between  $L_0$ ,  $\lambda_0$  and  $\beta_0$  in Figure 1 and Figure 2, the Equations (5.21), (5.22) and (5.23) can be expressed as Equation (5.24).

$$\begin{cases} \varepsilon_c = \frac{\sqrt{(2\pi R)^2 \tan^2 \beta_0 + \frac{\pi^2 (D_{c0} + 4D_{b0} + D_{w0})^2 (1 + \varepsilon_l)^2}{\cos^2 \beta_0}}}{\pi (D_{c0} + 4D_{b0} + D_{w0})} - 1 \\ \varepsilon_b = \frac{\sqrt{(2\pi R)^2 \tan^2 \beta_0 + \frac{\pi^2 (D_{c0} + 4D_{b0} + D_{w0})^2 (1 + \varepsilon_l)^2}{\cos^2 \beta_0}}}{\pi (D_{c0} + 4D_{b0} + D_{w0})} - 1 \\ \varepsilon_w = (1 + \varepsilon_l) \cos \beta_0 - 1 \end{cases} \quad (5.24)$$

By substituting Equations (5.20) and (5.24) into Equation (5.19), the helical radius of the base braid  $R$  in the second stage is:

$$R = \frac{D_{c0} \left( 1 + \nu_c - \nu_c \frac{\sqrt{(2\pi R)^2 \tan^2 \beta_0 + \frac{\pi^2 (D_{c0} + 4D_{b0} + D_{w0})^2 (1 + \varepsilon_l)^2}}{\pi (D_{c0} + 4D_{b0} + D_{w0})}}{2} \right) + 2D_{b0} \left( 1 + \nu_b - \nu_b \frac{\sqrt{(2\pi R)^2 \tan^2 \beta_0 + \frac{\pi^2 (D_{c0} + 4D_{b0} + D_{w0})^2 (1 + \varepsilon_l)^2}}{\pi (D_{c0} + 4D_{b0} + D_{w0})}} \right) + \frac{D_{w0} (1 + \nu_w - \nu_w (1 + \varepsilon_l) \cos \beta_0)}{2}}{2} \quad (5.25)$$

Based on the Equations (5.20), (5.24) and (5.25), the Poisson's ratio of the structure in the second stage is:

$$\nu = \frac{D_{c0} \left( \nu_c - \nu_c \frac{\sqrt{(2\pi R)^2 \tan^2 \beta_0 + \frac{\pi^2 (D_{c0} + 4D_{b0} + D_{w0})^2 (1 + \varepsilon_l)^2}}{\pi (D_{c0} + 4D_{b0} + D_{w0})}}{\varepsilon_l (D_{c0} + 4D_{b0} + D_{w0})} \right) + 4D_{b0} \left( \nu_b - \nu_b \frac{\sqrt{(2\pi R)^2 \tan^2 \beta_0 + \frac{\pi^2 (D_{c0} + 4D_{b0} + D_{w0})^2 (1 + \varepsilon_l)^2}}{\pi (D_{c0} + 4D_{b0} + D_{w0})}}{\varepsilon_l (D_{c0} + 4D_{b0} + D_{w0})} \right) + \frac{D_{w0} (1 + \nu_w - \nu_w (1 + \varepsilon_l) \cos \beta_0) - 2D_{w0}}{\varepsilon_l (D_{c0} + 4D_{b0} + D_{w0})}}{\varepsilon_l (D_{c0} + 4D_{b0} + D_{w0})} \quad (5.26)$$

### 5.3 Model validation

In order to validate the accuracy of the established analytical model, the results calculated from the mathematic formulations generated in the model were compared with those obtained from the experiment testing. In this case, the initial values of geometrical parameters in the model are set to be the same as those of Sample HL1 and R1a which were investigated in Chapter 4 and are relisted in Table 5.1. The

Poisson's ratio values as a function of tensile strain obtained from the experiment and theoretical calculation are shown in Figure 5.8. It can be found that the Poisson's ratio value calculated from the analytical model are much larger than those from the experiment due to the model is established only based on the geometry relationships without considering the interaction between component yarns. Another reason is that the interlacement between stiff yarn and other elastic braiding yarns in both HL and R1 structures are not considered in the model and thus the shape of stiff yarn in the model is different from its shape in real state. In the meantime, it is due to this ignorance of the interlacement between stiff yarn and other elastic braiding yarns that the geometrical model here cannot discriminate the difference between these two structures. However, since the Poisson's ratio – strain obtained from the model have the same variation trend with those obtained from the experimental testing, and the tensile strain where the negative Poisson's effect is activated is almost same to that of R1 and HL, this model is capable of predicting the overall Poisson's ratio behavior trend of these two structures. Therefore, the model is used to qualitatively analysis the effect of the structural parameters on the negative PR behaviour of the structure HL and R1 in this study.

Table 5.1 The geometrical parameters in the initial state used for theoretical calculation.

Initial diameter			Poisson's ratio			Initial wrap angle of stiff yarn
core yarn $D_{c0}$	Braiding yarn $D_{b0}$	Stiff yarn $D_{w0}$	Core yarn $\nu_c$	Braiding yarn $\nu_b$	Stiff yarn $\nu_s$	
2.2 mm	0.7 mm	0.7 mm	0.32	0.47	0.65	35°

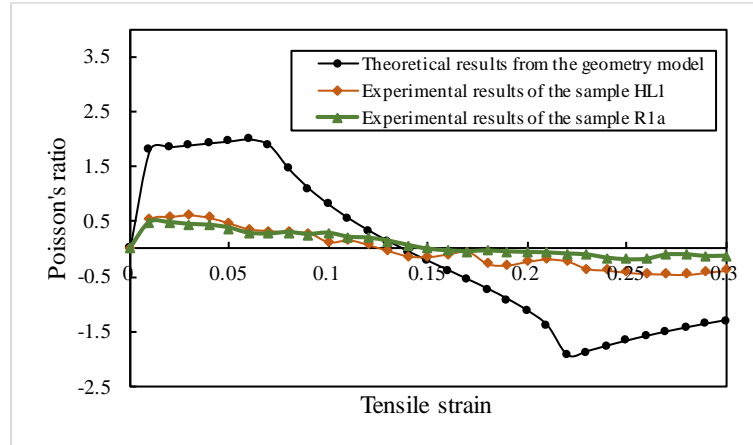


Figure 5.8 The comparison between results calculated from the established model and experimental results obtained from the testing for structures HL and R1.

## 5.4 Effects of parameters on the Poisson's ratio based on the analytical model

### 5.4.1 Effects of initial wrap angle of stiff yarn

In Chapter 6, it was found that the initial wrap angle could be used to tailor the Poisson's ratio of structure HL and a lower initial wrap angle would result in early activation of negative PR effect as well as a higher maximum negative PR value. This finding was validated by the results calculated from the analytical model, as shown in Figure 5.9. Besides that, it can also be found from the Figure 5.9 that the higher initial wrap angles would not only alleviate the auxetic behaviour of the structure but also could eliminate it; for example, the structure with an initial wrap angle of  $50^\circ$  presented a conventional positive Poisson's ratio when stretched. This is mainly because the stiff yarn in the structure with higher initial wrap angle has a longer length than that in the structure with lower initial wrap angle. Thus, larger tensile strains are required to straighten the stiff yarn completely. However, as the diameter component yarns decrease with the increase of the tensile strains. The diameter of the structure is much smaller than its initial value at large strains. Thus, even though the stiff yarn could

displace the structure laterally at large stains, the transverse length of the structure is still smaller than its initial diameter and thus presenting a positive Poisson's ratio. On the other hand, it is interesting to note that the structures with an initial wrap angle of 20° and 30° presented a similar Poisson's ratio after a tensile strain of 0.16. The probable reason is that the main deformation of the structure after the maximum Poisson's ratio value is the contraction of components yarns. As the Poisson's ratio and the initial diameter of used component yarns are same for the structures in Figure 5.9, the Poisson's ratio of them presented similar values at higher tensile strains.

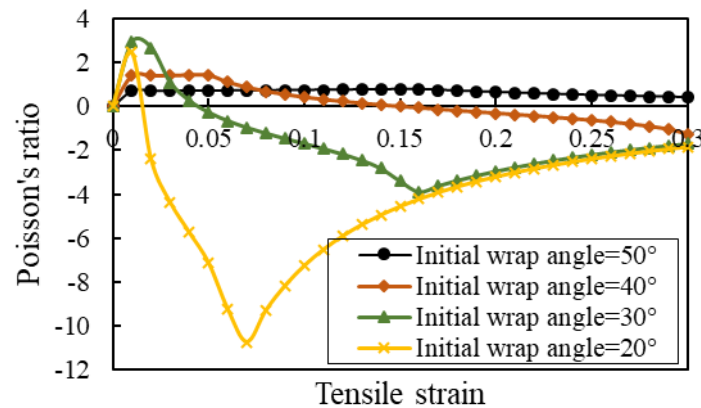


Figure 5.9 Effects of the initial wrap angle of the stiff yarn.

#### 5.4.2 Effects of the diameter of component yarns

In Chapter 4, the effects of diameters of elastic braiding yarns and core yarn had been analysed. Here, effects of the diameter of all three component yarns would be investigated by using the established analytical model. The Poisson's ratio – strain curves for structures with different core yarn diameters, different braiding yarn diameters and different stiff yarn diameters are presented in Figure 5.10a, 5.10b and 5.10c respectively.

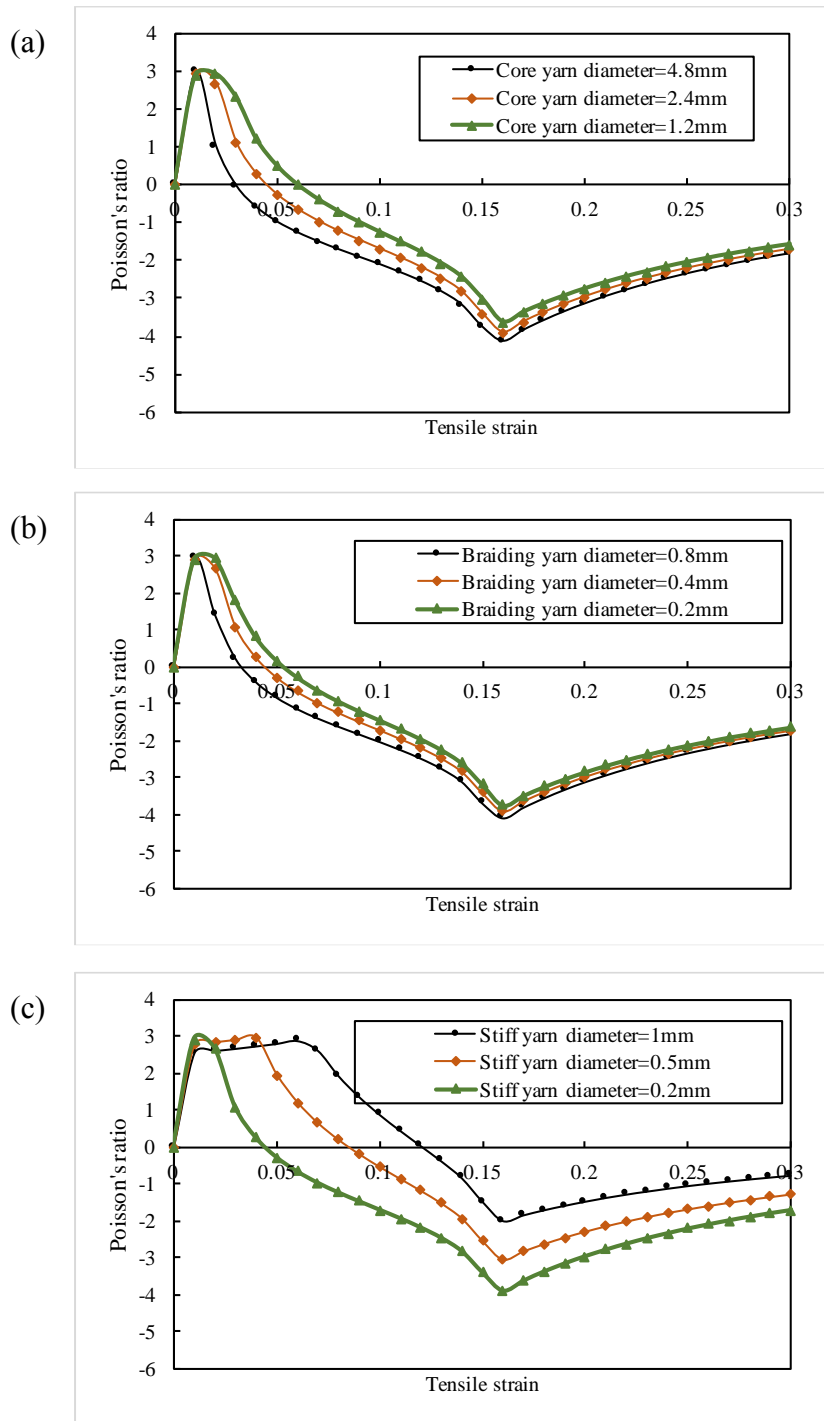


Figure 5.10 Effects of the diameter of components yarns on the negative PR effect of the structure: (a) effects of core yarn diameters; (b) effects of braiding yarn diameters; (c) effects of stiff yarn diameters.

As shown in Figure 5.10a and Figure 5.10b, the structure with larger core yarn diameter and larger braiding yarn diameter presented an early activation of the auxetic

behaviour as well as a larger maximum Poisson's ratio when stretched. This can be attributed to the fact that the increase of core yarn diameter and braiding yarn diameter would increase the lateral displacement caused by the stiff yarn and thus lower the Poisson's ratio of the structure. On the other hand, however, it can be found that the effect of the braiding yarn diameter is not as evident as that of the core yarn diameter. This is mainly because the diameter of braiding yarn is small compared to that of the core yarn and thus the changes in its diameter have less impact on the Poisson's ratio of the structure.

In contrast with the above, it can be found that the structure with larger stiff yarn diameter a delayed activation of the auxetic behaviour as well as a smaller maximum Poisson's ratio when stretched (Figure 5.10c). This is because the increase of the stiff yarn diameter would lessen the diameter difference between it and the whole structure. Therefore, less lateral displacement of the structure could be caused by the straightening of it. As a result, smaller negative Poisson's effect is exhibited in the structure with larger stiff yarn diameter.

#### **5.4.3 Effects of the Poisson's ratio of component yarns**

Besides the above two types of parameters, the influence of another material parameter, i.e., the Poisson's ratio of the component yarns, was analyzed here. The Poisson's ratio – strain curves for structures with different core yarn Poisson's ratios, different braiding yarn Poisson's ratio and different stiff yarn Poisson's ratio are presented in Figure 5.11a, Figure 5.11b and Figure 5.11c respectively.

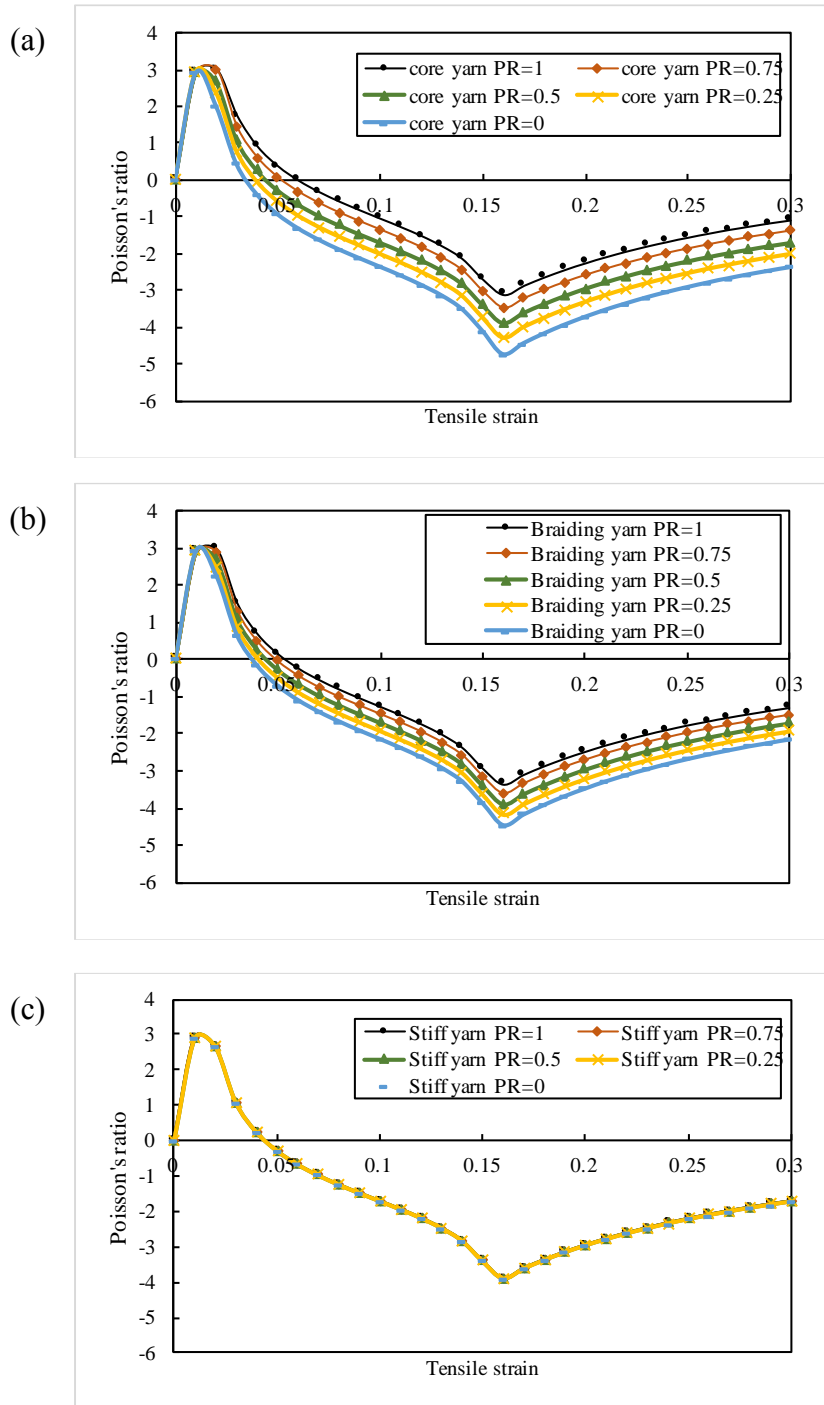


Figure 5.11 Effects of the Poisson's ratio of components yarns on the negative PR effect of the structure: (a) effects of core yarn Poisson's ratios; (b) effects of braiding yarn Poisson's ratios; (c) effects of stiff yarn Poisson's ratios.

As shown Figure 5.11a and Figure 5.11b, the maximum negative PR value of the structure increased with the decrease of the Poisson's ratio of the core yarn and

braiding yarns. This is because the contraction of the components is a major deformation of the structure when stretched beside its lateral displacement. As Poisson's ratio defines the ratio between the changes in width and length direction, components with lower Poisson's ratio has smaller diameter contraction when stretched. Therefore, the structure constructed by components with lower Poisson's ratio has a smaller diameter reduce and thus presents a lower Poisson's ratio. However, this effect is not evident for the stiff yarn, as shown in the Figure 5.11c, because the diameter of the stiff yarn is much smaller than those of the braiding yarns and the core yarn. Therefore, the change in the Poisson's ratio of it has less impact on the Poisson's ratio of the structure

## 5.5 Conclusions

In this chapter, the influence of structural parameters on the negative PR effect is studied via the theoretical analysis. Geometry relationships between the Poisson's ratio of the structure and its seven parameters were established for structure HL and R1 to investigate the effects of these structural parameters on negative PR effect of the structure. Based on the theoretical analysis, following conclusions could be obtained.

- The effects of the initial wrap angle of the stiff yarn on negative PR effect of the structure are evident. A lower initial wrap angle would result in a larger maximum Poisson's ratio value of the structure.
- The effects of the component diameter of component yarns on negative PR effect of the structure are apparent but not evident as the initial wrap angle. The structure with larger core yarn diameter, larger braiding yarn diameter and smaller stiff yarn diameter will present a larger maximum Poisson's ratio value.
- The effects of the Poisson's ratio of component yarns on negative PR effect of the structure are not as evident as previous two parameters, especially for that

of the stiff yarn. A lower initial wrap angle would result in a larger maximum Poisson's ratio value of the structure.

## **CHAPTER 6 CONCLUSIONS AND FUTURE WORK**

### **6.1 Conclusions**

This thesis is concerned with a systematic study of braided structures with negative PR. Its principal objects include design and fabrication of novel auxetic tubular braided structures, assessment of their negative PR behaviour under uniaxial loading condition, identification of the relationships between Poisson's ratio of the structure with its structural parameters via both experimental and theoretical analysis. The developed auxetic tubular braids show potential in commercial values, and the experimental and theoretical investigations on them laid a foundation for the further study of auxetic braids, auxetic fabrics as well as other auxetic materials. The main findings and achievements can be concluded as follows.

#### **6.1.1 Design and fabrication of the novel braided structures with negative PR**

In this study, six novel tubular braided structures with negative PR effect were successfully designed and fabricated via using two approaches, i.e., to wrap or insert extra stiff yarns onto the tubular braided structure and to employ both stiff yarns and elastic yarns in the braided structure. With the unique helical and trapezoidal geometry design in structure, all developed braids presented a shape change from a straight line to a crimp curve and therefore displaying a lateral size expansion as well as negative PR when stretched. As these developed auxetic braids could be fabricated using a slightly modified or a conventional circular braiding technology, they can be produced expertly with low cost.

#### **6.1.2 Experimental investigation on the developed six auxetic braided structures**

A tensile testing system consists of an Instron 5544 Universal Testing Machine, a high-

resolution CMOS camera and a computer was employed in order to assess the Poisson's ratio of developed auxetic braids. The results showed that all manufactured braids exhibited high negative PR behaviour when stretched and maintained this behaviour until the end of the testing. A similar variation trend of the Poisson's ratio value, which first increases and then decrease with the increase of the longitudinal tensile strain was exhibited in all developed six braided structures. Among them, the braid with an extra stiff yarn helically wrapped the tubular braided structure presented the largest maximum negative PR under tension. Meanwhile, different Poisson's ratio values were measured in different planes for two structures, a negative value in one plane and positive value in its orthogonal plane. On the other hand, by comparing the negative PR effect of samples with different parameter settings, it was found that auxetic braided structure with a larger core yarn diameter, a larger braiding yarn diameter, a smaller stiff yarn diameter, component materials with lower Poisson's ratio and a lower initial wrap angle presented a better negative PR effect when stretched.

### **6.1.3 Theoretical analysis of the developed six auxetic braided structures**

An analytical model based on geometrical relationships between components yarns was established in order to predict the Poisson's ratio of auxetic braided structure under extension. The accuracy of it was validated by comparing its results with the obtained experimental data. By using the established model, the effects of structural parameters, namely initial wrap angle of stiff yarn, the diameter of component yarns and the Poisson's ratio of component yarns, were thoroughly evaluated.

## **6.2 Contributions**

Materials and structures with negative PR, termed auxetics, have gained increased scientific interest in the past three decades due to their counter-intuitive behaviour and

enhanced properties. In contrast with the achievement of negative PR in textile fibers, yarns, knitted and woven or nonwoven fabrics, the development of auxetic braid is lagging. Given that, the completion of this study provides a way to design and fabricate novel auxetic braided structures with feasible approaches. The emerging of these novel auxetic braids may tackle the problems existed in the use of conventional positive Poisson's ratio braided products. On the other hand, the relationship between the negative PR effect of the developed auxetic braid and its parameters were found through the experiment work and theoretical analysis conducted in this study. Meanwhile, the deformation behaviour of these structures under uniaxial tension was clearly revealed. The developed analytical model could also be used to optimize the developed structure for desired performance criteria besides being the starting point for the analysis of structural influence on the negative PR effect and the approaches for designing auxetic tubular braid proposed in this study, i.e., to wrap or insert extra stiff yarns onto the base braided structure and to employ both stiff and elastic yarns in braided structure itself, could be utilized to develop various kinds of braids with different cross-sectional shapes.

### **6.3 Limitations**

Due to the constraints in time and resources, there were still limitations in this study, including:

- The experiment and theoretical investigation on the effect of different parameter settings on the Poisson's ratio did not cover all the auxetic tubular structure developed in this study.
- In the current analytical model, the crimp of stiff yarn in the initial state is not considered. Thus, the Poisson's ratio values of two structures calculated from analytical model failed to match the experimental results ideally.

- It is noticed that the stiff yarns in the structures R1, R2 and R3 are interlaced with other elastic braiding yarns and thus the path of it in the structure in the initial state is not in a helical shape but more like a sinusoidal wave, as shown in Figure 5.8a. This initial sinuous shape could influence the activation of the negative PR effect of the structure because the stiff yarn needs to be straightened before it could displace the structure laterally. However, the effect of it had not been evaluated in this study.
- In this study, the negative PR effect has been achieved only on the tubular braided structures. Other braided structures wait to be explored.

#### **6.4 Recommendation for future work**

Based on the work described in this thesis, the research on auxetic braided structures can be further enhanced and extended by the following:

- The effect of different parameter settings on the Poisson's ratio could be investigated by the experimental and theoretical analysis used in this study.
- In future analytical models, the crimp of stiff yarn in the initial state can be considered so that the accuracy of the theoretical results could be improved. Overall, it is believed that there could be three deformation stages in future analytical models instead of two deformation stages in the current analytical model. The new three stages could include the first stage where the stiff yarn changes its initial crimp shape into a helical shape, the second stage where the stiff yarn become straight and displace the braided structure laterally and the third stage where the diameter of the structure starts to decrease continuously.
- Tubular braided structures with different braiding patterns, such as diamond braid (stiff yarn goes on and under one elastic yarn), regular braid (stiff yarn goes on and under two elastic yarns) could be utilized to construct new auxetic

tubular braided structures because they have the different interlacement numbers between yarns and thus has different crimp shape of the stiff yarn. The negative PR effect of them can then be investigated and compared to analysis the influence of crimp shape of stiff yarn on the negative PR effect.

- Other braided structure, such as flat braid braided structure, 3D braided structures and braided structures with variable cross-sections, could be explored to design and fabricate braids with negative PR by using the two approaches developed in this study, i.e., to wrap or insert extra stiff yarns onto the base braided structure and to employ both stiff and elastic yarns in braided structure itself.

## REFERENCES

1. Kyosev, Yordan, *Braiding technology for textiles: principles, design and processes*. 2014: Elsevier.
2. Evans, K. E., M. A. Nkansah, I. J. Hutchinson, and S. C. Rogers, *Molecular Network Design*. Nature, 1991. **353**(6340): p. 124-124.
3. Alderson, K. L., A. Fitzgerald, and K. E. Evans, *The strain dependent indentation resilience of auxetic microporous polyethylene*. Journal of Materials Science, 2000. **35**(16): p. 4039-4047.
4. Lakes, RS and K Elms, *Indentability of conventional and negative Poisson's ratio foams*. Journal of Composite Materials, 1993. **27**(12): p. 1193-1202.
5. Scarpa, F and FC Smith, *Passive and MR fluid-coated auxetic PU foam—mechanical, acoustic, and electromagnetic properties*. Journal of intelligent material systems and structures, 2004. **15**(12): p. 973-979.
6. Wang, Z. Y. and H. Hu, *Auxetic materials and their potential applications in textiles*. Textile Research Journal, 2014. **84**(15): p. 1600-1611.
7. Sloan, MR, JR Wright, and KE Evans, *The helical auxetic yarn—a novel structure for composites and textiles; geometry, manufacture and mechanical properties*. Mechanics of Materials, 2011. **43**(9): p. 476-486.
8. Liu, Yanping, Hong Hu, Jimmy KC Lam, and Su Liu, *Negative Poisson's ratio weft-knitted fabrics*. Textile Research Journal, 2010. **80**(9): p. 856-863.
9. Hu, H., Z. Y. Wang, and S. Liu, *Development of auxetic fabrics using flat knitting technology*. Textile Research Journal, 2011. **81**(14): p. 1493-1502.
10. Ugbohue, S. C., Y. K. Kim, S. B. Warner, Q. G. Fan, C. L. Yang, O. Kyzymchuk, and Y. N. Feng, *The formation and performance of auxetic textiles. Part I: theoretical and technical considerations*. Journal of the Textile Institute, 2010. **101**(7): p. 660-667.
11. Alderson, K., A. Alderson, S. Anand, V. Simkins, S. Nazare, and N. Ravirala, *Auxetic warp knit textile structures*. Physica Status Solidi B-Basic Solid State Physics, 2012. **249**(7): p. 1322-1329.
12. Wright, J. R., M. K. Burns, E. James, M. R. Sloan, and K. E. Evans, *On the design and characterisation of low-stiffness auxetic yarns and fabrics*. Textile Research Journal, 2012. **82**(7): p. 645-654.
13. Zulifqar, Adeel, Tao Hua, and Hong Hu, *Development of uni-stretch woven fabrics with zero and negative Poisson's ratio*. Textile Research Journal, 2017: p. 0040517517715095.
14. Ng, W. S. and H. Hu, *Woven Fabrics Made of Auxetic Plied Yarns*. Polymers, 2018. **10**(2): p. 226.
15. Poisson, Siméon Denis, *Traité de mécanique, 2 vols*. Courcier, Paris, 1811.

16. Poisson, Siméon Denis, *Note sur les vibrations des corps sonores*. Ann. Chim. Phys, 1827. **36**: p. 86-93.
17. Greaves, G. N., A. L. Greer, R. S. Lakes, and T. Rouxel, *Poisson's ratio and modern materials*. Nat Mater, 2011. **10**(11): p. 823-837.
18. Lakes, R. S., *Negative-Poisson's-Ratio Materials: Auxetic Solids*. Annual Review of Materials Research, Vol 47, 2017. **47**(1): p. 63-81.
19. Love, AEH, *A Treatise on the Theory of Elasticity*. Cambridge Univ. Press, Cambridge, ed, 1927. **4**: p. 15.
20. Love, AEH, *A Treatise on the Mathematical Theory of Elasticity, 643 pp.* 1944, Dover Publications, New York, NY, USA.
21. Fung, Yuan-cheng, *Foundations of solid mechanics*. 1965: Prentice Hall.
22. Milton, Graeme W, *Composite materials with Poisson's ratios close to—1*. Journal of the Mechanics and Physics of Solids, 1992. **40**(5): p. 1105-1137.
23. Wang, YC and RS Lakes, *Composites with inclusions of negative bulk modulus: extreme damping and negative Poisson's ratio*. Journal of composite materials, 2005. **39**(18): p. 1645-1657.
24. Rouxel, Tanguy, H Ji, T Hammouda, and A Moréac, *Poisson's ratio and the densification of glass under high pressure*. Physical review letters, 2008. **100**(22): p. 225501.
25. Rouxel, Tanguy, *Elastic Properties and Short-to Medium-Range Order in Glasses*. Journal of the American Ceramic Society, 2007. **90**(10): p. 3019-3039.
26. Kelly, A, WR Tyson, and AH Cottrell, *Ductile and brittle crystals*. Philosophical magazine, 1967. **15**(135): p. 567-586.
27. Banerjee, Anirban, *Advances in physical metallurgy*. 1996: CRC Press.
28. Yang, Wei, Zhong-Ming Li, Wei Shi, Bang-Hu Xie, and Ming-Bo Yang, *Review on auxetic materials*. Journal of materials science, 2004. **39**(10): p. 3269-3279.
29. Choi, JB and RS Lakes, *Design of a fastener based on negative Poisson's ratio foam*. Cellular Polymers, 1991. **10**(3): p. 205-212.
30. Ai, L and X-L Gao, *Metamaterials with negative Poisson's ratio and non-positive thermal expansion*. Composite Structures, 2017. **162**: p. 70-84.
31. Ge, Zhaoyang, Hong Hu, and Shirui Liu, *A novel plied yarn structure with negative Poisson's ratio*. The Journal of The Textile Institute, 2016. **107**(5): p. 578-588.
32. Ha, Chan Soo, Michael E Plesha, and Roderic S Lakes, *Chiral three-dimensional isotropic lattices with negative Poisson's ratio*. physica status solidi (b), 2016. **253**(7): p. 1243-1251.
33. Ha, C. S., E. Hestekin, J. H. Li, M. E. Plesha, and R. S. Lakes, *Controllable thermal expansion of large magnitude in chiral negative Poisson's ratio lattices*.

- Physica Status Solidi B-Basic Solid State Physics, 2015. **252**(7): p. 1431-1434.
34. Ge, Z. Y. and H. Hu, *Innovative three-dimensional fabric structure with negative Poisson's ratio for composite reinforcement*. Textile Research Journal, 2013. **83**(5): p. 543-550.
  35. Li, D., L. Dong, and R. S. Lakes, *The properties of copper foams with negative Poisson's ratio via resonant ultrasound spectroscopy*. Physica Status Solidi B-Basic Solid State Physics, 2013. **250**(10): p. 1983-1987.
  36. Hou, Xiaonan, Hong Hu, and Vadim Silberschmidt, *A novel concept to develop composite structures with isotropic negative Poisson's ratio: effects of random inclusions*. Composites Science and Technology, 2012. **72**(15): p. 1848-1854.
  37. Miller, W, Z Ren, CW Smith, and KE Evans, *A negative Poisson's ratio carbon fibre composite using a negative Poisson's ratio yarn reinforcement*. Composites Science and Technology, 2012. **72**(7): p. 761-766.
  38. Miller, W, PB Hook, Christopher W Smith, X Wang, and Kenneth E Evans, *The manufacture and characterisation of a novel, low modulus, negative Poisson's ratio composite*. Composites Science and Technology, 2009. **69**(5): p. 651-655.
  39. Kocer, C., D. R. McKenzie, and M. M. Bilek, *Elastic properties of a material composed of alternating layers of negative and positive Poisson's ratio*. Materials Science and Engineering a-Structural Materials Properties Microstructure and Processing, 2009. **505**(1-2): p. 111-115.
  40. Grima, J. N., R. Gatt, N. Ravirala, A. Alderson, and K. E. Evans, *Negative Poisson's ratios in cellular foam materials*. Materials Science and Engineering a-Structural Materials Properties Microstructure and Processing, 2006. **423**(1-2): p. 214-218.
  41. Ravirala, Naveen, Kim L Alderson, Philip J Davies, Virginia R Simkins, and Andrew Alderson, *Negative Poisson's ratio polyester fibers*. Textile research journal, 2006. **76**(7): p. 540-546.
  42. N. Grima, Joseph, Andrew Alderson, and Kenneth E. Evans, *An alternative explanation for the negative Poisson's ratios in auxetic foams*. Journal of the Physical Society of Japan, 2005. **74**(4): p. 1341-1342.
  43. Brandel, B. and R. S. Lakes, *Negative Poisson's ratio polyethylene foams*. Journal of Materials Science, 2001. **36**(24): p. 5885-5893.
  44. Wang, Y. C., R. Lakes, and A. Butenhoff, *Influence of cell size on re-entrant transformation of negative Poisson's ratio reticulated polyurethane foams*. Cellular Polymers, 2001. **20**(6): p. 373-385.
  45. Xu, Bing, Francisco Arias, Scott T Brittain, Xiao-Mei Zhao, Bartosz Grzybowski, Salvatore Torquato, and George M Whitesides, *Making negative Poisson's ratio microstructures by soft lithography*. Advanced materials, 1999. **11**(14):

- p. 1186.
46. Baughman, R. H., J. M. Shacklette, A. A. Zakhidov, and S. Stafstrom, *Negative Poisson's ratios as a common feature of cubic metals*. *Nature*, 1998. **392**(6674): p. 362-365.
  47. Zhang, R. G., H. L. Yeh, and H. Y. Yeh, *A preliminary study of negative Poisson's ratio of laminated fiber reinforced composites*. *Journal of Reinforced Plastics and Composites*, 1998. **17**(18): p. 1651-1664.
  48. He, C. B., P. W. Liu, and A. C. Griffin, *Toward negative Poisson ratio polymers through molecular design*. *Macromolecules*, 1998. **31**(9): p. 3145-3147.
  49. Larsen, U. D., O. Sigmund, and S. Bouwstra, *Design and fabrication of compliant micromechanisms and structures with negative Poisson's ratio*. *Journal of Microelectromechanical Systems*, 1997. **6**(2): p. 99-106.
  50. Theocaris, P. S., G. E. Stavroulakis, and P. D. Panagiotopoulos, *Negative Poisson's ratios in composites with star-shaped inclusions: A numerical homogenization approach*. *Archive of Applied Mechanics*, 1997. **67**(4): p. 274-286.
  51. Choi, J. B. and R. S. Lakes, *Fracture toughness of re-entrant foam materials with a negative Poisson's ratio: Experiment and analysis*. *International Journal of Fracture*, 1996. **80**(1): p. 73-83.
  52. Chen, CP and RS Lakes, *Micromechanical analysis of dynamic behavior of conventional and negative Poisson's ratio foams*. *Journal of Engineering Materials and Technology*, 1996. **118**(3): p. 285-288.
  53. Pickles, A. P., K. L. Alderson, and K. E. Evans, *The effects of powder morphology on the processing of auxetic polypropylene (PP of negative Poisson's ratio)*. *Polymer Engineering and Science*, 1996. **36**(5): p. 636-642.
  54. Clarke, JF, RA Duckett, PJ Hine, IJ Hutchinson, and IM Ward, *Negative Poisson's ratios in angle-ply laminates: theory and experiment*. *Composites*, 1994. **25**(9): p. 863-868.
  55. Lakes, Roderic, *Advances in negative Poisson's ratio materials*. *Advanced Materials*, 1993. **5**(4): p. 293-296.
  56. Lakes, RS, *Design considerations for negative Poisson's ratio materials*. *ASME Journal of Mechanical Design*, 1993. **115**: p. 696-700.
  57. Choi, JB and RS Lakes, *Non-linear properties of polymer cellular materials with a negative Poisson's ratio*. *Journal of Materials Science*, 1992. **27**(17): p. 4678-4684.
  58. Yeganeh-Haeri, Amir, Donald J Weidner, and John B Parise, *Elasticity of a-cristobalite: a silicon dioxide with a negative Poisson's ratio*. *Science*, 1992. **257**(5070): p. 650-652.

59. Alderson, KL and KE Evans, *The fabrication of microporous polyethylene having a negative Poisson's ratio*. Polymer, 1992. **33**(20): p. 4435-4438.
60. Smith, WALLACE ARDEN. *Optimizing electromechanical coupling in piezocomposites using polymers with negative Poisson's ratio*. in *Ultrasonics Symposium, 1991. Proceedings., IEEE 1991*. 1991. IEEE.
61. Lakes, Roderic, *Deformation mechanisms in negative Poisson's ratio materials: structural aspects*. Journal of Materials Science, 1991. **26**(9): p. 2287-2292.
62. Warren, Thomas L, *Negative Poisson's ratio in a transversely isotropic foam structure*. Journal of applied physics, 1990. **67**(12): p. 7591-7594.
63. Caddock, BD and KE Evans, *Microporous materials with negative Poisson's ratios. I. Microstructure and mechanical properties*. Journal of Physics D: Applied Physics, 1989. **22**(12): p. 1877.
64. Friis, EA, RS Lakes, and JB Park, *Negative Poisson's ratio polymeric and metallic foams*. Journal of Materials Science, 1988. **23**(12): p. 4406-4414.
65. Lakes, R., *Foam Structures with a Negative Poisson's Ratio*. Science, 1987. **235**(4792): p. 1038-1040.
66. Herakovich, Carl T, *Composite laminates with negative through-the-thickness Poisson's ratios*. Journal of Composite Materials, 1984. **18**(5): p. 447-455.
67. Popereka, M. Y. and Balaguro.Vg, *Ferromagnetic Films Having a Negative Poisson Ratio*. Soviet Physics Solid State,Ussr, 1970. **11**(12): p. 2938-2943.
68. McAfee, J. and N. H. Faisal, *Parametric sensitivity analysis to maximise auxetic effect of polymeric fibre based helical yarn*. Composite Structures, 2017. **162**: p. 1-12.
69. Ng, W. S. and H. Hu, *Tensile and Deformation Behavior of Auxetic Plied Yarns*. Physica Status Solidi B-Basic Solid State Physics, 2017. **254**(12).
70. Magalhaes, R., P. Subramani, T. Lisner, S. Rana, B. Ghiassi, R. Figueiro, D. V. Oliveira, and P. B. Lourenco, *Development, characterization and analysis of auxetic structures from braided composites and study the influence of material and structural parameters*. Composites Part a-Applied Science and Manufacturing, 2016. **87**: p. 86-97.
71. Subramani, P., S. Rana, B. Ghiassi, R. Figueiro, D. V. Oliveira, P. B. Lourenco, and J. Xavier, *Development and characterization of novel auxetic structures based on re-entrant hexagon design produced from braided composites*. Composites Part B-Engineering, 2016. **93**: p. 132-142.
72. Zhou, L., L. L. Jiang, and H. Hu, *Auxetic composites made of 3D textile structure and polyurethane foam*. Physica Status Solidi B-Basic Solid State Physics, 2016. **253**(7): p. 1331-1341.
73. Zhang, G. H., O. Ghita, C. P. Lin, and K. E. Evans, *Varying the performance of*

- helical auxetic yarns by altering component properties and geometry.* Composite Structures, 2016. **140**: p. 369-377.
74. Sibal, A. and A. Rawal, *Design strategy for auxetic dual helix yarn systems.* Materials Letters, 2015. **161**: p. 740-742.
  75. Verma, Prateek, Meisha L Shofner, Angela Lin, Karla B Wagner, and Anselm C Griffin, *Inducing out-of-plane auxetic behavior in needle-punched nonwovens.* physica status solidi (b), 2015. **252**(7): p. 1455-1464.
  76. Zhang, G. H., O. Ghita, and K. E. Evans, *The fabrication and mechanical properties of a novel 3-component auxetic structure for composites.* Composites Science and Technology, 2015. **117**: p. 257-267.
  77. Lim, Teik-Cheng, *Semi-auxetic yarns.* physica status solidi (b), 2014. **251**(2): p. 273-280.
  78. Wang, Zhengyue and Hong Hu, *3D auxetic warp-knitted spacer fabrics.* physica status solidi (b), 2014. **251**(2): p. 281-288.
  79. Subramani, P., S. Rana, D. V. Oliveira, R. Figueiro, and J. Xavier, *Development of novel auxetic structures based on braided composites.* Materials & Design, 2014. **61**: p. 286-295.
  80. Alderson, KL, Andrew Alderson, G Smart, VR Simkins, and PJ Davies, *Auxetic polypropylene fibres: Part 1-Manufacture and characterisation.* Plastics, Rubber and Composites, 2002. **31**(8): p. 344-349.
  81. Dirrenberger, J., S. Forest, and D. Jeulin, *Effective elastic properties of auxetic microstructures: anisotropy and structural applications.* International Journal of Mechanics and Materials in Design, 2013. **9**(1): p. 21-33.
  82. Spadoni, A. and M. Ruzzene, *Elasto-static micropolar behavior of a chiral auxetic lattice.* Journal of the Mechanics and Physics of Solids, 2012. **60**(1): p. 156-171.
  83. Ma, Zheng-Dong, *Three-dimensional auxetic structures and applications thereof.* 2011: U.S. Patent No. 7,910,193. 22 Mar. 2011.
  84. Wright, J. R., M. R. Sloan, and K. E. Evans, *Tensile properties of helical auxetic structures: A numerical study.* Journal of Applied Physics, 2010. **108**(4): p. 044905.
  85. Liu, Y. P. and H. Hu, *A review on auxetic structures and polymeric materials.* Scientific Research and Essays, 2010. **5**(10): p. 1052-1063.
  86. Grima, J. N., P. S. Farrugia, R. Gatt, and D. Attard, *On the auxetic properties of rotating rhombi and parallelograms: A preliminary investigation.* Physica Status Solidi B-Basic Solid State Physics, 2008. **245**(3): p. 521-529.
  87. Dolla, William Jacob, Brian A Fricke, and Bryan R Becker, *Structural and drug diffusion models of conventional and auxetic drug-eluting stents.* Journal of

- Medical Devices, 2007. **1**(1): p. 47-55.
88. Gaspar, N., X. J. Ren, C. W. Smith, J. N. Grima, and K. E. Evans, *Novel honeycombs with auxetic behaviour*. Acta Materialia, 2005. **53**(8): p. 2439-2445.
  89. Stavroulakis, G. E., *Auxetic behaviour: appearance and engineering applications*. Physica Status Solidi B-Basic Solid State Physics, 2005. **242**(3): p. 710-720.
  90. Ravirala, N, Andrew Alderson, KL Alderson, and PJ Davies, *Expanding the range of auxetic polymeric products using a novel melt-spinning route*. physica status solidi (b), 2005. **242**(3): p. 653-664.
  91. Alderson, K. L., V. R. Simkins, V. L. Coenen, P. J. Davies, A. Alderson, and K. E. Evans, *How to make auxetic fibre reinforced composites*. Physica Status Solidi B-Basic Solid State Physics, 2005. **242**(3): p. 509-518.
  92. Grima, J. N., R. Gatt, A. Alderson, and K. E. Evans, *On the potential of connected stars as auxetic systems*. Molecular Simulation, 2005. **31**(13): p. 925-935.
  93. McMullan, Philip J, Satish Kumar, and Anselm C Griffin, *Textile fibres engineered from molecular auxetic polymers*. National Textile Center Annual Report, 2004.
  94. Evans, K. E., J. P. Donoghue, and K. L. Alderson, *The design, matching and manufacture of auxetic carbon fibre laminates*. Journal of Composite Materials, 2004. **38**(2): p. 95-106.
  95. Hook, PB, *Auxetic mechanisms, structures & materials*. 2003, Ph. D. thesis, School of Engineering and Computer Science, University of Exeter.
  96. Alderson, K. L., A. Alderson, G. Smart, V. R. Simkins, and P. J. Davies, *Auxetic polypropylene fibres Part 1 - Manufacture and characterisation*. Plastics Rubber and Composites, 2002. **31**(8): p. 344-349.
  97. Alderson, A, J Rasburn, KE Evans, and JN Grima, *Auxetic polymeric filters display enhanced de-fouling and pressure compensation properties*. Membrane Technology, 2001. **2001**(137): p. 6-8.
  98. Alderson, A and KE Evans, *Rotation and dilation deformation mechanisms for auxetic behaviour in the  $\alpha$ -cristobalite tetrahedral framework structure*. Physics and Chemistry of Minerals, 2001. **28**(10): p. 711-718.
  99. Alderson, A., J. Rasburn, S. Ameer-Beg, P. G. Mullarkey, W. Perrie, and K. E. Evans, *An auxetic filter: A tuneable filter displaying enhanced size selectivity or defouling properties*. Industrial & Engineering Chemistry Research, 2000. **39**(3): p. 654-665.
  100. Smith, C. W., J. N. Grima, and K. E. Evans, *A novel mechanism for generating*

- auxetic behaviour in reticulated foams: Missing rib foam model.* Acta Materialia, 2000. **48**(17): p. 4349-4356.
101. Grima, J. N. and K. E. Evans, *Auxetic behavior from rotating squares.* Journal of Materials Science Letters, 2000. **19**(17): p. 1563-1565.
  102. Evans, K. E. and A. Alderson, *Auxetic materials: Functional materials and structures from lateral thinking!* Advanced Materials, 2000. **12**(9): p. 617-628.
  103. Alderson, KL, RS Webber, and KE Evans, *Novel variations in the microstructure of auxetic ultra-high molecular weight polyethylene. Part 2: Mechanical properties.* Polymer Engineering & Science, 2000. **40**(8): p. 1906-1914.
  104. Alderson, K. L., A. Alderson, R. S. Webber, and K. E. Evans, *Evidence for uniaxial drawing in the fibrillated microstructure of auxetic microporous polymers.* Journal of Materials Science Letters, 1998. **17**(16): p. 1415-1419.
  105. Chan, N. and K. E. Evans, *Fabrication methods for auxetic foams.* Journal of Materials Science, 1997. **32**(22): p. 5945-5953.
  106. Alderson, KL, AP Kettle, PJ Neale, AP Pickles, and KE Evans, *The effect of the processing parameters on the fabrication of auxetic polyethylene.* Journal of materials science, 1995. **30**(16): p. 4069-4075.
  107. Burke, M., *A stretch of the imagination.* New Scientist, 1997. **154**(2085): p. 36-39.
  108. Friis, Elizabeth A, *Surgical implants incorporating re-entrant material.* U.S. Patent No. 5,035,713. 30 Jul. 1991.
  109. Simkins, V. R., A. Alderson, P. J. Davies, and K. L. Alderson, *Single fibre pullout tests on auxetic polymeric fibres.* Journal of Materials Science, 2005. **40**(16): p. 4355-4364.
  110. Boakye, A., Y. P. Chang, K. R. Rafiu, and P. B. Ma, *Design and manufacture of knitted tubular fabric with auxetic effect.* Journal of the Textile Institute, 2018. **109**(5): p. 596-602.
  111. Glazzard, Martha and Philip Breedon, *Weft-knitted auxetic textile design.* physica status solidi (b), 2014. **251**(2): p. 267-272.
  112. Ugbolue, S. C., Y. K. Kim, S. B. Warner, Q. G. Fan, C. L. Yang, O. Kyzymchuk, Y. N. Feng, and J. Lord, *The formation and performance of auxetic textiles. Part II: geometry and structural properties.* Journal of the Textile Institute, 2011. **102**(5): p. 424-433.
  113. Ma, P. B., Y. P. Chang, and G. M. Jiang, *Design and fabrication of auxetic warp-knitted structures with a rotational hexagonal loop.* Textile Research Journal, 2016. **86**(20): p. 2151-2157.
  114. Verma, Prateek, Meisha L Shofner, Angela Lin, Karla B Wagner, and Anselm C Griffin, *Induction of auxetic response in needle-punched nonwovens: Effects of*

- temperature, pressure, and time. physica status solidi (b)*, 2016. **253**(7): p. 1270-1278.
115. King, M. E., *Analytical Methods and Prehistoric Textiles*. American Antiquity, 1978. **43**(1): p. 89-96.
  116. Ko, Frank K, Christopher M Pastore, and Andrew A Head, *Atkins & Pearce Handbook of Industrial Braiding*. 1989: Atkins & Pearce.
  117. Cheang, Sarah, *Cornrow Culture*. MacGuffin, 2016. **3**: p. 133-137.
  118. Blakesley, Gilbert H, *Lace-braiding machine*. U.S. Patent No. 861,703. 30 Jul. 1907.
  119. Cobb, Henry Z, *Braided fabric for hose*. Google Patents: U.S. Patent No. 1,104,777. 28 Jul. 1914.
  120. Walter, Erwin, *Method of manufacturing multi-core cables*. U.S. Patent No. 2,936,670. 17 May 1960.
  121. Branscomb, D., D. Beale, and R. Broughton, *New Directions in Braiding*. Journal of Engineered Fibers and Fabrics, 2013. **8**(2): p. 11-24.
  122. Némoz, Guy, Loïc Dréano, and David Bigaud. *3D braided preforms for shaped composite material*. in *Proceedings of the European Conference on Spacecraft Structures, Materials and Mechanical Testing*. 2005. Materials and Mechanical Testing.
  123. Langer, H, A Pickett, B Obolenski, H Schneider, M Schneider, and E Jacobs. *Computer controlled automated manufacture of 3D braids for composite*. in *Euromat Symp Munich, Germany*. 2000.
  124. Rana, Soheli and Raul Fanguero, *Braided Structures and Composites: Production, Properties, Mechanics, and Technical Applications*. Vol. 3. 2015: CRC Press.
  125. Du, Zhaoqun, Ming Zhou, Hongling Liu, and Linge He, *Study on negative Poisson's ratio of auxetic yarn under tension: Part 1—Theoretical analysis*. Textile Research Journal, 2015. **85**(5): p. 487-498.